THE
PHYSICAL REVIEW

A journal of experimental and theoretical physics established by E. L. Nichols in 1893

SECOND SERIES, VOL. 73, NO. 3 FEBRUARY 1, 1948

The Scattering of High Energy Neutrons by Protons

M. CAMAC AND H. A. BETHE
Cornell University, Ithaca, New York
(Received October 10, 1947)

The scattering has been calculated, using the exact formula, for neutron energies between 20 and 80 Mev, with ranges of 2.0 and 2.8×10^{-13} cm for the nuclear force and using ordinary, exchange, and symmetric forces. The maximum of the scattered intensity at 180° is sensitive to the range of the forces; experiments with neutrons from 30 to 60 Mev would permit a rather conclusive determination of the range. The total cross section for forces of the exchange type is much smaller than that obtained from the Born approximation, even at 80 Mev.

THE scattering of neutrons by protons at energies from 20 to 80 Mev has been calculated, making different assumptions about the nuclear forces. Throughout the calculation a pure central force was used and the tensor force neglected. A square well potential was assumed in each case.

The range of the nuclear forces was taken to be either 2.8 or 2.0×10^{-13} cm[2]. The first of these values is the one commonly assumed and is in agreement with the results from proton-proton scattering at low energies.[1] The smaller range is suggested, especially for the triplet interaction, by the experiments on scattering of neutrons by para-hydrogen.[2] We realize that this smaller range may result in disagreement with the experimental total cross section in the range from 2–5 Mev.

The three customary[3] types of forces were assumed, namely: ordinary forces, exchange forces, and "symmetric" forces, i.e., those derived from the symmetric meson theory which are proportional to the operator $\sigma_1\cdot\sigma_2\tau_1\cdot\tau_2$ (σ = spin, τ = isotopic spin). On the basis of the recent experiments made with the Berkeley[4] cyclotron, ordinary forces may be considered as excluded and symmetric forces as the most likely.

The exact theory of scattering[5] was used throughout. For the determination of the phase shifts δ_l, a convenient method was developed which is described in the appendix. The depth of the potential well for the triplet interaction was determined to fit the binding energy of the deuteron, 2.19 Mev. The depth of the singlet interaction was determined to give the cross section of 20 barns for the scattering of slow neutrons by protons. The well depths, for the triplet and singlet interaction respectively, are then 21.3 and 11.9 Mev for the longer range, and 36.6 and 24.0 Mev for the shorter range of the forces.

The results for the phase shifts of the triplet and singlet states are given in Table I. As is to

[1] G. Breit, H. M. Thaston, and L. Eisenbud, Phys. Rev. 55, 1018 (1939).
[2] R. B. Sutton, T. Hall, E. E. Anderson, H. S. Bridge, J. W. DeWire, L. S. Lavatelli, E. A. Long, T. Snyder, and R. W. Williams, Phys. Rev. 72, 1147 (1947); See also C. S. Wu, L. J. Rainwater, W. W. Havens and J. R. Dunning, Phys. Rev. 69, 236 (1946).
[3] W. Rarita and J. Schwinger, Phys. Rev. 59, 556 (1941).
[4] E. M. MacMillan, private communication.
[5] N. F. Mott and H. S. W. Massey, *The Theory of Atomic Collisions* (Oxford University Press, 1933), p. 24.

be expected, the phase shifts for ordinary forces are all positive, while for the two other types, the phase shifts for odd l are negative (repulsive force). For a given energy and given l, the negative phase shift for the exchange force is smaller than the corresponding positive one for the ordinary force, because a repulsive potential is less effective than an attractive potential of the same magnitude. For the symmetric theory, the phase shifts δ_l are smaller than the corresponding ones for exchange forces in the triplet states of odd l, but larger in the singlet states, because the forces are multiplied by factors $\frac{1}{3}$ and 3, respectively. For the ordinary force, the phase shift generally decreases with increasing l for a given energy; however, this is reversed for $l=0$ and 1 when the wave-length inside the potential well becomes less than twice the range of the nuclear forces: this is a peculiar effect for a square well which can be verified directly from the formulas for the phase shifts.

The scattered intensity in the center-of-mass system, was calculated as a function of angle, and expressed in terms of a power series in $\cos\theta$, thus:

$$d\sigma = 2\pi C \sin\theta d\theta (A_0 + A_1 \cos\theta + \cdots + A_n \cos^n\theta + \cdots), \quad (1)$$

$$C = \lambda^2/16.$$

The coefficients A_n and C are given in Table II. It is interesting to note that the coefficient A_0 which gives directly the scattering through 90°, is determined entirely by the phase shifts for *even* l because the spherical harmonics of odd l vanish for $\theta=90°$. Therefore, the 90° scattering is independent of the type of forces assumed (always neglecting tensor forces).

In Table III, we have given the differential scattering cross sections at 180°, 90° and 0° corresponding to protons projected forward, at 45° and at 90° in the laboratory system. We have also given the ratio of the scattered intensities at 180° and 90°. It is seen that this ratio increases rapidly with energy for exchange and symmetric forces as is to be expected. For ordinary forces, there is first a decrease which again is expected, but then, at the higher energies, an increase; this is due to the well-known phenomenon[6] that the scattered intensity has a secondary maximum in the backward direction if the exact scattering formula is used. This maximum does not appear in the Born approximation and has been investigated in some detail for proton-neutron scattering by Marshak and Ashkin.[7] An illustration of the backward maximum is given in Fig. 1.

The maximum of the intensity at 180° for

TABLE I. Phase shifts (in degrees).

	Range 2.0×10^{-13} cm						Range 2.8×10^{-13} cm					
	Triplet			Singlet			Triplet			Singlet		
	Ord.	Exch.	Sym.	Ord.	Exch.	Sym.	Ord.	Exch.	Sym.	Ord.	Exch.	Sym.
20 Mev												
0	86.5			57.9			75.4			47.8		
1	6.4	−2.6	−1.07	3.35	−1.9	−4.0	20.5	−6.7	−2.9	8.0	−4.4	−9.1
2	0.13			0.08			0.75			0.4		
30 Mev												
0	76.1			53.0			63.2			41.0		
1	11.3	−4.4	−1.85	5.8	−3.2	−6.7	31.0	−10.6	−4.6	12.6	−7.0	−14.4
2	0.22			0.13			1.9			0.9		
3							0.08	−0.08	−0.03	0.04	−0.04	−0.17
40 Mev												
0	68.5			48.6			54.5			35.7		
1	16.3	−6.3	−2.7	8.4	−4.6	−9.5	37.5	−14.4	−6.2	16.4	−9.5	−19.5
2	0.65			0.4			3.6			1.75		
3	0.02	−0.02	−0.01	0	0	−0.03	0.20	−0.17	−0.05	0.10	−0.08	−0.27
80 Mev												
0	49.4			36.0			34.8			22.1		
1	31.0	−13.4	−5.6	17.2	−9.8	−20.1	40.2	−26.1	−10.5	22.0	−16.5	−36.2
2	3.1			1.9			13.8			6.5		
3	0.18	−0.17	−0.05	0.12	−0.08	−0.25	1.6	−1.2	−0.4	0.8	−0.7	−2.1
4							0.1			0.05		

[6] The phenomenon is due to the fact that the Legendre polynomials P_l alternate between +1 and −1 at 180° which permits only very incomplete destructive interference between the contributions of various values of l, whereas at other angles the values of P_l are more erratic and destructive interference more effective.

[7] Marshak and Ashkin, Phys. Rev., to be published.

TABLE II. Coefficients in Fourier expansion of differential cross section. See Eq. (1).

Energy	Range in 10^{-13} cm	Force	C in 10^{-26} cm²	A_0	A_1	A_2	A_3	A_4	A_5	A_6	A_7
20 Mev	2.0	ord.	26.0	14.8	+2.0	+1.5	+0.16				
	2.0	exch.	26.0	14.8	−0.36	+0.32	−0.07				
	2.0	sym.	26.0	14.8	−0.71	+0.27	−0.04				
	2.8	ord.	26.0	13.2	+15.1	+14.5	+2.5	+0.29			
	2.8	exch.	26.0	13.2	−1.6	+2.4	−0.95	+0.19			
	2.8	sym.	26.0	13.2	−2.0	+1.9	−0.60	+0.28			
30 Mev	2.0	ord.	17.3	13.8	+7.0	+4.7	+0.44	+0.04			
	2.0	exch.	17.3	13.8	−1.4	+0.95	−0.19	+0.02			
	2.0	sym.	17.3	13.8	−2.1	+0.81	−0.12				
	2.8	ord.	17.3	10.4	+28.0	+32.4	+8.9	+1.7	+0.17		
	2.8	exch.	17.3	10.4	−3.2	+6.5	−3.7	+1.2	−0.17		
	2.8	sym.	17.3	10.4	−3.3	+5.2	−2.3	+1.7	−0.09		
40 Mev	2.0	ord.	13.0	+12.2	+12.9	+10.1	+1.9	+0.3			
	2.0	exch.	13.0	12.2	−2.5	+2.3	−0.8	+0.2			
	2.0	sym.	13.0	12.2	−2.4	+2.0	−0.5	+0.2			
	2.8	ord.	13.0	7.4	+31.2	+46.3	+18.8	+5.2	+0.9	+0.2	
	2.8	exch.	13.0	7.4	−3.6	+11.8	−9.0	+3.8	−0.7	+0.1	
	2.8	sym.	13.0	7.4	−3.8	+9.6	−5.5	+3.6	−0.4	+0.1	
80 Mev	2.0	ord.	6.49	6.5	+25.3	+38.0	+15.2	+3.1	+0.8	+0.1	
	2.0	exch.	6.49	6.5	−4.7	+10.9	−7.6	+3.0	−0.5	+0.1	
	2.0	sym.	6.49	6.5	−4.0	+9.5	−4.9	+3.1	−0.35	+0.1	
	2.8	ord.	6.49	0.59	+3.3	+37.2	+65.2	+54.5	+24.2	+7.2	+1.4
	2.8	exch.	6.49	0.59	+4.8	+15.5	−36.4	+47.7	−17.5	+5.6	−1.2
	2.8	sym.	6.49	0.59	+2.0	+9.5	−23.5	+45.2	−10.5	+5.4	−0.6

exchange and symmetric forces should be observable already at 20 Mev neutron energy (in the laboratory system) if the nuclear forces have a range of 2.8×10^{-13} cm; it becomes quite marked at 30 and very pronounced at 40 Mev. For the shorter range, nearly twice as much energy is required to produce the same asymmetry in the scattering; this is a direct consequence of the fact that the depth of the potential wells is nearly twice as great as for the longer range. Because of this great sensitivity of the angular distribution to the range of the forces, it seems very much worth while to make scattering experiments in the intermediate energy range, from about 20 to 60 Mev; such experiments would be especially conclusive after the symmetry properties of the forces have been established by experiments at higher energy. Intermediate energies have also the advantage that relativistic corrections will be unimportant, while they may be appreciable at 100 Mev. Also, probably the influence of tensor forces is relatively smaller at intermediate energies.

Figure 1 gives the angular distribution of the scattered neutrons in the center-of-mass system at 80 Mev neutron energy, for the various assumptions about the forces. The very deep minimum near 90° for $a=2.8\times10^{-13}$ is largely an accidental effect; there is near cancellation of the contributions from $l=0$ and $l=2$ to the

TABLE III.

Energy in	Range forces	Differential cross section in c.m. system per unit solid angle in 10^{-26} cm²: at $\theta=0°$	at $\theta=90°$	at $\theta=180°$	Ratio 180/90	Total scattering cross section in barns (10^{-24} cm²): Exact formula	Born approximation
20 Mev	2.0 ord	4.81	3.85	3.69	0.96	0.500	0.410
	2.0 exch	3.82	3.85	4.05	1.05	0.486	0.410
	2.0 sym	3.73	3.85	4.12	1.07	0.486	*
	2.8 ord	11.88	3.43	2.72	0.79	0.590	0.714
	2.8 exch	3.42	3.43	4.75	1.38	0.456	0.714
	2.8 sym	3.30	3.43	4.67	1.36	0.451	*
30 Mev	2.0 ord	4.48	2.38	1.92	0.81	0.333	0.336
	2.0 exch	2.27	2.38	2.83	1.19	0.306	0.336
	2.0 sym	2.14	2.38	2.91	1.22	0.305	*
	2.8 ord	14.08	1.79	1.28	0.72	0.466	0.529
	2.8 exch	1.89	1.79	4.37	2.44	0.277	0.529
	2.8 sym	2.00	1.79	3.97	2.22	0.268	*
40 Mev	2.0 ord	4.87	1.59	1.01	0.64	0.256	0.290
	2.0 exch	1.48	1.59	2.34	1.47	0.214	0.290
	2.0 sym	1.49	1.59	2.25	1.42	0.213	*
	2.8 ord	14.22	0.96	1.05	1.09	0.388	0.408
	2.8 exch	1.28	0.96	4.72	4.92	0.201	0.408
	2.8 sym	1.44	0.96	3.94	4.10	0.184	*
80 Mev	2.0 ord	5.78	0.42	0.42	1.00	0.155	0.165
	2.0 exch	0.50	0.42	2.16	5.14	0.0880	0.165
	2.0 sym	0.65	0.42	1.85	4.40	0.0837	*
	2.8 ord	12.57	0.038	3.52	92.6	0.203	0.206
	2.8 exch	1.24	0.038	7.75	204	0.131	0.206
	2.8 sym	4.32	0.038	6.05	159	0.111	*

* Very close to value for ordinary and exchanges forces.

scattered amplitude, and higher l's do not yet contribute appreciably. (At higher energies, this accidental cancellation disappears but there is a general tendency for the cross section to decrease, so that $\sigma(90°)$ actually stays low.) But even with $a=2\times10^{-13}$, the ratio between 180° and 90° is 5.1 and 4.4, respectively, for exchange and symmetric forces. It is apparent that the range of the forces is more important for the ratio 180°/90° than their type, i.e., whether they are pure exchange or symmetric, and this is even true for the 0° scattering. Moreover, the tensor forces will greatly increase the scattering at 90° while not affecting it appreciably at 180°; therefore, it would be premature to draw conclusions on the range or the type of nuclear forces by comparing the present calculations with experiment.

In Table III we have also given the total cross section. It is striking that at the higher energies the total cross section is much smaller for exchange than for ordinary forces. This is due to the fact that $|\delta_l|$ is much smaller for exchange than for ordinary forces for any odd value of l. We mentioned before that this is caused by the repulsive character of the exchange force in states of odd l. The main contribution to the total cross section at 80 Mev for ordinary forces comes from $l=1$; this contribution is very much reduced for exchange forces. The difference is more pronounced for the shorter range, because in this case the potential has a greater magnitude. This effect will gradually decrease with further increase in energy..

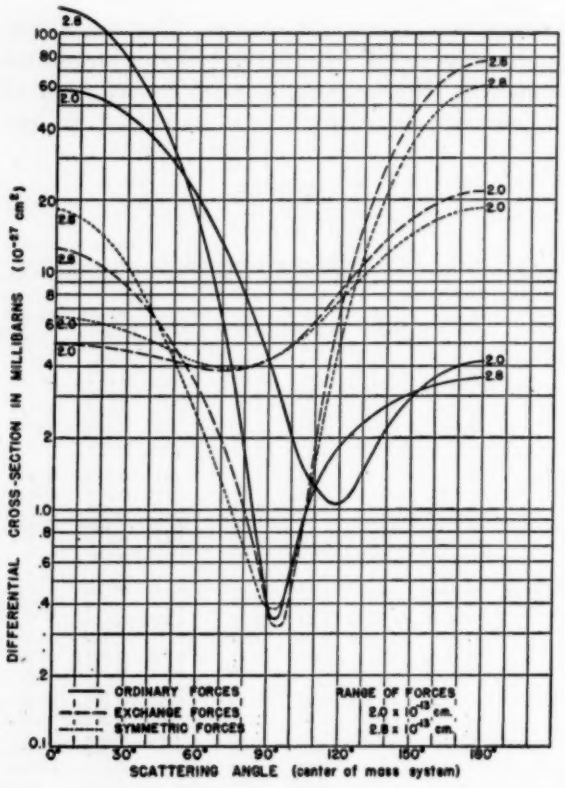

FIG. 1. Angular distribution of scattering of 80 Mev neutrons by protons.

We have also listed the cross sections according to the Born approximation. At 80 Mev there is quite good agreement between the Born approximation and the exact cross section in the case of ordinary forces. For the exchange types, the exact calculation gives much lower cross sections. The agreement in the case of ordinary forces is due to a compensation between two effects: the exact calculation will, in general, give greater phase shifts than the Born approximation for an attractive potential, but the cross section is proportional to $\sin^2\delta_l$ in the exact theory instead of δ_l^2 in the Born approximation. In the case of a repulsive potential, the exact δ_l is smaller in absolute magnitude than the Born approximation value, and the replacement of δ_l^2 by $\sin^2\delta_l$ causes a further reduction in the cross section. For the symmetric force, the calculations in the Born approximation were not carried out explicitly, but it was found that the result is nearly the same as for exchange forces. The same is seen to be true in the exact theory.

Since the nuclear forces appear to be of the exchange or symmetric type, the total cross section at 80 Mev, and probably still at higher energies, is considerably smaller than the value derived from the Born approximation. This tends to bring about better agreement with the experimental value of the cross section of about 0.08 barns[4] at 90 Mev. Shorter range of the forces would also help to lower the cross section and thereby improve the agreement with experiment. But it must again be remembered that these results may be modified by tensor forces, and that also relativistic corrections may easily have an effect of about 10 percent. The sign of these corrections is unknown.

At lower energies, agreement between Born approximation and exact calculation is not to be

expected. Considering the magnitude of the nuclear potential, the actual agreement at the lower energies is surprisingly good. It might be expected that the Born approximation gives too large a cross section at lower energies—this, at least, is its behavior in most problems of *atomic* collisions. In contrast to this expectation, the Born approximation cross section is smaller than the exact one for 20 Mev and $a=2.0\times10^{-13}$ cm. This can be understood from a calculation at zero energy; here the Born approximation would give 0.6 barns as against the correct value of 20 barns. (With $a=2.8\times10^{-13}$, the Born approximation gives 1.8 barns.) The high value from the exact calculation is known to be caused by a resonance effect which, of course, cannot be simulated by the Born approximation. Since the latter gives a cross section which increases montonically with decreasing energy, it must fall below the actual cross section already at some finite energy.

APPENDIX

The radial wave function for a given l inside the potential well is given by

$$v=r^{-\frac{1}{2}}J_{l+\frac{1}{2}}(\kappa r), \tag{2}$$

and outside the potential well by:

$$u=Ar^{-\frac{1}{2}}Z_{l+\frac{1}{2}}(kr), \tag{3}$$

where Z is the generalized Bessel function,

$$Z_{l+\frac{1}{2}}(kr)=J_{l+\frac{1}{2}}(kr)\cos\delta_l-N_{l+\frac{1}{2}}(kr)\sin\delta_l, \tag{4}$$

where J is the Bessel and N the Neumann function, and

$$k^2=ME/\hbar^2, \quad \kappa^2=M(E+V_0)/\hbar^2. \tag{5}$$

E is the energy in the center-of-mass system and V_0 the depth of the potential. The two functions u and v must join with continuous derivative at $r=a$. Setting the logarithmic derivatives equal, we obtain the condition:

$$k\frac{Z_{l+\frac{1}{2}}'(ka)}{Z_{l+\frac{1}{2}}(ka)}=\kappa\frac{J_{l+\frac{1}{2}}'(\kappa a)}{J_{l+\frac{1}{2}}(\kappa a)}, \tag{6}$$

where the prime denotes differentiation with respect to the argument. Equations (6) and (4) serve to determine the phase shift δ.

Equation (6) may be simplified by using the following relations between the generalized Bessel function:

$$\begin{aligned} Z_p'(x)&=Z_{p-1}(x)-(p/x)Z_p(x),\\ Z_{p+1}(x)&=(2p/x)Z_p(x)-Z_{p-1}(x). \end{aligned} \tag{7}$$

Therefore, we have

$$\frac{Z_{l+\frac{1}{2}}'(x)}{Z_{l+\frac{1}{2}}(x)}=-\frac{l+\frac{1}{2}}{x}+\frac{Z_{l-\frac{1}{2}}(x)}{Z_{l+\frac{1}{2}}(x)} \tag{8}$$

$$=-\frac{l+\frac{1}{2}}{x}+\cfrac{1}{\cfrac{2l-1}{x}-\cfrac{Z_{l-3/2}}{Z_{l-1}}} \tag{9}$$

$$=-\frac{l+\frac{1}{2}}{x}+\cfrac{1}{\cfrac{2l-1}{x}-\cfrac{1}{\cfrac{2l-3}{x}-\cfrac{Z_{l-5/2}}{Z_{l-3/2}}}}.$$

Continuing to express the Bessel functions by those of lower order, we finally arrive at the ratio,

$$\frac{Z_{-\frac{1}{2}}(ka)}{Z_{\frac{1}{2}}(ka)}=\cot(ka+\delta). \tag{10}$$

Equating both sides of Eq. (6), the term $-(l+\frac{1}{2})/x$ cancels and we obtain

$$\cfrac{k}{\cfrac{2l-1}{ka}-\cfrac{1}{\cfrac{2l-3}{ka}-\cfrac{1}{\cdots-\cfrac{1}{\cfrac{1}{ka}-\cot(ka+\delta)}}}}$$

$$=\cfrac{\kappa}{\cfrac{2l-1}{\kappa a}-\cfrac{1}{\cfrac{2l-3}{\kappa a}-\cfrac{1}{\cdots-\cfrac{1}{\cfrac{1}{\kappa a}-\cot\kappa a}}}}. \tag{11}$$

This can be solved and gives the formula,

$$\cot(ka+\delta)=\cfrac{1}{ka}-\cfrac{1}{\cfrac{3}{ka}-\cfrac{1}{\cfrac{5}{ka}-\cfrac{1}{\cdots-\cfrac{1}{\cfrac{2l-1}{ka}-\cfrac{ka}{\kappa a}\left(\cfrac{2l-1}{\kappa a}-\cfrac{1}{\cfrac{2l-3}{\kappa a}-\cfrac{1}{\cdots-\cfrac{1}{\cfrac{1}{\kappa a}-\cot\kappa a}}}}\right)}}}}. \tag{12}$$

The use of this formula obviates the necessity of calculating the explicit formulae for the Bessel functions of high order. It also reduces the numerical work for higher l partly to that already done for lower l.

In some cases, the potential is repulsive and greater than the energy of the system. In this case κ comes out imaginary, and if we use $\kappa'=|\kappa|$ instead, we must replace Eq. (12) by

$$\cot(ka+\delta)=\cfrac{1}{ka}-\cfrac{1}{\cfrac{3}{ka}-\cfrac{1}{\cfrac{5}{ka}-\cfrac{1}{\cdots-\cfrac{1}{\cfrac{2l-1}{ka}+\cfrac{ka}{\kappa' a}\left(\cfrac{2l-1}{\kappa' a}+\cfrac{1}{\cfrac{2l-3}{\kappa' a}+\cfrac{1}{\cdots+\cfrac{1}{\cfrac{1}{\kappa' a}-\coth\kappa' a}}}}\right)}}}}. \tag{13}$$

Note the change of sign and the change from cot to coth.

It is worth noting that in actual calculations with Eq. (13) and occasionally with (12), especially for large l, the two terms which have to be added in each denominator, tend to cancel each other so that considerable numerical accuracy is needed.

For the higher values of l it is convenient to use the recursion formula derived from perturbation theory:

$$\delta_l=\delta_{l-1}\frac{(ka)^2}{(2l+1)(2l+3)}. \tag{14}$$

This formula was found to be quite accurate if the phase was less than 1°.

The Scattering of Neutrons of Energy between 12.0 Mev and 13.0 Mev by Protons

J. S. LAUGHLIN AND P. G. KRUGER
Department of Physics, University of Illinois, Urbana, Illinois

(Received September 25, 1947)

The angular distribution of the recoil protons projected during the scattering of neutrons by protons has been investigated in a methane-filled, high pressure cloud chamber. A deuterium gas target bombarded with 10 Mev deuterons provided the high energy neutron source. The spectrum of the neutrons from this source, which entered the cloud chamber through a collimator, was surveyed and showed a group of high energy neutrons superimposed on a continuous background. Examination of the data with rigorous selection criteria to determine those recoils projected by the scattering of neutrons between 12.0 Mev and 13.0 Mev yielded a total of 1573 recoil protons. The azimuthal and recoil angle distributions of these protons have been analyzed. A ratio of the differential cross sections for neutron scattering in the backward direction to scattering in a direction perpendicular to that of the incident neutron beam, of unity (spherically symmetric scattering) or slightly greater than unity can be consistent with these data.

THEORETICAL predictions concerning the angular distribution to be expected in the scattering of high energy neutrons by protons vary widely, depending on the nature of the forces assumed for the neutron-proton interaction. Because of the fundamental importance of obtaining a more accurate knowledge of the nature of the neutron-proton interaction, this study of the angular distribution of recoil protons from the scattering of high energy neutrons has been made. Several other authors[1–3] have also mentioned the desirability of obtaining further data on the scattering of high energy neutrons by protons.

In this report the experimental study of the scattering of neutrons between 12.0 Mev and 13.0 Mev in energy is described. The angular distribution was studied in a methane-filled, high pressure (25 atmospheres) cloud chamber. The University of Illinois cyclotron was used to bombard deuterium gas with 10 Mev deuterons for the neutron source.

Previous experiments[4–6] indicated that at lower energies (2.6 Mev) the neutron-proton scattering process is spherically symmetric. However, the results of other experimenters at high energies (12.5 Mev to 14.0 Mev) have indicated large deviations from spherically symmetric scattering. Amaldi and his collaborators[7] reported a determination of the ratio of the differential cross sections for scattering of 12.5 Mev neutrons in the backward direction to the scattering in a perpendicular direction with respect to the incident neutron beam in the center-of-mass system of 0.71 ± 0.04 and a ratio of 0.53 ± 0.03 for neutrons with an average energy of 13.3 Mev. They employed proportional counters in triple coincidence to detect the recoil protons. Champion and Powell[8] employed photographic emulsions as detectors to study the same problem. Their results with neutrons of about 13.0 Mev energy were first reported to be in general agreement with those of Amaldi. Later results by Powell[9] indicate spherically symmetric scattering in the center-of-mass system.

The high pressure cloud chamber was used in this experimental study of the angular distribution of the neutron-proton scattering process. The chamber body was constructed by the Westinghouse Electric and Manufacturing Com-

[1] William Rarita, Julian Schwinger, and H. A. Nye, Phys. Rev. 59, 209 (1941).
[2] Lamek Hulthén, Phys. Rev. 63, 383 (1943).
[3] W. Pauli, *Meson Theory of Nuclear Forces* (Interscience Publishers, Inc., New York, 1946) p. 56.
[4] P. G. Kruger, W. E. Shoupp, and F. W. Stallman, Phys. Rev. 52, 678 (1937).
[5] T. W. Bonner, Phys. Rev. 52, 685 (1937).
[6] P. I. Dee and C. W. Gilbert, Proc. Roy. Soc. 163, 265 (1937).
[7] E. Amaldi, D. Bocciarelli, B. Ferretti, and G. C. Trabacchi, Naturwiss. 30, 582 (1942).
[8] F. C. Champion and C. F. Powell, Proc. Roy. Soc. A183, 64 (1944).
[9] G. Wentzel, Rev. Mod. Phys. 19, 10 (1947); (see footnote 38).

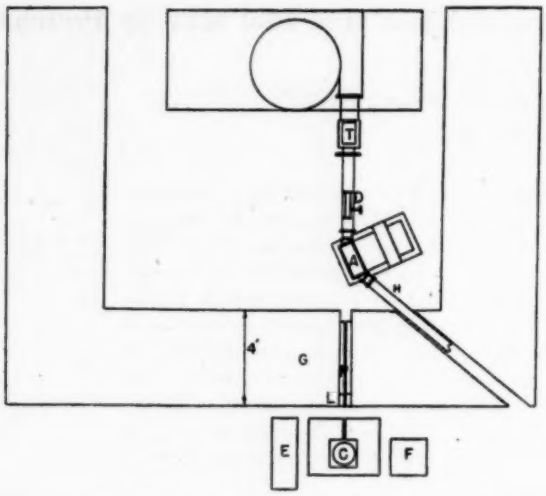

FIG. 1. Experimental arrangement. *T* indicates location of copper target containing a hole, *D* the deuterium target, *A* the analyzer magnet, *P* the paraffin collimator, *L* the lead collimator, *C* the high pressure cloud chamber, *E* the air compressor, *F* the control panel, *G* the shielding tanks around the cyclotron, and *H* the exit tube.

pany,[10] and was modified and the system completed at the University of Illinois. The cloud chamber interior has an inside diameter of $5\frac{3}{4}$ inches and a height of 3 inches. Expansion is caused by reducing the pressure underneath the piston. The cloud chamber operation was controlled by a cam system which, in conjunction with time delay relays, permitted sensitive and independent adjustment of the cycle time and of the time intervals between operation of the various components of the cloud chamber system. Illumination was provided by a mercury capillary arc. A reflector and double lens system concentrated the light for illuminating the cloud chamber in a parallel well-defined beam. A sweep-field voltage of about 2000 volts was applied between expansions. The cycle time was varied between two and three minutes, depending on equilibrium conditions in the chamber. The camera used was so designed that the film was accurately positioned and this position exactly reproducible. The camera used 35 mm film and contains an $f/2$ Ektar lens of 45 mm focal length. Each photograph contained three views of the chamber, a central view and two reflected views from two parallel mirrors perpendicular to the light beam and mounted rigidly in the mirror box which supported the camera above the chamber.

The vapor for track formation was provided by 10 cc of a 60 percent solution of isopropyl alcohol in distilled water. After evacuation, the chamber was filled with 99 percent pure methane gas to a gauge pressure of 335 pounds per square inch. The impurity in the methane consisted of higher order hydrocarbons.

The incident neutrons were detected by observing recoil protons projected from elastic collisions. The energy of the incident neutron E_n and the proton recoil E_p are related by the expression $E_p = E_n \cos^2\phi$, where ϕ is the recoil angle of the proton relative to the direction of the incident neutron in the laboratory system.

Three quantities were measured for each proton track, the recoil angle ϕ, the azimuthal angle θ, and its length L. The angle between the vertical direction and the projection of the proton track in a plane normal to the incident neutron beam is the azimuthal angle for that track. To measure these quantities, the tracks were reprojected through the same optical system in which they were photographed. Upon reprojection, the film was accurately positioned in the camera and illuminated by an arc. The three stereoscopic views of each track were projected on a ground glass screen. This screen, mounted on two rigid side arms attached to the stereoscopic mirror system, allowed one degree of rotational freedom and one degree of translational freedom. The viewing screen was adjusted until the stereoscopic images of a given proton track coincided and were in focus. A measuring engine was then used to measure the ϕ, θ, and L. This engine contained a lucite ruler graduated in millimeters. Adjustment of two bearings allowed this ruler to assume any direction and coincide with any proton track focused on the screen. Each of these bearings contained a pointer and an associated scale graduated in degrees. One of these indicated the recoil angle ϕ, while the other indicated the azimuthal angle θ. Thus ϕ, θ, and L could be simultaneously recorded. The length of each track was read to the nearest millimeter and the lengths were reproducible to one millimeter. The angles were read to the nearest degree. The recoil angle readings were reproducible after removing the film, replacing it and

[10] The cloud chamber was made available to the University of Illinois through Dr. W. E. Shoupp of the Westinghouse Electric and Manufacturing Company Research Laboratory.

readjusting for coincidence of the stereoscopic images, to within $\pm 2°$ and the azimuthal angles to within $\pm 4°$.

The direction of the incident neutrons was well known, since the neutrons were collimated by passing through a hole one-half inch in diameter through the water tanks surrounding the cyclotron. The collimation consisted of a tubular paraffin plug three feet long, with an outside diameter of six inches and an inside diameter of one-half inch. This paraffin plug, together with a lead plug six inches long with the same diameters, was placed in a cylindrical pipe through the water tanks. The cloud chamber was shielded from gamma-rays by lead blocks eleven inches thick placed around the chamber. A $\frac{3}{8}$-inch hole was bored through these blocks in a straight line with the collimator hole through the water tanks surrounding the cyclotron. The water in these tanks was saturated with boron, which aided in reducing to a negligible amount the number of neutrons which escaped through the tanks surrounding the cyclotron. The cloud chamber was so aligned with respect to the collimator that the neutrons passed through the center of the chamber along a diameter. In the photographs, over 95 percent of all proton tracks started in the central one-half inch diameter cylinder. Considering the relative volume of this cylinder to the illuminated volume of the chamber, less than one-half of one percent of the tracks originating in the central cylinder could have been due to stray neutrons. The collimation was thus successful in localizing the direction and path of the neutrons through the chamber.

A prolific source of high energy neutrons was necessary to make the cloud chamber method of studying the angular distribution possible. The neutrons from various targets bombarded by 10 Mev deuterons were investigated in a position at right angles to the incident deuteron beam before a satisfactory source was finally achieved in the forward direction. With the collimator and cloud chamber in the position at right angles to the deuteron beam, thin and thick targets of lithium, copper, beryllium, and aluminum were bombarded and the neutron energies and proton recoil intensities observed.[11] None of these targets gave a sufficient number of high energy neutrons to make a cloud chamber examination of the scattering problem feasible.

The d,d reaction is known to give a single monoenergetic group of neutrons when bombarded with monoenergetic deuterons:

$$_1D^2 + {}_1D^2 = {}_2He^3 + {}_0n^1 + 3.26 \text{ Mev}.$$

The highest energy neutrons are ejected in the forward direction from the target, so the high pressure cloud chamber was stationed in front of the forward porthole of the water tanks. Figure 1 shows the general experimental arrangement. The deuteron beam passed through a one-inch hole in a copper target at T. After passing through the deuterium target at D, the deuteron beam was deflected by the analyser magnetic field at A and passed part way down the exit tube H. This prevented neutrons from sources other than the target entering the cloud chamber. The current in the analyzer magnet coils was increased somewhat above the value which would send the beam completely through the exit tube outside the tanks, so that it terminated on the exit tube well inside the water tank. The combined effect of the water and boron in these tanks made negligible the number of neutrons of energy above a few Mev passing through the tanks. The deuterium gas target holder is shown in Fig. 2. The end foils were one and one-half mil Duralumin foil. The stopping power of the deuterium gas for a 10 Mev deu-

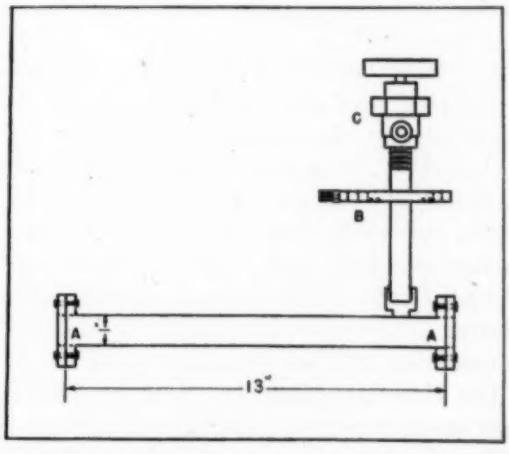

FIG. 2. Deuterium gas target. Location of the Duralumin windows is indicated by A, B indicates the flange which made a vacuum seal to the entrance tube, and C indicates the valve.

[11] J. S. Laughlin and P. G. Kruger, Phys. Rev. 71, 484 (1947).

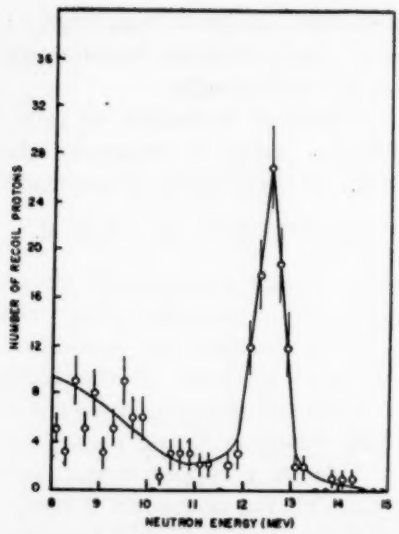

FIG. 3. Spectrum of recoil protons projected by neutrons from the deuterium gas target bombarded with 10 Mev deuterons.

teron was 0.52 Mev. Duralumin foils were chosen for the target windows, since they made it possible to use thicknesses with sufficiently high tensile strength to withstand atmospheric pressure which still had a low stopping power, and since both the aluminum and copper neutron spectrum observed in the right angle position had very low relative intensities for high energy neutrons above 9 Mev. Duralumin consist of about 94 percent aluminum, 4.2 percent copper, 0.7 percent manganese, 0.5 percent magnesium, 0.2 percent silicon, and 0.4 percent iron. The target could be evacuated and filled with gas without disturbing the vacuum of the cyclotron chamber.

0.85 Mev was the calculated maximum spread in the energy of the neutrons produced in this target resulting from inhomogeneity in energy of the incident deuterons, straggling in the foils, variation of magnetic field in the cyclotron during operation, and thickness of target. The median absolute energy was calculated to be 12.5 ± 0.2 Mev. The intensity of this group relative to the continuous background could not be predicted.

The cloud chamber was used to survey the high energy neutron spectrum of this target; collimation arrangement and about 900 photographs were taken for this purpose. The cyclotron deuterium arc was struck 0.05 sec. after each expansion had started. This insured that the chamber was about three-fourths expanded before irradiation.

In the calculation of the neutron energies, a single value of the stopping power was employed, since the spectrum was being examined over only the high energy range where the stopping power of methane has very small dependence on the proton energy. At a gauge pressure of 301.5 pounds per square inch, the stopping power of the chamber was 17.9 and each measured track length was multiplied by this amount. A range-energy curve constructed from a table published by Pollard and Davidson[12] was used to convert these lengths into proton energies. The relation $E_n=E_p/\cos^2\phi$ was then used to obtain the energies of the incident neutrons. Those tracks which were distinct, fully illuminated, entirely in the chamber, and which originated in the neutron beam along a diameter of the chamber were suitable for data. Although all tracks with scattering angles up through 50° were measured, only those at angles equal to or less than 40° were used in the calculations for the spectral survey. A total of 161 of the measured tracks corresponded to a neutron energy greater than 8 Mev. Figure 3 shows the results plotted in number of recoil protons versus neutron energy. A definite group of fairly energetically homogeneous neutrons strong in intensity relative to that of the immediately neighboring energy regions is present. Though there is not a sufficient number of tracks in this survey for good statistics, the intensity between 11 Mev and 12 Mev appears less than 20 percent of that between 12 Mev and 13 Mev. The width of the group appears to be over 1.25 Mev, as compared with a calculated maximum of 0.85 Mev. Multiple small angle scattering in the collimator, pressure variation in the cloud chamber, and errors in measurement probably account for this additional spread.

The average yield of tracks per picture was increased to more than one high energy track every two pictures by applying the cyclotron arc voltage at the beginning of the expansion and increasing the stability of the cyclotron arc operation. This was effective since the chamber

[12] E. C. Pollard and W. L. Davidson, *Applied Nuclear Physics* (John Wiley and Sons, Inc., 1942), Appendix 7.

was now exposed a longer time to the incident neutrons, and even when the arc delayed in firing, it was more likely to produce some deuterons sufficiently early for use. The compressed chamber gauge pressure was set at 335 pounds per square inch. The scattering data were taken in 36 runs, each "run" consisting of continuous operation of the chamber for approximately three hours between changing of rolls of film in the camera. The tracks were measured with the apparatus and procedure already described. As before, only those proton tracks which were distinct, fully in the light beam, wholly inside the chamber, and which originated in the path of the neutron beam across a diameter of the chamber, were considered as valid for data. Most of the tracks appeared uniformly dense along their lengths, with a slight increase in density near their terminal end. The maximum and minimum proton ranges that could correspond to a 12.0 Mev to 13.0 Mev neutron were known from a calculation to be described, and

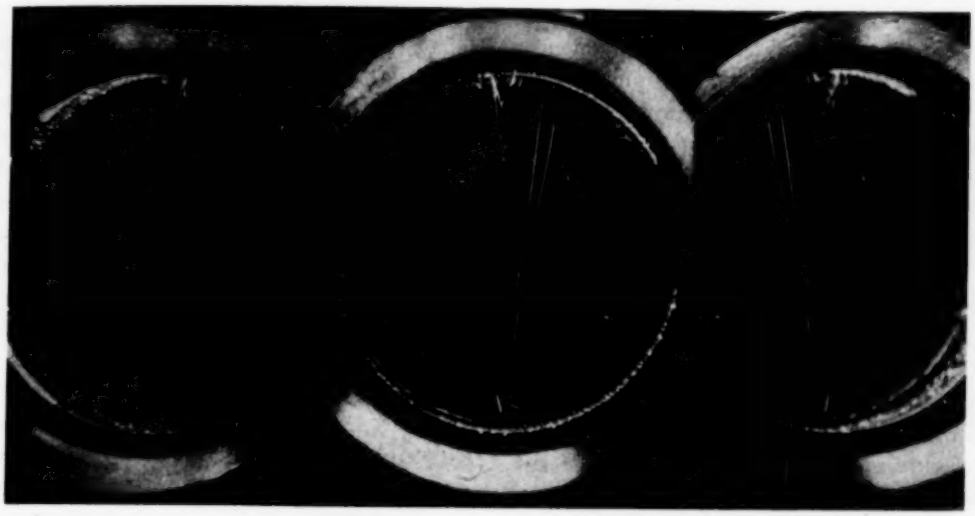

FIG. 4. Recoil protons in the high pressure cloud chamber. The expansion ratio was adjusted to minimize density of the electron tracks.

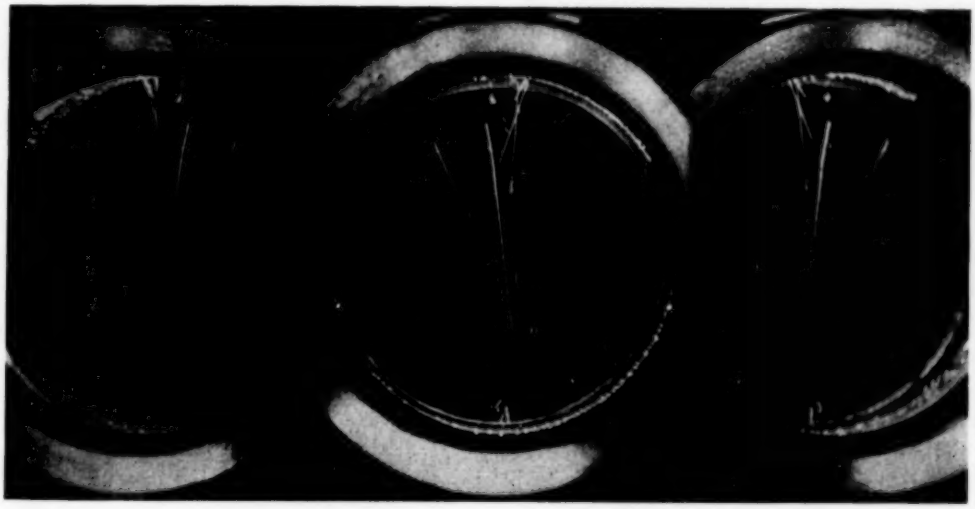

FIG. 5. Recoil protons in the high pressure cloud chamber. The effect of collimation is evident. The less dense tracks are electron tracks.

TABLE I. Cloud chamber stopping power.

Recoil angle interval, degrees	Stopping power Max. pressure	Min. pressure
0–10	19.35	17.30
11–20	19.36	17.31
21–30	19.42	17.40
31–40	19.55	17.50
41–50	19.75	17.65

particular care was exercised to measure all tracks that could possibly fall within this region. Energetically the examined region extended from below 10.5 Mev to above 14.5 Mev, with certainty that no tracks in the pertinent region were missed. Figures 4 and 5 show some pictures of the proton tracks. These pictures show more than one proton track and thus show the effect of collimation of the neutrons. Over 1900 tracks were measured.

Five cases of 3-prong tracks were recorded on the photographs. Energy and momentum conservation considerations required that all of the prongs be proton tracks. These were, therefore, instances in which neutron-proton scattering was followed by proton-proton scattering.

Using the maximum and minimum pressures in the chamber and the stopping power of the gas, the maximum and minimum lengths of the protons recoiled from collisions with neutrons of energy between 12.0 Mev and 13.0 Mev were calculated as a function of recoil angle. The maximum and minimum gauge pressures were 335 pounds per square inch and 298 pounds per square inch, respectively, which correspond to absolute pressures of 23.8 atmospheres and 21.3 atmospheres. For each recoil angle in one-degree intervals the energy of the proton recoils corresponding to 12.0 Mev and 13.0 Mev neutrons and their ranges in air were calculated from the relation $E_p = E_n \cos^2\phi$ and from the range-energy curve. Before this length in air was converted into the track length in the chamber, the variation of the stopping power of methane with proton energy was evaluated from the curves given by Bethe.[13] This variation was small and is more important from the standpoint of consistency rather than accuracy. The median proton energy corresponding to the median recoil angle in each 10° recoil angle interval was taken as the average proton energy for each of these intervals. The length in air corresponding to these proton energies was obtained and the stopping power of methane determined for each length. The chamber stopping power as a function of recoil angle in 10° intervals for maximum and minimum pressure is given in Table I. These maximum and minimum stopping powers, together with the lengths of the recoil proton tracks determined for each recoil angle, yielded the maximum and minimum ranges of a proton projected by a neutron with energy between 12.0 Mev and 13.0 Mev as a function of recoil angle ϕ. These ranges are given in Table II.

The tracks in the data which fell within the range limits corresponding to their measured recoil angle ϕ were tabulated simultaneously in 5° recoil angle intervals and 10° azimuthal angle intervals. This tabulation was also repeated for those tracks which either fell within the range limits corresponding to their measured recoil angle ϕ or also those of the neighboring recoil angles $\phi \pm 1°$. This tabulation was also repeated for larger recoil angle intervals. Though the error in measurement of the recoil angle was as much as $\pm 2°$, since the neutron spectrum was peaked between the 12.0 Mev and 13.0 Mev limits used, the overlapping of the range limits for neighboring recoil angles was apparently

TABLE II. Maximum and minimum proton track length allowed for each recoil angle.

Recoil angle degrees	Track length limits cm	Recoil angle degrees	Track length limits cm	Recoil angle degrees	Track length limits cm
0	8.20–10.55	21	6.35–8.3	41	3.0 –3.9
1	8.2 –10.5	22	6.2 –8.0	42	2.8 –3.6
2	8.1 –10.5	23	6.1 –7.8	43	2.7 –3.4
3	8.1 –10.5	24	5.9 –7.6	44	2.5 –3.2
4	8.00–10.40	25	5.8 –7.4	45	2.4 –3.0
5	8.00–10.4	26	5.6 –7.2	46	2.3 –2.9
6	8.0 –10.4	27	5.4 –7.0	47	2.1 –2.7
7	7.9 –10.3	28	5.3 –6.8	48	2.0 –2.5
8	7.9 –10.3	29	5.1 –6.6	49	1.8 –2.4
9	7.8 –10.15	30	4.9 –6.3	50	1.7 –2.2
10	7.7 –10.0	31	4.7 –6.0	51	1.6 –2.0
11	7.65– 9.9	32	4.5 –5.8	52	1.5 –1.9
12	7.54– 9.75	33	4.3 –5.6	53	1.4 –1.7
13	7.44– 9.6	34	4.15–5.4	54	1.3 –1.6
14	7.28– 9.5	35	4.0 –5.1	55	1.2 –1.5
15	7.19– 9.3	36	3.8 –4.9	56	1.1 –1.4
16	7.08– 9.2	37	3.7 –4.7	57	0.97–1.25
17	6.98– 9.0	38	3.5 –4.5	58	0.87–1.14
18	6.88– 8.9	39	3.3 –4.3	59	0.77–1.0
19	6.67– 8.7	40	3.1 –4.1	60	0.66–0.90
20	6.55– 8.5				

[13] H. A. Bethe, Rev. Mod. Phys. 9, 275 (1937).

sufficient to include most of the tracks whose measured recoil angle had an error of $\pm 2°$. As a consequence, the $\phi \pm 0°$ and $\phi \pm 1°$ scattering angle tabulations differed by small percentages. The 1573 tracks selected with the $\phi \pm 0°$ recoil angle selection criterion are used in this analysis, though essentially similar results are obtained on the basis of the 1636 tracks selected with the less rigorous $\phi \pm 1°$ recoil angle selection criterion. An analysis based on the tracks selected with the less rigorous $\phi \pm 1°$ recoil angle selection criterion was reported earlier.[14]

The total number of tracks measured in 10° recoil angle intervals has been plotted against their ranges in the chamber. These plots are shown in Fig. 6. The total number is the sum of the solid and dashed plots, where the solid lines represent the tracks which fell within the calculated ranges for the measured recoil angle. These are not spectrum plots, since tracks of the same length could correspond to different neutron energies. This is because, as shown in Table II, tracks of different lengths corresponding to the same recoil angle were acceptable. Since the proton energy varies as the squares of the cosine of the scattering angle ϕ, the change in proton energy for a given change in recoil angle will increase as the angle ϕ increases. Also a given change in length will be relatively more important energy-wise at the lower proton energies (larger recoil angle ϕ) since their ranges are shorter. For these reasons, the overlapping of different energies into a single range will increase as the recoil angle increases. However, at the smaller recoil angles the different energies will be more spread apart and the range plot will bear more of a resemblance to a spectrum plot. The plot for the recoil angle interval 0°–10° would therefore represent the spectrum within statistical limitations.

As described above, the experimental data were tabulated according to their azimuthal distribution. Since the neutron-proton scattering process is azimuthally symmetrical, the number in each azimuthal angle interval should be constant if all the tracks were fully within the illuminated region of the cloud chamber. The following factors influence the actual azimuthal distribution:

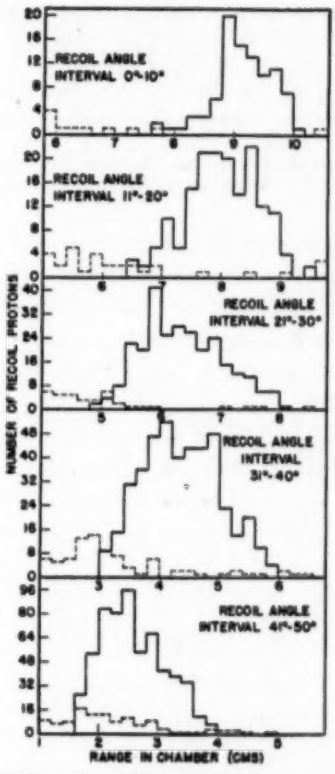
RECOIL ANGLE INTERVAL 0°-10°
RECOIL ANGLE INTERVAL 11°-20°
RECOIL ANGLE INTERVAL 21°-30°
RECOIL ANGLE INTERVAL 31°-40°
RECOIL ANGLE INTERVAL 41°-50°
NUMBER OF RECOIL PROTONS
RANGE IN CHAMBER (CMS)

FIG. 6. Number of recoil protons *vs.* range in the high pressure cloud chamber. The solid plot indicates the number of recoil protons selected by use of the $\phi \pm 0°$ recoil angle selection criterion. The dashed plot shows some of the recoil protons excluded by this criterion. The recoil angle intervals are in the laboratory system.

(a) the finite height of the volume illuminated by the parallel light beam,
(b) the finite diameter of the neutron beam,
(c) the spread of lengths in each recoil angular interval.

The expected azimuthal distribution can be calculated on the basis of purely geometrical considerations. In Fig. 7, $2d$ represents the height of the light beam, while r represents the projection of a recoil in a plane normal to the neutron beam. The quantity r is given numerically by the relation $r = L \sin\phi$. θ' is the largest azimuthal angle at which r is still included in the light beam. Because of the finite size of the neutron beam, a track that starts above center will have less chance of being seen in the upper half but more chance of being seen in the lower half. For such a track the value of θ' above center (θ_a') will be smaller, while the corre-

[14] J. S. Laughlin and P. G. Kruger, Phys. Rev. 71, 736 (1947).

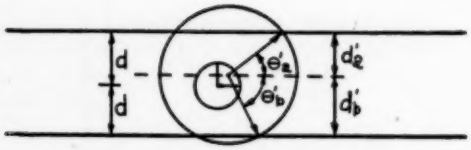

FIG. 7. Geometrical relation between the neutron beam and the illuminated chamber volume.

sponding value of θ' below center (θ_b') will be larger, than if it started at the center. The distribution of neutrons can be considered uniform in the one-half inch diameter circle, so the probability P of the track being illuminated will be determined for one quadrant. If y represents the vertical distance from the center at which the track originates, the remaining distance to the upper and lower edges of the light beam will be $d_a'=d-y$ and $d_b'=d+y$, respectively. The maximum value of y will be $b=\frac{1}{4}$ inch. The expression for P now becomes:

$$P=\left[\int_0^b\int_0^{(b^2-y^2)^{\frac{1}{2}}}\frac{2}{\pi}\sin^{-1}\frac{d-y}{r}dxdy+\int_0^b\int_0^{(b^2-y^2)^{\frac{1}{2}}}\frac{2}{\pi}\sin^{-1}\frac{d+y}{r}dxdy\right]\frac{1}{dxdy}.$$

The quadrant was divided into ten segments and the expression for P integrated numerically. For each 10° recoil angle interval, this calculation has been carried out for the maximum and minimum values of r that occur in that interval. The azimuthal distributions obtained from these values of r should be the extremes, and the experimental azimuthal distribution would be expected to fall between these extremes. The azimuthal distribution was considered in 20° azimuthal angle intervals. Each azimuthal angular interval was weighted according to the probability of a track originating from each quadrant segment being seen in that azimuthal interval, this weight in turn being weighted by the fractional area of the quadrant belonging to that particular segment. These weights were then determined in each 20° azimuthal interval for each segment and added, yielding the relative probability of a track being illuminated in each 20° azimuthal interval. Figure 8 shows the plotted results. The dashed lines represent the calculated extreme azimuthal angle distributions, while the solid line is the experimental distribution. Probable errors, a measure of statistical uncertainty ($0.6745(n)^{\frac{1}{2}}$) are indicated. The data have been "folded over" azimuthally for the experimental plots so that all of the data are represented in the one azimuthal quadrant indicated, e.g., in Fig. 9 in the 0° to 10° recoil angle interval 25 tracks are plotted in the 70° to 90° azimuthal angle interval. This includes tracks from the 70° to 109° and 250° to 289° azimuthal angular intervals.

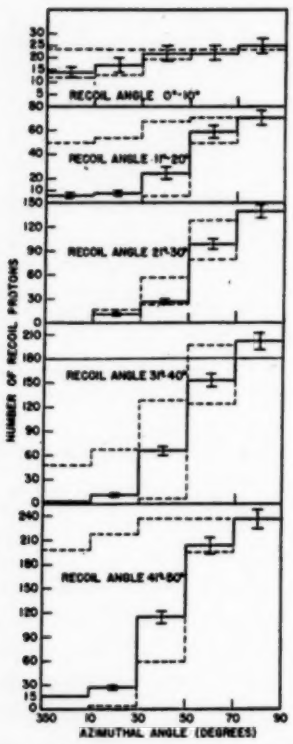

FIG. 8. Azimuthal distribution of the recoil protons. The dashed plots indicate the calculated maximum and minimum limits for the number of recoil protons which could have been observed under the limitation of the cloud chamber geometry relative to the observed number plotted in the solid graph. The number of recoil protons plotted in a given azimuthal angle interval includes all those in the corresponding azimuthal angular interval in all four quadrants of the azimuthal plot. For instance, the number plotted in the azimuthal interval 70° to 90° includes those observed in the intervals 70° to 90°, 90° to 110°, 250° to 270°, and 270° to 290°.

The coincidence of the dashed lines for certain end intervals indicates that all the tracks should have been seen in those azimuthal intervals. Accordingly, the experimental data were normalized to coincide for those intervals. If all the data occurring in the various azimuthal intervals are to be used, an azimuthal correction factor

TABLE III. Experimental data for angular distribution of recoil protons with azimuthal correction factor of unity.

Recoil angle interval in center-of-mass system	Total no. of recoil protons	No. of recoil protons in fully illuminated azimuthal intervals	Length correction factors	Corrected no. of recoil protons	Solid angle of indicated recoil and azimuthal angle intervals	Corrected no. of recoil protons per unit solid angle	Relative no. of recoil protons per unit solid angle
0– 21	93	47*	2.78	131	0.1845	708	1.21±0.12
21– 41	166	71	2.31	164	0.250	656	1.12±0.09
41– 61	277	140	1.84	258	0.378	682	1.17±0.06
61– 81	435	203	1.41	286	0.459	623	1.07±0.05
81–101	593	238	1.19	284	0.485	584	1.00±0.04

* No. of recoil protons in those azimuthal intervals corresponding to 50° to 90°.

would be necessary. However, if the light beam had been sufficiently deep, all tracks would have been illuminated over their full length in all the azimuthal intervals and thus would have been measured. In this case, both the calculated extremes would have been horizontal lines. Therefore, the area under a horizontal line extended across from the end interval represents the number of tracks that would have been seen if no correction were necessary. An azimuthal correction factor would be unnecessary if only those data were used which fell in those azimuthal angular intervals in which all the tracks were fully illuminated. In the final analysis in Table III only these data appearing in these particular end azimuthal zones are employed, and the azimuthal correction factors are consequently unity and do not appear.

The actual experimental azimuthal distribution would be expected to fall between the calculated extreme azimuthal distributions. If the assumptions could be made that the spectrum of the high energy neutron group was completely symmetrical, that the neutrons entered the chamber in uniform numbers throughout the expansion, and that the different track lengths above and below the median track lengths in each recoil angle interval were equally probable, the experimental distribution would be expected to be halfway between the calculated extremes. Though these simplifying assumptions are not necessarily valid, for the purpose of comparison with the results in Table III, the calculated extreme azimuthal distributions are represented in Table IV by correction factors based on the median of the calculated azimuthal distributions. The calculated azimuthal correction factor is the ratio of the area under the horizontal line extended across from the end interval at 90° to 0° to the area under the median of the calculated distribution between azimuthal angles 0° and 90°. An examination of the plots shows that the experimental azimuthal distribution falls within the calculated extremes in a reasonable manner. In the azimuthal angular interval from 0° to 30° in the plot for the 41° to 50° recoil angle interval the experimental points are markedly low. Although great care was taken to measure all pertinent tracks, the most plausible explanation for the low values of these particular experimental points is that some tracks were missed. In the azimuthal positions of the viewing screen in which most of the tracks occurred and were measured, the tracks in this particular azimuthal and recoil angular interval would have the shortest projections of any of the tracks ex-

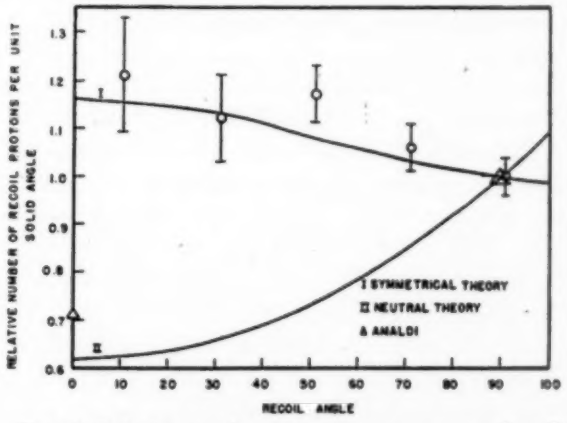

FIG. 9. Relative number of recoil protons per unit solid angle in center-of-mass system normalized to unity at the 90° recoil angle. This indicates a ratio of unity or somewhat greater than unity for backward scattering of neutrons to that at right angles with respect to the incident neutron beam. The angular distributions predicted by a symmetrical type of theory and a neutral type of theory are plotted. A comparison is also made with some of Amaldi's experimental results.

TABLE IV. Experimental data for angular distribution of recoil protons with calculated azimuthal correction factor.

Recoil angle interval in center-of-mass system	Number of recoil protons	Calculated azimuthal correction factor	Length correction factor	Corrected no. of recoil protons	Solid angle of indicated recoil and azimuthal angle interval	Corrected no. of recoil protons per unit solid angle	Relative no. recoil of protons per unit solid angle
0– 21	93	1.12	2.78	290	0.415	698	1.25±0.09
21– 41	166	1.81	2.31	692	1.125	615	1.10±0.06
41– 61	277	2.19	1.84	1115	1.698	658	1.18±0.05
61– 81	435	2.10	1.41	1287	2.083	617	1.11±0.04
81–101	557*	1.22	1.19	810	1.452	557	1.00±0.03

* Does not include recoils in azimuthal angle intervals corresponding to 0° to 30°.

amined. For this reason, the calculated azimuthal correction factor in Table IV for the 81°–101° recoil angle interval (center of mass system) is based on the azimuthal region 30° to 90° and on the corresponding regions in the other three azimuthal quadrants, i.e., 90° to 150°; 210° to 270°; and 270° to 330°.

A length correction factor is necessary since the track length is different for each different recoil angle. The recoil protons have a uniform probability of originating at any point in the neutron beam which is along a diameter of the chamber, However, the distance along this path in which the track can originate and end within the chamber will increase with decreasing track length and increasing recoil angle. The ratio of the diameter of the cloud chamber to that portion of the diameter in which the track can originate and be entirely within the chamber is the length correction factor. The average length of track in each recoil angle interval was calculated, and the ratio then geometrically determined. The length correction factors are listed in Tables III and IV.

The analysis of the data is given in Table III. The first column lists the recoil angle intervals in the center-of-mass system into which the data have been analyzed. The second column gives the total number of proton recoils which satisfied the $\phi \pm 0°$ recoil angle selection criterion. The third column gives the number of recoil protons in those azimuthal angle intervals which were fully illuminated. Unless otherwise noted, these azimuthal intervals were those corresponding to the 70° to 90° interval in the first azimuthal quadrant. The fourth column gives the length correction factors. The fifth column contains the number of recoils after application of the length correction factor. The sixth column gives the solid angle corresponding to the indicated recoil and azimuthal angular intervals. The seventh column gives the number of corrected tracks per unit solid angle. The last column gives the ratio of the number of recoil protons per unit solid angle in the center-of-mass system in the indicated recoil angle interval to the number in the 81° to 101° recoil angle interval. Probable errors, based on the number of tracks in the third column, are also indicated.

In Table IV is an analysis on the basis of the calculated azimuthal correction factors. The second column gives the total number of tracks in the indicated recoil angle intervals. The number of tracks in the 81°–101° interval does not include those between azimuthal angles corresponding to 0° and 30°. The third column contains the calculated azimuthal correction factors based on a median of the calculated extreme distributions. The fourth column contains the length correction factors, and the fifth the corrected number of recoil tracks. The sixth shows the solid angle corresponding to the indicated recoil and azimuthal angle interval. The seventh column shows the corrected number of recoils per unit solid angle. The last column gives the ratios defined above. The general trend of the ratios in Table IV is in agreement with that of Table III. The analysis in Table III is considered more reliable since the azimuthal correction factors have been eliminated.

In Fig. 9 the experimental data of Table III are compared with two theoretical curves. A form of the "symmetrical" theory yields the expression as given by Rarita, Schwinger, and Nye.[15]

[15] William Rarita, Julian Schwinger, and H. A. Nye, Phys. Rev. 59, 209 (1941).

$$\sigma \sim (1-0.080\cos\phi+0.077\cos^2\phi)$$

for the distribution in the center-of-mass system. This distribution is denoted by I in Fig. 9. The "cut-off neutral theory of Bethe[16] as calculated by Kittel and Breit[17] for 16 Mev neutrons gave the expression:

$$\sigma \sim (1+0.46\cos\phi+0.094\cos^2\phi).$$

This distribution is plotted as II in Fig. 9.

[16] H. A. Bethe, Phys. Rev. **57**, 390 (1940).
[17] C. Kittel and G. Breit, Phys. Rev. **56**, 744 (1939).

With regard for the statistical limitations present in these data, it appears that a ratio of the differential cross sections for the scattering of neutrons in the backward direction to the scattering of neutrons in the direction perpendicular to that of the incident neutron beam equal to unity (spherically symmetric scattering), or slightly greater than unity can be consistent with these data. This result favors meson nuclear force theories of the "symmetrical" type and is in disagreement with "neutral" theories or any theory involving ordinary forces only.

PHYSICAL REVIEW VOLUME 73, NUMBER 3 FEBRUARY 1, 1948

Range-Energy Relations for Protons in Substances Containing C, H, O, A, and Xe*,**

J. O. HIRSCHFELDER† AND J. L. MAGEE‡
Los Alamos Scientific Laboratory, Los Alamos, New Mexico

(Received October 6, 1947)

The Bethe theory was used to calculate the stopping power of protons in C, H, O, A, and Xe. The range-energy curves for protons in glycerol tristearate ($C_{57}H_{110}O_6$), paraffin ($(CH_2)_n$), argon, and xenon are presented. The calculations for C, H, and paraffin are carried to 15 Mev, whereas all the others are only given up to 3 Mev.

BETHE'S[1] method can be used to determine the range-energy relations for fast protons passing through various substances. The functional form of the equations is valid provided that the energy is larger than around 0.1 Mev. Actually we have used these equations down to energies of 0.005 Mev in order to calculate the absolute value of the range (even rather large errors in the stopping power over this energy interval do not appreciably effect the value of the range for high energy protons). The method is semi-empirical in the sense that the effective ionization potential for the electrons in the outermost shell is adjusted to fit an experimental value of an alpha particle range. The other constants in the equations are chosen *a priori* from theoretical considerations.

I. THEORETICAL EQUATIONS

The change of energy, E(Mev), with residual range, R(cm), for protons is given by:

$$dE/dR=2\pi e^4(M/m)N(B/E). \quad (1)$$

Here, $M/m=1836.6$, which is the ratio of mass of proton to mass of electron; e is the electronic charge (for our purposes it is convenient to take $e^2=14.397\times10^{-8}$ electron volt cm); and N is the number of atoms per cc. The dimensionless quantity B is called the stopping number. For a gas under standard conditions, Eq. (1) becomes:

$$dE/dR=0.006094B/E. \quad (2)$$

The stopping number is closely related to the atomic stopping cross section (electron volt cm²):

$$\sigma\times10^{15}=0.2392B/E, \quad (3)$$

* This paper is a revision of part of the material contained in the declassified Los Alamos Report LADC-124.

** This document is based on work performed at Los Alamos Scientific Laboratory of the University of California under Government Contract W-7405-eng-36 and the information contained therein will appear in Division V of the National Nuclear Energy Series (Manhattan Project Technical Section) as part of the contribution of the Los Alamos Laboratory.

† Now in the Department of Chemistry, University of Wisconsin.
‡ Now at Argonne National Laboratory.

[1] H. Bethe, *Handbuch der Physik* Vol. 24 Part I, p. 521; M. Livingston and H. Bethe, Rev. Mod. Phys. 9, 263 (1937); J. Ashkin, H. Bethe, and V. Weisskopf, LADC-116 (1943); N. F. Mott and H. S. W. Massey, *The Theory of Atomic Collisions* (Oxford University Press, 1933), p. 224.

in which σ is defined so that

$$dE/dR = N\sigma \times 10^{-6}. \quad (4)$$

According to Bethe's theory, the stopping number can be expressed in form:

$$B = \Sigma_i q_i f_i b_i. \quad (5)$$

Here q_i is the number of electrons in the ith shell; f_i is the effective oscillator strength of an electron in the ith shell. The sum, $\Sigma_i q_i f_i$, is equal to the atomic number if all transitions are effective; we have assumed this to be true.

For electrons in the K shell, Bethe has shown that:

$$b_i = B_K(\eta)/1.81, \qquad \eta \leqslant 1 \quad (6a)$$

$$= (\log_e 3.63\eta) - C_K(1/\eta)/1.81. \qquad \eta \geqslant 1 \quad (6b)$$

Here B_K and C_K are the functions[2] shown in Fig. 1. The parameter η is given by the equation:

$$\eta = \frac{E}{(M/m)I_K'} = \frac{E}{1836.6 I_K'}. \quad (7)$$

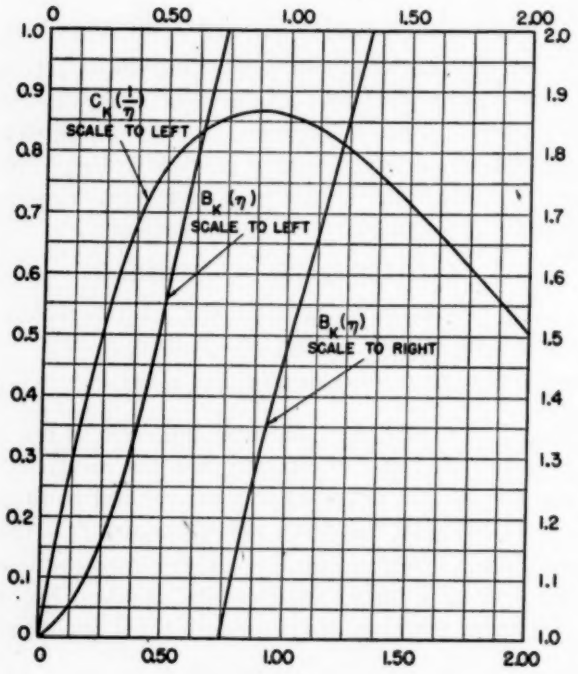

FIG. 1.

[2] The values of $C_K(1/\eta)$ were taken from Fig. 28 in Livingston and Bethe's article (see reference 1). The values of $B_K(\eta)$ for η greater than 0.75 were recalculated to be consistent with the values of $C_K(1/\eta)$.

TABLE I.

	ThC′–RaC′	RaC′–ThC	ThC–Po
$E=(1/8)(E\alpha_1+E\alpha_2)$	2.0570	1.7167	1.4190
$+\frac{dE}{dR}=\frac{(E\alpha_1-E\alpha_2)}{4(R_1-R_2)}$	0.1606	0.1842	0.2107
$B=\frac{E}{0.0060943}\frac{dE}{dR}$	54.21	51.89	49.06
$(B_{\text{calculated}})$	(54.59)	(51.34)	(47.98)

Here I_K' is not the true ionization potential of the electrons in the K shell, but the ionization potential which one would calculate using Slater's screening constants.[3]

$$I_K' = 13.60 Z_{\text{eff}}^2 \times 10^{-6} \text{ (Mev)}. \quad (8)$$

In Eq. (6), one would expect the argument 4η in the logarithm but 3.63η appears instead, because the electrons instead of always being ionized to the lowest continuous state are on the average excited to a state of energy $1.103 I_K'$ above their normal atomic level.

In order to have a complete theory for the stopping number, we would have to derive expressions for b_i for electrons in the L, M, etc. shells. This would be a very difficult task. However, Bethe suggested to us that it would be a good approximation to use the functional form for b_K given in Eq. (6) for b_i in all shells. The argument η is then given in terms of an effective ionization potential I_i', in place of I_K' given by the equation:

$$I_i' = 13.60 Z_{\text{eff}}^2 \times 10^{-6}/n_i^2 \text{ (Mev)}. \quad (9)$$

Here n_i is the effective principal quantum number of the ith shell. By far the biggest contribution to the stopping number comes from the outer shell and the biggest uncertainty in B arises from the exact value of I' taken for the outer shell. It is, therefore, reasonable to adjust the value of I' for the outer shell so that the calculated value of B agrees with some experimental value. This experimental value of B may be taken from the stopping power of α-particles since, at high energies, the α-particles should have the same value of σ as protons of one-fourth the energy. This equality does not

[3] J. Slater, Phys. Rev. 36, 57 (1930).

hold for low energies where the charge on the alpha-particles vary.

The range, R, is calculated by numerical integration of

$$R=\int_0^E (dR/dE)dE, \tag{10}$$

where

$$dR/dE=39.25/\sigma\times 10^{15}. \tag{11}$$

Here dR/dE is calculated at energy intervals of 0.1 Mev and the integral is evaluated numerically. The small value of R corresponding to energies lying between 0.0 and 0.005 Mev are estimated by making the assumption that dR/dE is proportional to $E^{\frac{1}{2}}$ for these energies.

Another quantity of interest is the distance, $\bar{X}$, along the proton path from the point where the energy is E to the ionization centroid.

$$\bar{X}=R-(1/E)\int_0^E RdE. \tag{12}$$

The integration is carried out numerically as in the calculation of the range. If $R=\beta E^{\frac{1}{2}}$, then $\bar{X}=0.6R$. Actually, this relation is very nearly true at high energies.

II. CALCULATIONS FOR ARGON

The calculations for argon proceeded as follows. For the K and L shells we used Slater's[3] screening constants and Honl's[4] oscillator strengths. The average oscillator strength for the electrons in the M shell was chosen so that the sum of all of the oscillator strengths equaled the total number of electrons in the atom. The stopping power of argon for protons can then be expressed in the form:

$$\begin{aligned}B_A=&\frac{1.44}{1.81}B_K(\eta_K)\\&+7.76[\log_e 3.63\eta_L-C_K(1/\eta_L)/1.81]\\&+(18-1.44-7.76)[\log_e 3.63E\\&-\log_e 1836.6I'-C_K(1/\eta_M)/1.81].\end{aligned} \tag{13}$$

Here the only undetermined parameter is I', the effective ionization potential of the electrons in the M shell. It is possible to adjust the value of I' to agree with the experimental measurements of the range of alpha particles in argon. The details of this adjustment require some explanation.

The ranges of different species of α-particles are known for both argon and air. The relative ranges were measured by Harper and Salaman[5] and the absolute value of the (mean) ranges in air and the initial energies were measured by Holloway and Livingston.[6]

TABLE II. Argon range-energy relations.

E Mev	$\sigma\times 10^{15}$ cm^2	R cm	$\bar{X}$ cm	$E dR/dE$
0.005	7.5	0.0523	0.023	0.026150
0.010	12.3	0.0729	0.027	0.031907
0.015	17.1	0.0863	0.028	0.034425
0.02	21.94	0.0964	0.030	0.035776
0.03	29.55	0.1115	0.034	0.039843
0.04	32.96	0.1239	0.037	0.047628
0.05	34.57	0.1355	0.040	0.056765
0.06	35.124	0.1467	0.043	0.067040
0.07	35.033	0.1579	0.047	0.07842
0.08	34.570	0.1692	0.051	0.09082
0.10	33.064	0.1931	0.063	0.11870
0.15	29.072	0.2563	0.095	0.20250
0.20	25.855	0.3280	0.134	0.30358
0.25	22.989	0.4086	0.180	0.42680
0.30	20.834	0.4980	0.232	0.56511
0.4	17.601	0.7039	0.355	0.89192
0.5	15.432	0.94277	0.500	1.2716
0.6	13.833	1.2119	0.663	1.7023
0.7	12.604	1.5096	0.846	2.1797
0.8	11.610	1.8344	1.044	2.7043
0.9	10.792	2.1853	1.260	3.2729
1.0	10.108	2.5614	1.491	3.8827
1.1	9.522	2.9616	1.739	4.5338
1.2	9.011	3.3855	2.000	5.2264
1.3	8.563	3.8325	2.276	5.9582
1.4	8.160	4.3022	2.566	6.7334
1.5	7.807	4.7941	2.871	7.5405
1.6	7.4887	5.3075	3.189	8.3851
1.7	7.1996	5.8421	3.520	9.2669
1.8	6.9345	6.3976	3.865	10.187
1.9	6.6924	6.9738	4.223	11.142
2.0	6.468	7.5705	4.594	12.135
2.1	6.2599	8.1873	4.976	13.166
2.2	6.0675	8.8243	5.373	14.230
2.3	5.8885	9.4809	5.782	15.329
2.4	5.7220	10.157	6.203	16.461
2.5	5.5653	10.853	6.637	17.630
2.6	5.4187	11.567	7.082	18.831
2.7	5.2809	12.301	7.540	20.066
2.8	5.1496	13.054	8.011	21.339
2.9	5.0271	13.825		22.640
3.0	4.9098			23.980

[4] Honl, Zeits. f. Physik. **84**, 14 (1933).

[5] G. I. Harper and E. Salaman, Proc. Roy. Soc. A127, 175 (1930).

[6] M. Holloway and M. Livingston, Phys. Rev. **54**, 18 (1938).

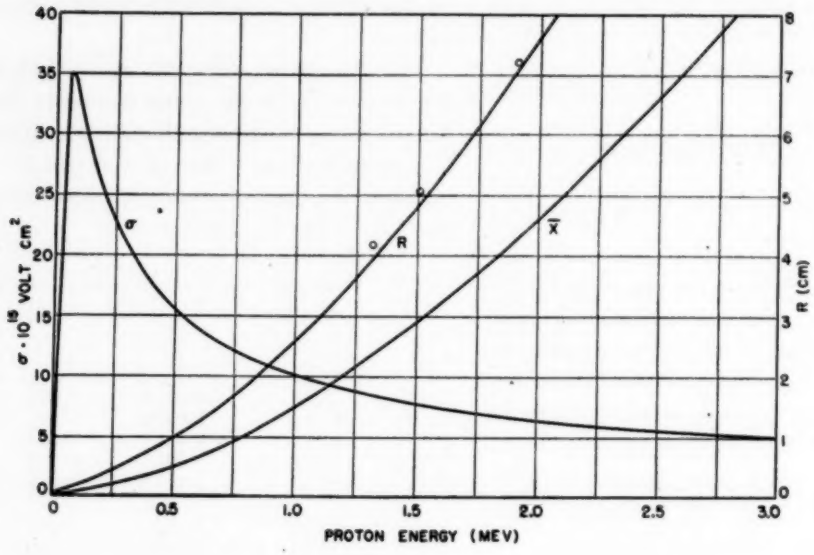

FIG. 2.

ThC′: $E=8.7759$, $R_A=8.570/0.958=8.946$,
RaC′: $E=7.6802$, $R_A=6.907/0.954=7.240$,
ThC: $E=6.0537$, $R_A=4.730/0.940=5.032$,
Po: $E=5.2984$, $R_A=3.842/0.929=4.136$.

These ranges correspond to protons having one-fourth the energy of these α-particles. First, we used pairs of ranges to determine (dE/dR) and attributed this derivative to the mean value of the energy for the pair. The best fit for B_A was obtained by taking $I'=27.06\times10^{-6}$ Mev in Eq. (13) and calculating the values of B given in Table I. The calculated ranges are about 0.25 cm smaller than the α-particle ranges for the same velocity. This corresponds to the fact that α-particles have about 0.25 cm larger range in air than protons of the same velocity. Using this value of I', $\eta_M=E/0.04970$, and we obtain the the following equations for the stopping power of argon:

$E\geqslant 1.0$ Mev,

$$B_A=0.7956B_K(\eta_K)-4.287C_K(1/\eta_L)-4.862C_K(1/\eta_M)+38.131\log_{10}E+46.364. \quad (14a)$$

$0.05\leqslant E\leqslant 1.0$ Mev,

$$B_A=0.7956B_K(\eta_K)+4.287B_K(\eta_L)-4.862C_K(1/\eta_M)+20.263\log_{10}E+37.761. \quad (14b)$$

$E\leqslant 0.05$ Mev,

$$B=0.7956B_K(\eta_K)+4.287B_K(\eta_L)+4.862B_K(\eta_M). \quad (14c)$$

The values of σ, R, and $\bar{X}$ as functions of E are given in Table II and shown in Fig. 2.

TABLE III. Constants in the stopping power equation for xenon.

Shell	Z_{eff}	Ionization potential Mev	η	Oscillator strength* f
1 s	53.70	39.218×10^{-3}	$E/72.028$	0.59
2 sp	49.85	8.449×10^{-3}	$E/15.518$	0.72
3 sp	42.75	2.762×10^{-3}	$E/5.072$	0.80
3 d	32.85	1.631×10^{-3}	$E/2.995$	1.09
4 sp	26.25	0.6845×10^{-3}	$E/1.257$	1.00
4 d	14.85	0.2191×10^{-3}	$E/0.4023$	1.25
5 sp	8.25	$0.01036^*\times10^{-3}$	$E/0.019027$	1.16

* This value was fitted from experimental results of stopping power for alphas in xenon.

III. CALCULATIONS FOR XENON

The constants in the stopping power equation for xenon are given in Table III. Values of Z_{eff} and the ionization potentials have been calculated using Slater's rules.[3]

The measurement of the stopping power of alphas in xenon has not been made very accurately. The several values found in the literature do not agree. It was decided to use Mano's value (Livingston and Bethe, reference 1, p. 272) of 3.76 for the stopping power for 6 Mev alphas in xenon relative to air. This figure determines the ionization potentials for the 5s and 5p electrons.

Thus we obtained for the stopping power of xenon:

$3.0 \geqslant E \geqslant 1.25$,

$$B_{Xe}=0.6519B_K(\eta_1)+3.182B_K(\eta_2)+3.757B_K(\eta_3)+5.525B_K(\eta_4)-4.420C_K(1/\eta_5)-7.182C_K(1/\eta_6)-5.127C_K(1/\eta_7)+69.723\log_{10}E+85.803. \quad (15a)$$

$1.25 \geqslant E \geqslant 0.40$,

$$B_{Xe}=0.6519B_K(\eta_1)+3.182B_K(\eta_2)+3.757B_K(\eta_3)+5.525B_K(\eta_4)+4.420B_K(\eta_5)-7.182C_K(1/\eta_6)-5.127C_K(1/\eta_7)+52.302\log_{10}E+77.319. \quad (15b)$$

$0.40 \geqslant E \geqslant 0.02$,

$$B_{Xe}=0.6519B_K(\eta_1)+3.182B_K(\eta_2)+3.757B_K(\eta_3)+5.525B_K(\eta_4)+4.420B_K(\eta_5)+7.182B_K(\eta_6)-5.127C_K(1/\eta_7)+21.368\log_{10}E+48.730. \quad (15c)$$

$0.02 \geqslant E$,

$$B=0.6519B_K(\eta_1)+3.182B_K(\eta_2)+3.757B_K(\eta_3)+5.525B_K(\eta_4)+4.420B_K(\eta_5)+7.182B_K(\eta_6)+5.127B_K(\eta_7). \quad (15d)$$

The calculated results for xenon are given in Table IV. Curves showing the range and cross sections are given in Fig. 3.

IV. STOPPING POWER OF CARBON

The stopping power of carbon has been calculated by Bethe.[1] His figures give the stopping number relative to air as a function of range. Since we require both the range-energy relationship and the change in energy with range it seemed advisable to make a complete recalculation. Apparently Bethe did not use any experimental data for carbon in his calculation, but instead evaluated the effective ionization potential, I', by extrapolating from the values for nitrogen and oxygen. We made a careful survey of the experimental values for the ranges of α-particles in carbon containing gases and found that they led to relative stopping powers which agree well with Bethe's calculations.

The oscillator strength of the K electrons may be estimated from the Hartree wave function for oxygen in the manner explained by Bethe (Livingston and Bethe, reference 1, p. 265).

$$f_{1s}=1-(1/3)\times 0.15=0.95.$$

Then the stopping number for carbon can be written:

$$B_C=(6-1.90)[\log_e 3.63\eta_L-(1/1.81)C_K(1/\eta_L)]+(1.90/1.81)B_K(\eta_K), \quad (16)$$
$$\eta_K=E/(1836.6\times 441.86\times 10^{-6})=E/0.811520,$$
$$\eta_L=E/(1836.6I_L').$$

The value of I_L' must be adjusted to make B_C

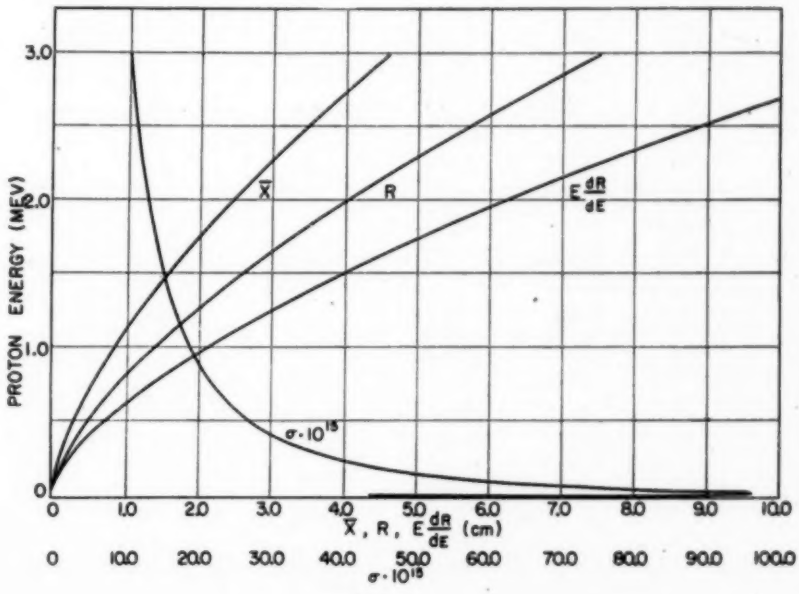

FIG. 3.

agree with experimental data for some value of the energy.

The best sequence of α-particle range measurement was made by Bragg[7] in 1905 and 1906 through use of the ionization method. His data are presented in the first two columns of Table V. Since this work was done at an early date, it is probable that Bragg's source was not good and his measurements of range were probably inaccurate. However, the relative ranges should be insensitive to the purity of the source (provided that the same source is used for all gases) and insensitive to the method of measuring range (provided it is the same for all gases). To get the absolute (extrapolated) ranges, we made use of Holloway and Livingston's results[6]):

$$(R_{air})_{RaC'}=6.953;\quad (R_{air})_{RaA}=4.685,$$
$$(E_\alpha)_{RaC'}=7.6802;\quad (E_\alpha)_{RaA}=5.9981.$$

The stopping numbers were obtained from the difference in the ranges (by the same method that we used in the argon) and these stopping numbers are ascribed to protons having a velocity halfway between the velocity of the RaC' and the RaA α-particles. These values of B are given in Table V.

The stopping number is supposed to be an additive property almost independent of the state of chemical binding. On this account we can use this set of stopping numbers to obtain a number of different estimates of B_C.

$$\left.\begin{aligned} B_{CO_2}-B_{O_2}&=B_C=24.10,\\ B_{CO}-\tfrac{1}{2}B_{O_2}&=B_C=24.17,\\ \tfrac{2}{3}B_{C_2H_2}-\tfrac{1}{3}B_{CH_4}&=B_C=24.32,\end{aligned}\right\} B_C=24.20.$$

$$\left.\begin{aligned} B_{C_2H_4}-B_{CH_4}&=25.39,\\ 2B_{C_2H_6}-3B_{CH_4}&=B_C=26.85,\end{aligned}\right\}$$ Ignore because of difficulty of obtaining pure C_2H_4 and C_2H_6 in 1905 and 1906.

These results show that the stopping number is very nearly additive and that $B_C=24.20$. The stopping power of carbon relative to 1/2(air) is then:

$$B_C/\tfrac{1}{2}B_{air}=0.918, \qquad (17)$$

According to Bethe's calculations (reference 1,

TABLE IV. Xenon range-energy relations.

E Mev	$\sigma\times10^{18}$ cm^2	R cm	$\bar{X}$ cm	EdR/dE
0.005	43.6268	0.00900	0.00409	0.0044979
0.010	75.0735	0.01259	0.00459	0.0052277
0.015	90.8713	0.01490	0.00496	0.0064784
0.02	96.1544	0.01697	0.00552	0.0081632
0.04	90.4829	0.02539	0.00911	0.017350
0.05	84.5617	0.02988	0.01133	0.023206
0.06	79.3856	0.03467	0.01384	0.029662
0.08	70.9833	0.04513	0.01956	0.044231
0.10	63.2072	0.05686	0.02622	0.062091
0.15	51.1904	0.09163	0.04665	0.11500
0.20	44.0168	0.13318	0.07148	0.17832
0.30	35.5828	0.23319	0.13154	0.33087
0.40	30.6465	0.35258	0.20350	0.51224
0.50	27.2376	0.48880	0.28566	0.72045
0.60	24.7589	0.64020	0.37704	0.95106
0.70	22.7846	0.80566	0.47698	1.2058
0.80	21.1880	0.98447	0.58513	1.4818
0.90	19.8589	1.1759	0.70103	1.7786
1.0	18.7458	1.3795	0.82444	2.0936
1.1	17.7874	1.5946	0.95490	2.4270
1.2	16.9314	1.8208	1.0922	2.7815
1.3	16.1795	2.0581	1.2364	3.1534
1.4	15.5181	2.3058	1.3868	3.5406
1.5	14.9227	2.5638	1.5438	3.9450
1.6	14.3839	2.8318	1.7070	4.3656
1.7	13.8931	3.1095	1.8762	4.8023
1.8	13.4476	3.3966	2.0511	5.2531
1.9	13.0239	3.6933	2.2321	5.7255
2.0	12.6331	3.9994	2.4189	6.2132
2.1	12.2705	4.3147	2.6116	6.7166
2.2	11.9311	4.6390	2.8098	7.2367
2.3	11.6212	4.9724	3.0139	7.7673
2.4	11.3341	5.3145	3.2233	8.3102
2.5	11.0644	5.6649	3.4378	8.8678
2.6	10.8071	6.0239	3.6577	9.4419
2.7	10.5592	6.3913	3.8828	10.035
2.8	10.3248	6.7673	4.1135	10.643
2.9	10.1065	7.1515	4.3492	11.261
3.0	9.8972	7.5439	4.5901	11.896

TABLE V. α-particle range and stopping number.

	$(R_{air}/R_{gas})_{RaC'}$	$(R_{air}/R_{gas})_{RaA}$	Stopping Number B for $E=1.710$ Mev
air	1.000	1.000	52.70
O_2	1.064	1.057	56.11
CO	0.985	0.976	52.23
CO_2	1.505	1.488	80.21
CH_4	0.860	0.880	42.73
C_2H_2	1.118	1.121	57.84
C_2H_4	1.349	1.369	68.12
C_2H_6	1.514	1.526	77.52
C_5H_{12}	3.544	3.595	179.13
$C_4H_{10}O$	3.437	3.471	175.27

[7] Bragg, Phil. Mag. 10, 617 (1906); 10, 318 (1905).

p. 274) for a mean range in air of

$$\tfrac{1}{2}(6.953+4.685)=5.819 \text{ cm},$$

this ratio should be 0.924. The agreement is excellent.

Since Bragg's methods were undoubtedly crude compared to modern standards, we examined the more recent work of Mader[8] on air, oxygen, and carbon dioxide.[9] Mader only studies the α-particles from Po, but he effectively measured the ionization as a function of range.

TABLE VI. Glycerol tristearate ($C_{57}H_{110}O_6$) range-energy relations.

E Mev	B_C	B_H	B_O	R' mg/cm²	EdR'/dE mg/cm²
0.005	0.128	0.041	0.046	0.026	0.0128
0.010	0.464	0.146	0.125	0.035	0.0143
0.015	0.968	0.307	0.252	0.041	0.0154
0.02	1.614	0.485	0.437	0.046	0.0167
0.03	2.847	0.817	0.900	0.054	0.0216
0.04	3.941	1.104	1.511	0.061	0.0279
0.05	4.909	1.351	2.240	0.068	0.0350
0.10	8.263	2.178	5.279	0.106	0.0834
0.15	10.36	2.673	7.959	0.151	0.1493
0.20	11.84	3.012	10.038	0.205	0.2321
0.30	13.92	3.472	13.169	0.338	0.4440
0.40	15.47	3.790	15.418	0.501	0.7117
0.50	16.72	4.030	17.172	0.693	1.0318
0.60	17.74	4.222	18.596	0.913	1.4033
0.70	18.68	4.383	19.813	1.160	1.820
0.80	19.46	4.523	20.878	1.433	2.286
0.90	20.18	4.647	21.828	1.731	2.796
1.0	20.83	4.756	22.672	2.054	3.351
1.1	21.43	4.854	23.449	2.401	3.949
1.2	21.98	4.946	24.171	2.772	4.589
1.3	22.49	5.028	24.828	3.166	5.271
1.4	22.96	5.104	25.435	3.583	5.995
1.5	23.40	5.177	26.628	4.022	6.748
1.6	23.81	5.244	27.173	4.483	7.554
1.7	24.20	5.305	27.669	4.966	8.399
1.8	24.57	5.363	28.147	5.471	9.286
1.9	24.92	5.418	28.594	5.998	10.209
2.0	25.25	5.469	29.031	6.546	11.173
2.1	25.57	5.519	29.445	7.115	12.177
2.2	25.87	5.566	29.842	7.705	13.216
2.3	26.16	5.611	30.216	8.317	14.295
2.4	26.45	5.654	30.579	8.948	15.410
2.5	26.71	5.695	30.928	9.601	16.565
2.6	26.96	5.735	31.259	10.274	17.760
2.7	27.21	5.773	31.584	10.967	18.989
2.8	27.45	5.811	31.891	11.680	20.256
2.9	27.68	5.847	32.197	12.414	21.558
3.0	27.90	5.882	32.482	13.167	22.897

TABLE VII. Paraffin $(CH_2)_n$ range-energy relation.

E Mev	B_C	B_H	R' mg/cm²
0.005	0.12790	0.04088	0.02322
0.010	0.46420	0.14586	0.03197
0.015	0.96813	0.30663	0.03732
0.02	1.6135	0.48509	0.04143
0.03	2.8467	0.81714	0.04824
0.04	3.9409	1.1043	0.05462
0.05	4.9086	1.3513	0.06096
0.10	8.2625	2.1775	0.09613
0.15	10.364	2.6731	0.13860
0.2	11.839	3.0121	0.18908
0.3	13.916	3.4722	0.31370
0.4	15.467	3.7898	0.46833
0.5	16.719	4.0295	0.65115
0.6	17.744	4.2218	0.86101
0.7	18.683	4.3825	1.09677
0.8	19.459	4.5233	1.35759
0.9	20.181	4.6471	1.64291
1.0	20.832	4.7564	1.95202
1.1	21.430	4.8544	2.28446
1.2	21.977	4.9464	2.63976
1.3	22.486	5.0281	3.01756
1.4	22.964	5.1044	3.41751
1.5	23.403	5.1767	3.83930
1.6	23.813	5.2435	4.28273
1.7	24.201	5.3052	4.74757
1.8	24.565	5.3629	5.23363
1.9	24.922	5.4176	5.74061
2.0	25.253	5.4694	6.26829
2.1	25.566	5.5187	6.81661
2.2	25.873	5.5658	7.38533
2.3	26.162	5.6108	7.97427
2.4	26.445	5.6539	8.58326
2.5	26.711	5.6953	9.21214
2.6	26.963	5.7351	9.86087
2.7	27.211	5.7734	10.52932
2.8	27.446	5.8108	11.21735
2.9	27.676	5.8470	11.92483
3.0	27.898	5.8820	12.65163
3.5	28.907	6.0528	16.57086
4.0	29.758	6.1863	20.95967
4.5	30.513	6.3041	25.81139
5.0	31.183	6.4094	31.11793
5.5	31.789	6.5048	36.87259
6.0	32.336	6.5918	43.06963
6.5	32.840	6.6718	49.70417
7.0	33.313	6.7459	56.77056
7.5	33.746	6.8149	64.26439
8.0	34.154	6.8794	72.18204
8.5	34.531	6.9401	80.52013
9.0	34.895	6.9972	89.27502
10.0	35.551	7.1026	108.0222
11.0	36.141	7.1979	128.4035
12.0	36.676	7.2849	150.4002
13.0	37.169	7.3650	173.9955
14.0	37.627	7.4391	199.1717
15.0	38.054	7.5081	225.9125

[8] M. Mader, Zeits. f. Physik **77**, 601 (1932).

[9] The authors appreciate the help of Dr. M. Holloway in the interpretation of Mader's results.

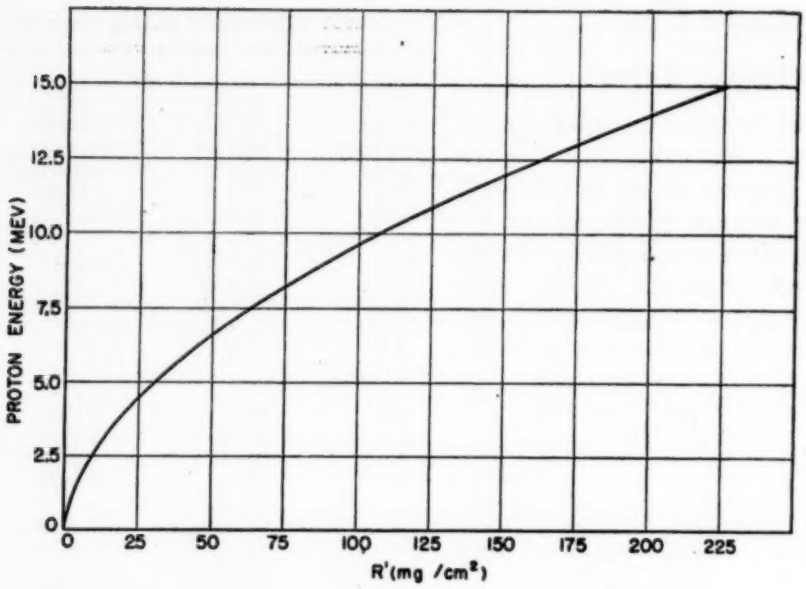

FIG. 4.

As closely as we could tell from his graphs,

$$(dE/dR)_{CO_2}/\tfrac{1}{2}(dE/dR)_{air} = 3.18 - B_{CO_2}/(\tfrac{1}{2}B_{air}), \quad (18)$$

$$(dE/dR)_{O_2}/\tfrac{1}{2}(dE/dR)_{air} = 2.28 - B_{O_2}/(\tfrac{1}{2}B_{air}). \quad (19)$$

So that

$$B_C/(\tfrac{1}{2}B_{air}) = 3.18 - 2.28 = 0.90. \quad (20)$$

The range Po α-particles in air is 3.870 for which Bethe gives $B_C/(\frac{1}{2}B_{air}) = 0.928$. This difference is within the accuracy of our interpretation of Mader's results.

We were unable to find any other experimental data which would have a bearing on the stopping power of carbon. Thus we decided to adjust I' to fit Bethe's value of $B_C/(\frac{1}{2}B_{air}) = 0.924$, i.e., $B_C = 24.33$, for $E = 1.710$ Mev. This gives $I' = 18.72 \times 10^{-6}$ Mev and the equation for B_C becomes:

$E \gtrsim 0.8$,

$$B_C = 9.4406 \log_{10}(E/0.0094704) - 2.2652 C_K(1/\eta_L) + 4.3749 \log_{10}(E/0.22356) - 1.0497 C_K(1/\eta_K). \quad (21a)$$

$0.03 \lesssim E \lesssim 0.8$,

$$B_C = 0.4406 \log_{10}(E/0.0094704) - 2.2652 C_K(1/\eta_L) + 1.0497 B_K(\eta_K). \quad (21b)$$

$E \lesssim 0.03$,

$$B_C = 2.2652 B_K(\eta_L) + 1.0497 B_K(\eta_K). \quad (21c)$$

In the above,

$$\eta_K = E/0.811520, \quad \eta_L = E/0.034378.$$

The value of B_C are given in Table VI.

V. STOPPING POWER OF OXYGEN

The stopping power of oxygen has been calculated by Ashkin (La-12-R) for low energies. We required the values for high energies and decided to make a complete recalculation.

Since Livingston and Bethe[1] give the oscillator strength for oxygen: $f_{1s} = 0.905$, we can write down the equation for the stopping number of oxygen:

$$B_O = 6.19[\log_e 3.63\eta_L - C_K(1/\eta_L)/1.81] + 1.81 \log_e \eta_K - C_K(1/\eta_K). \quad (22)$$

Here,

$$\eta_L = E/(1836.6I'), \quad \eta_K = E/(1836.6I_K') = E/1.4809.$$

Joliot-Curie[10] has prepared a table of the stopping powers of oxygen relative to air as a function of velocity. For $V = 2.0 \times 10^9$ cm/sec.

[10] Joliot-Curie, *Tables Annuelles* (1938), Vol. 26, Section 44, p. 19.

corresponding to a proton energy of 2.095 Mev:

$$\frac{(dE/dR)_{O_2}}{(dE/dR)_{air}}=\frac{B_{O_2}}{B_{air}}=1.065. \quad (23)$$

Or making use of the stopping numbers for air obtained from Holloway and Livingston's measurements:

$$B_O=\tfrac{1}{2}B_{O_2}=1.065\times(56.04/2)=29.44. \quad (24)$$

From this, it follows that our value of I' should equal 47.2 ev.

The equation for the stopping number for oxygen is then:

$E\geqslant 1.5$ Mev,

$$B_O=18.421\log_{10}E-3.4199C_K(1/\eta_L)-C_K(1/\eta_K)+24.741. \quad (25a)$$

$0.09\leqslant E\leqslant 1.6$ Mev,

$$B_O=14.253\log_{10}E-3.4199C_K(1/\eta_L)+B_K(\eta_K)+22.496. \quad (25b)$$

$E\leqslant 0.09$ Mev,

$$B_O=3.4199B_K(\eta_L)+B_K(\eta_K). \quad (25c)$$

The values of B_O are given in Table VI where

$$\eta_K=E/1.4809, \quad \eta_L=E/0.09036.$$

VI. STOPPING POWER OF HYDROGEN

The calculation of the stopping power of hydrogen does not offer any particular difficulties.

$$B_H=\log_e 3.63\eta-(1/1.81)C_K(1/\eta), \quad (26)$$

where

$$\eta=E/(1836.6I').$$

The value of I' is adjusted to fit the experimental data.

Joliot-Curie[10] has prepared a table of the stopping power of hydrogen relative to air as a function of velocity. For $V=2.0\times10^9$ cm/sec. corresponding to a proton energy of 2.095 Mev,

$$B_{H_2}/B_{air}=0.1971.$$

On making use of the value of B_{air} obtained from Holloway and Livingston's[6] measurements,

$$B_H=\tfrac{1}{2}B_{H_2}=0.1971\times56.04/2=5.52.$$

From this it follows that $I'=16.26$ ev and $\eta=E/0.029863$.

$E\geqslant 0.03$ Mev,

$$B_H=2.30259\log_{10}E-0.55248C_K(1/\eta)+4.800. \quad (27a)$$

$E\leqslant 0.03$ Mev,

$$B_H=(E/1.81)B_K(\eta). \quad (27b)$$

The values of B_H are given in Table VI.

VII. RANGE OF PROTONS IN GLYCEROL TRISTEARATE ($C_{57}H_{110}O_6$)

The range of protons in glycerol tristearate is easy to calculate from the stopping numbers of carbon, hydrogen, and oxygen (B_C, B_H, and B_O). Since the stopping numbers are supposed to be additive, the stopping number B_p, for glycerol tristearate, is:

$$B_p=57B_C+110B_H+6B_O. \quad (28)$$

If R' is the range expressed in milligrams of glycerol tristearate per cm^2, the energy loss Eq. (2) becomes:

$$dE/dR'=1.616\times10^{-4}B_p/E. \quad (29)$$

The range is then found by integration and the results are shown in Table VI.

VIII. RANGE OF PROTON IN PARAFFIN, $(CH_2)N$

The range of proton in paraffin was calculated in the same manner as for glycerol tristearate. Here

$$B_p=B_C+2B_H, \quad (30)$$

and

$$dE/dR'=0.010271B_p/E. \quad (31)$$

Here R' is the range of the protons in milligrams of paraffin per cm^2 and E is the proton energy in Mev. The rest of the calculations proceed as in the case of the glycerol tristearate. The results are shown in Table VII and Fig. 4.

Momentum Conservation in the Beta-Decay of P^{32} and the Angular Correlation of Neutrinos with Electrons

CHALMERS W. SHERWIN
University of Illinois, Urbana, Illinois
(Received October 27, 1947)

It is possible, by evaporation of carrier free P^{32}, to produce what appear to be monolayer beta-active sources. These sources maintain their characteristics for several hours in a good vacuum. The momentum of the recoil ion is measured by timing its flight in a field-free space. Recoil momentum spectra are observed at 180°, 135°, 90°, and 45° with respect to the electrons. It is shown that (a) momentum is not conserved between the electron and the recoil nucleus, (b) the experimental data are in disagreement with any hypothesis in which the neutrino and the electron are most probably emitted in the same hemisphere, (c) for recoil ions above about 25 ev energy, the observed recoil momentum spectra agree rather well with those spectra calculated on the assumption of a $(1-\beta\cos\theta)$ neutrino-electron angular correlation function, and (d) below 25 ev too many recoils are observed compared to any neutrino theory which gives agreement for high momentum recoils. Since the reason for the disagreement below 25 ev is not understood, the selection of the $(1-\beta\cos\theta)$ function must be regarded as tentative.

I. INTRODUCTION

IT has been known for a long time that energy is not conserved in beta-decay if only the beta-particle and the nucleus are considered. A number of experiments have been performed to see if momentum is also not conserved between the beta-particle and the recoil nucleus. Leipunski,[1] Crane and Halpern,[2] Allen,[3] Jacobsen,[4] Wright,[5] and Fowler, Lauritsen *et al.*[6] all report with different degrees of certainty that momentum is in fact not conserved between the beta-particle and the nucleus. A point of particular interest in momentum measurements is whether the experimental results can be interpreted by assuming the existence of a neutrino whose direction has some definite angular correlation with the direction of the beta-particle. The various formulations of Fermi's beta-decay theory[7] predict different angular correlations between the beta-particle and the neutrino.

The experiments referred to above are about equally divided between employing a radioactive gas, or using a thin radioactive deposit on a surface as the source of the beta-particles and the recoils. It is now possible to obtain carrier free, radioactive P^{32} from Clinton Laboratories. This material is so free from even inert contamination (0.6 to 3 milligrams of non-volatile matter per millicurie) that it greatly increases the possibility of forming a true monolayer surface. If a monolayer, or less, can be formed by evaporation in a high vacuum, for example, one might hope that the most serious difficulty encountered in the use of the thin surface radioactive source, namely, scattering and energy loss of the recoils at the surface, can be greatly reduced.

II. THE PRINCIPLE OF THE EXPERIMENTAL METHOD

The principle involved in the experiments about to be described is to measure the momentum of the recoil nucleus by measuring its time of flight in a field-free space. Zero time is taken to be the time at which an electron, going in a selected direction, is detected. An electron multiplier detects the recoil nucleus, also going in some selected direction, at a later time. Since the mass of the recoil nucleus is known, it is possible to calculate the magnitude of its momentum from its measured time of flight. It presumably escapes from the monolayer source with small change of either energy or momentum. A cathode-ray tube displays a horizontal sweep starting whenever an electron is detected. The recoil nucleus, when detected, causes a vertical deflection which can be recorded either visually or photographically. The cathode-ray tube display permits a wide range of the recoil momen-

[1] A. I. Leipunski, Proc. Camb. Phil. Soc. **32**, 301 (1936).
[2] H. R. Crane and J. Halpern, Phys. Rev. **53**, 789 (1938); **56**, 232 (1939).
[3] J. S. Allen, Phys. Rev. **61**, 689 (1942).
[4] J. C. Jacobsen and O. Kofoed-Hansen, Mat. Fys. Medd. **23**, Nr. 12 (1945).
[5] B. T. Wright, Phys. Rev. **71**, 839 (1947).
[6] R. F. Christy, E. R. Cohen, W. A. Fowler, C. C. Lauritsen, and T. Lauritsen, Phys. Rev. **72**, 698 (1947).
[7] D. R. Hamilton, Phys. Rev. **71**, 456 (1947).

tum spectrum to be measured at one time. This is important because of the limited time (about 2 hours) that the monolayer surface maintains its characteristics.

Only charged recoil atoms can be given acceleration so that they will produce secondary electrons on the first dynode of the electron multiplier. Therefore an electron emitter, P^{32}, was chosen as the radioactive material. It is also free from any gamma-rays whose momenta can complicate matters. The singly-charged positive recoil ion, S^{32}, has a first ionization potential of 10.3 volts. It is necessary to use a surface whose work function is the order of 10 volts as the base upon which the P^{32} is evaporated so the positive S^{32} ions have a chance to escape without first being neutralized.

Since the recoil atoms are charged, care must be taken to give them a field-free space in which to travel before they are detected. Otherwise their direction and energy will be completely altered.

P^{32} has a calculated maximum recoil energy of 78-electron volts. It is hoped that surface binding energy will not seriously affect at least the higher momentum recoils. Barton[8] found that an appreciable fraction of RaE recoils, whose energy is the order of 1 ev, were able to escape from a surface.

III. DESCRIPTION OF THE APPARATUS

Figure 1 shows the measuring chamber used in the experiments. A thin mica sheet, S (1 to 1.5 mg/cm^2), has on it the evaporated radioactive surface. The total activity is usually about 1 to 3×10^4 electron per second. The size of the surface is about 1 cm by 0.6 cm. This surface is prepared in an adjoining evaporation chamber, as shown in Fig. 2. The details of the preparation of the surface will be discussed in the next section.

After its formation the surface S is moved to the measuring chamber through the magnetically operated valve, C. Both chambers are maintained by separate pumps at a pressure between 1 and 3 times 10^{-7} mm of Hg, so that from the time of its formation, the surface is in a vacuum.

The inside of the measurement chamber is covered with a grounded beryllium film. There is a grounded grid in front of the electron multiplier made of 0.0025-cm tungsten wire knitted into a mesh with an average hole size of about 0.06 cm. This permits about 80 percent transmission. The Geiger counter ports, Fig. 1, are also protected by a similar grounded grid. Thus no external field can penetrate the space surrounding the source.

The electron multiplier is a 12-stage, beryllium-coated unit following the design of J. S. Allen.[9] It is outgassed by induction heating after each exposure to air to obtain maximum gain (50,000 to 100,000). It is followed by feed-back amplifiers with a total voltage gain of about 10^6, and a rise time of 0.1 microsecond.

The cathode-ray tube sweep, which starts upon the detection of the electron in the Geiger counter, is 15 microseconds long. It is calibrated by a one megacycle shock-excited oscillator. An edge lighted scale marked in one-half microsecond divisions is used to read the time of occurrence of the pulses from the recoil ions. The source is usually weak enough so that the recoils come at a convenient rate for recording by visual observation. The slight persistance of the type P1 screen aids greatly in this. The fact that results on a given source can be reproduced to within limits set by statistics indicated that this method of data collection does not contribute greatly to the error. When stronger sources with the necessary monolayer characteristics can

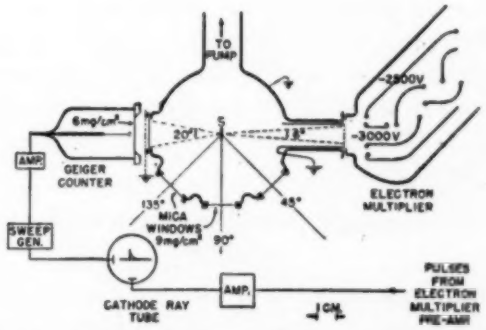

FIG. 1. Horizontal cross section of the measurement chamber. The monolayer P^{32} source is on S, facing the electron multiplier which detects the positive (sulfur) recoil ions. The electrons are detected by the Geiger counter which can be placed in front of any one of the four mica windows. Measurement of the time of flight of each recoil ion permits a calculation of its momentum. The field-free path of the recoil ions is 6.5 cm.

[8] A. W. Barton, Phil. Mag. 1, 835 (1926).

[9] J. S. Allen, Rev. Sci. Inst. 12, 582 (1941).

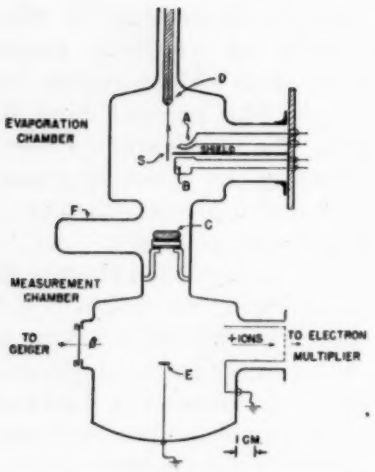

FIG. 2. Vertical cross section of the complete vacuum system. The source S can be raised, lowered, or rotated by the rod D which is magnetically controlled. S is first coated with LiF (or SiO_2) evaporated from a platinum filament A (or a tungsten coil at A). It is then lowered and coated with P^{32} from the platinum filament B. Gate C is opened magnetically, and S is lowered to E where it rests while observations are made.

be formed, a recording camera will be used to collect the data.

The mica windows fastened on with Dennison's American Express No. 2 red wax. A glass ring on the outside of the mica is also waxed to the mica, thus holding it from both sides. A copper washer with the edges rounded is placed in between the mica and the ground-glass port on the vacuum system. The rounded edges reduce danger of cracking in the mica as it bows inward under the pressure of the atmosphere.

Typical sets of data collected with this apparatus are shown in Fig. 3, and the momentum spectra of these recoils are shown in curves A of Fig. 4. The significance of this data will be discussed in a later section.

IV. PREPARATION OF THE MONOLAYER SOURCE

The production of a true monolayer source which causes a minimum of scattering of both electrons and recoil ions is the most critical part of this type of experiment. In previous experiments the thin radioactive sources used have probably not been monolayers. It might be expected that the evidence of energy loss and scattering of recoils present in these previous experiments, notably Allen's,[3] would be missing when large quantities of high activity carrier-free materials are available to form true monolayers. Proof that monolayer sources were actually formed in the experiments reported here is mostly indirect. It is deduced from the appearance of the recoil momentum spectra. However, the contamination of the radioactive material before evaporation was so low that a further purification during evaporation of a factor of 10 to 100 will produce monolayers of adequate activity.

First, a mica sheet (1 to 1.5 mg/cm^2) is coated in an auxillary vacuum system with a thin beryllium layer. In operation, this layer is grounded. The reason for this is to remove the effects resulting from electrostatic charge caused by the electrons leaving the radioactive surface. Some early measurements were in error because of this electrostatic charge. The mica plus beryllium surface is then placed in the evaporation chamber, Fig. 2, where it is further processed.

Since the sulfur recoil atoms have a first ionization potential of 10.3 volts, and since their velocities are low (order of 10^6 cm/sec.), they have small probability of escaping in a charged condition from a surface unless the work function of that surface is in the neighborhood of 10 volts. No metals have this high work function, and no charged recoils were observed to come from surfaces of Al, Be, and W, for example. A search was made for easily evaporated insulators which might have the electrons of the surface atoms strongly enough bound so that the recoil ions could escape charged. Freshly evaporated surfaces of SiO_2, LiF, and NaF were found to permit a measurable number, probably less than 10 percent, of the recoil ions to escape charged. Therefore in the evaporation chamber, Fig. 2, the first step is to evaporate an insulating film, a few wave-lengths of light in thickness, on top of the beryllium surface of S. A shield prevents this evaporating material from contaminating the platinum filament, B, on which some P^{32} is deposited.

The method of preparing the radioactive deposit on filament B, Fig. 2, will now be described. The P^{32} is obtained from the Clinton Laboratories in a pH 7.5 solution containing 10 millicuries of phosphorus in the form of $NaHPO_4$.

The non-volatile matter varied from 0.6 mg/mc up to 2 or 3 mg/mc. The nature of this non-volatile matter was unknown in all cases, and it appeared to vary from shipment to shipment since the evaporation characteristics of the P^{32} were quite different in different shipments.

To the original radioactive solution HCl is added until the pH is 3 or 4. Then 25 micrograms of $FeCl_3$ in solution is added, followed by the addition of NH_4OH. The solution is heated, to aid coagulation, and centrifuged. Usually, about 70 percent of the activity goes with the precipitate. This is washed and dissolved in 0.1 N HCl. Sometimes the material is re-precipitated several times without the addition of more $FeCl_3$. The phosphorus is presumably in the form of iron phosphate.

The next step is to calibrate the evaporation characteristics of the iron phosphate solution from the center of a standard platinum filament, 0.002 inch thick, 0.082 inch wide, and about 1.5 inch long. This calibration is done in terms of the current through the filament so that the temperature conditions can be easily and accurately reproduced.

About 0.1 millicurie of solution is evaporated to dryness in air on a clean platinum filament. This filament has been cleaned by previous heating in a vacuum to just below the melting point. The loaded filament is placed in an auxillary vacuum system having a mica window in front of the active deposit on the filament. A Geiger counter measures the activity of the filament as a function of the heat treatment. A magnetically operated shutter prevents the radioactive material from depositing on the mica window during evaporation. In the best case, 80 percent of the original activity of the filament disappeared after two or three minutes heating in the temperature range of 1000°C to 1120°C. Usually it required a temperature range of 750°C to 1180°C. Measurements on different filaments loaded with radioactive P^{32} from a given solution showed very reproducible evaporation characteristics.

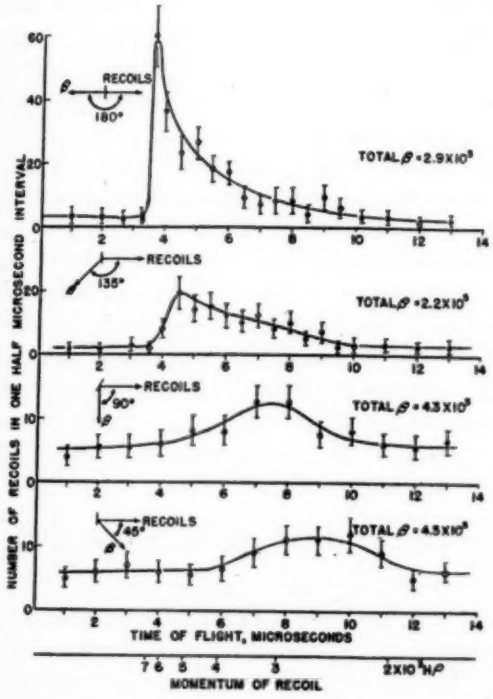

FIG. 3. Typical time of flight diagrams for the recoil ions from P^{32}. The radioactive source has a foundation layer of LiF upon which the thin layer of P^{32} is deposited by a double evaporation process. The recoil-momentum spectra, corresponding to these diagrams, are shown in curves *A* of Fig. 4. The geometry of the detection system is shown in Fig. 1. "Total β" means the total number of electrons detected while the data were being collected.

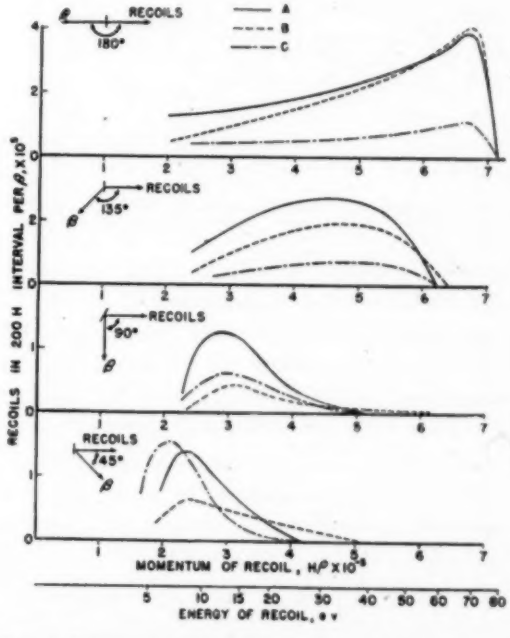

FIG. 4. Some momentum spectra of recoil ions from P^{32}. For *A*, the base surface is LiF with the P^{32} deposited by a double evaporation process. For *B*, the base surface is LiF with the P^{32} deposited by a single evaporation. For *C*, the base is SiO_2, with the P^{32} deposited by a single evaporation. *Note:* The symbol ρ should follow the letter H in the label of the abscissa.

Once the evaporation characteristics of a given solution of P^{32} is known, the filament, B, in Fig. 2 is loaded with about 0.1 mc, and the filament (or coil) at A is charged with the insulator to be used to form the base surface. When the pressure is low enough (2×10^{-7} mm of Hg), the insulator is evaporated on to the surface S. With S protected by the shield, filament B is heated in exactly the same sequence as the test sample. At the selected point in the evaporation curve, the surface S is lowered so it is exposed to B. B is then heated to some higher temperature for about 30 or 40 seconds, and then turned off. When a single evaporation process is performed in the manner described, it is usually necessary to make several trials to find the region on the evaporation characteristic curve which gives good sources.

After the evaporation process is completed, the surface S is lowered into the measurement chamber, a process which takes about one minute. It takes several more minutes to collect enough data to determine the general characteristics of the recoil spectrum, but there is no evidence of any change in the recoil spectrum for a period of one or two hours providing the pressure is 1 or 2 times 10^{-7} mm of Hg. The ground-glass gate, C, can be left open after the evaporation process is completed without contaminating the measurement chamber. No radioactivity is found in the liquid air cooled traps on the pumps.

When the evaporation curve has poor characteristics, i.e., wide temperature range necessary to cause the majority of activity to disappear, a double evaporation process is used. A clean platinum filament is used in an auxillary vacuum system as a "catcher." It intercepts the evaporating radioactive material from a heated filament. The "catcher" is exposed only during the most favorable evaporation region of the heated filament (1000°C to 1200°C). The "catcher" has no visible deposit. Not even interference fringes are visible. It has an activity of about 1/20 or 1/40 millicurie. The evaporation characteristics of the "catcher" are now measured in the auxiliary system. It is found that 80 percent of the activity disappears at a much lower temperature (between 640°C and 940°C) than was the case for the original material. This probably means that the P^{32} deposit on the "catcher" has a different chemical form than it had before the first evaporation. A freshly prepared "catcher" is placed in the regular evaporation chamber, Fig. 2. It is found to give good and consistent results in preparing what appear to be monolayer sources on the surface S if S is exposed during the favorable evaporation region (640°C to 900°C) of the "catcher."

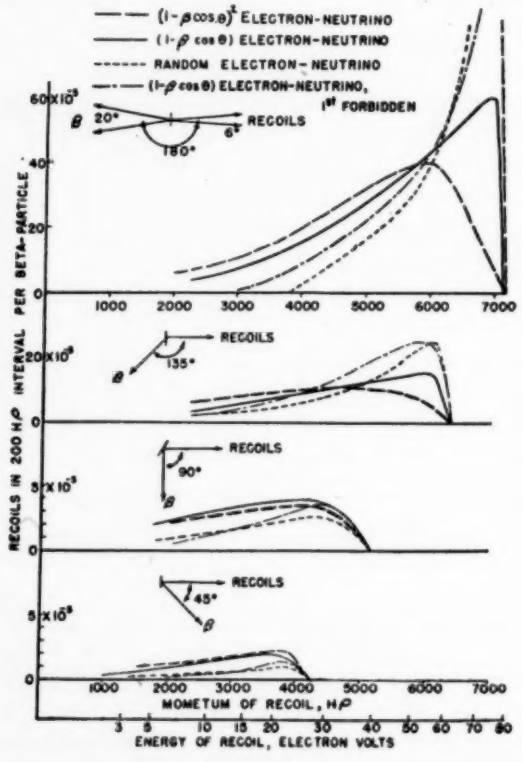

FIG. 5. Theoretical recoil momentum spectra based on the neutrino hypothesis. The geometry of the detection system is shown in Fig. 1. The 180° random neutrino peak is at 360×10^{-6} and the $(1-\beta\cos\theta)$ first forbidden peak is at 135×10^{-6}.

V. DESCRIPTION OF SOME TYPICAL DATA

Figure 3 shows a typical set of time of flight data. The data was collected in time intervals ranging from $\frac{1}{4}$ microsecond to one microsecond, but in the diagram all points are normalized to the number in a $\frac{1}{2}$-microsecond interval. Short time of flight corresponds to high momentum, as can be seen from the momentum scale in Fig. 3. The total number of beta-particles detected during the observation time for each curve is noted on the diagrams. Observation

time per curve varied from about 15 to 45 minutes.

The pulses observed from 0 to 3.5 microseconds are the random background. These pulses are partly due to recoils unrelated to the particular electron which started the sweep, and partly due to electrons. The electron multiplier is about 5 or 10 percent as efficient as a Geiger counter for P^{32} electrons.

It is a straightforward calculation to change the time of flight diagram of Fig. 3 into the momentum diagram, curve *A*, Fig. 4. The non-linear relation between time of flight and momentum makes the sharp peak of the 180° case in Fig. 3 to be greatly attenuated in Fig. 4. The momentum diagrams are plotted in terms of recoils in a $200H\rho$ interval per electron. This is the form in which the theoretical momentum diagrams, based on the assumption of the existence of the neutrino, are presented in Fig. 5.

The delays in the measuring system are small and constant. After the recoil passes the grid in front of the electron multiplier, it is calculated that the ions take a nearly constant time of 0.46 microsecond to be accelerated and to reach the sensitive region of the first dynode. From there on, the pulse from the ion is delayed only by the amplifier which has a rise time of about 0.1 microsecond and a voltage gain of about 10^6.

Delays in the Geiger counter have been measured,[10] and found to be the order of 0.1 microsecond.

When data are collected in tenth microsecond intervals, a number of recoils are observed to have the maximum energy of 78 ev, which corresponds to a 3.5-microsecond time of flight. This maximum energy is calculated from the known maximum electron momentum of $7200H\rho$. The experimental error in this measurement is estimated at ± 0.2 microsecond, or ± 8 ev. Recoils are observed out to 14 microseconds, corresponding to an energy of 5 ev.

VI. A DISCUSSION OF SOME ERRORS

Some consideration will now be given to the sources of errors which can affect the shape of the recoil momentum spectra.

It has been assumed up to now that the observed delayed pulses are really due to mass

[10] C. W. Sherwin, Phys. Rev. **71**, 479 (1947).

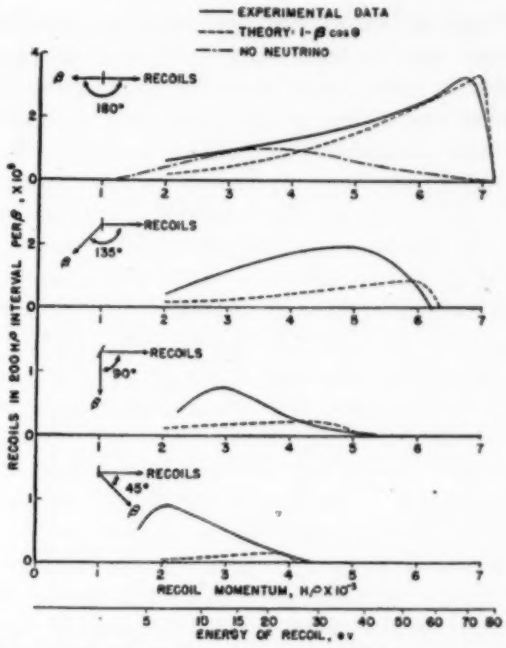

FIG. 6. Comparison of experimental data with the $(1-\beta\cos\theta)$. neutrino hypothesis. This neutrino-electron angular correlation function is predicted by the scalar and pseudoscalar forms of beta-interaction. The experimental data are the average of four different runs, including the three shown in Fig. 4. The curve for the case of "no neutrino" is identical in form to the electron spectrum, since in this case the electron and the recoil nucleus always have equal and opposite momentum. All the curves calculated on the assumption of the $(1-\beta\cos\theta)$ neutrino-electron correlation function shown in Fig. 5 have been divided by 18.5 before plotting them in Fig. 6. This normalizes the amplitudes of the theoretical and experimental curves for the 180° case.

32 ions. This assumption was confirmed by measuring the mass of these ions in the following manner. A grounded grid was placed 2 or 3 millimeters in front of the surface *S*, Fig. 1. The conducting layer of surface *S* was then placed at a positive potential of 100 volts. Upon reaching the grid, the ions have a total energy of $(E+100)$ ev, where E is their initial energy, if, as is assumed, they are singly charged. The new minimum time of flight was measured as 2.3 microseconds. If one assumes that the mass of the ion is 32 (0.532×10^{-22} gram) and that its initial energy is about 80 ev, one predicts a minimum time of flight of 2.4 microseconds. This mass measurement is accurate to only about ± 30 percent mainly because of the short time intervals involved, but the possibility that some spurious effect was producing ions of a different mass is ruled out.

There is the possibility that electrostatic charges on the radioactive surface will cause errors. In fact, before the conducting grounded surface was added to the mica, an electrostatic potential, constantly increasing at about 10 or 20 volts per hour appeared on the surface. This was due to the negative beta-particles leaving. Since few charged recoils escape, a positive charge collects on the active surface. This causes a gradual speeding up of all the recoil ions in a direction normal to the surface *S*. In one case a potential of about 500 volts was observed 36 hours after the radioactive surface was formed. This effect was completely removed after the conducting, grounded, beryllium film was added to *S*, because of the greatly increased electrostatic capacity of the radioactive layer with respect to ground. The extreme thinness of the insulating layer of SiO_2 or LiF makes this capacity of the order of several thousand centimeters compared to a capacity of the order of 1 centimeter when no conducting film is present.

There is the possibility that the chemical nature of the foundation surface on which the P^{32} layer is deposited may effect the recoil momentum spectra. Good agreement on a number of runs with SiO_2, LiF, and NaF as the foundation surfaces reduces this possibility.

Related to the above point, there is the possibility that the positive ion "neutralization efficiency" of the surface will have an effect on the recoil spectra. The number of recoils in a given time of flight interval per electron detected varied by over a factor of 4 without changing the shape or the relative amplitude of the recoil momentum curves in any appreciable way. On the average, LiF permits about two or three times as many recoils to escape charged as does quartz. NaF was less efficient than quartz, and for that reason the data on it are very limited.

There is the possibility that the contaminating material evaporated with the P^{32} will cause some sort of selective effect on the escape of the recoil ions. This source of error is reduced by the fact that P^{32} deposits from different shipments from the Clinton Laboratories, on the platinum filament, have rather different evaporation characteristics. This indicates that there are different amounts, and probably different kinds of inert contamination materials. The recoil spectra are very similar. Furthermore, the double evaporation process in which the second evaporation occurs at a much lower temperature than the first evaporation gives the same recoil spectra.

There is the possibility that the orientation of the path of the recoils with respect to the normal to surface *S*, Fig. 1, will affect the recoil spectrum. In most of the measurements the surface *S* was oriented approximately normal to the line between the surface and the electron multiplier. An exception to this is the case where the electron-recoil angle is 90°. Here the surface (Fig. 1) is rotated about an axis normal to the paper through about 30°, so that the electrons can get to the Geiger counter without passing through the mica backing of the surface *S*. Some experiments were done at 180° to test the effect on the recoil spectrum of the orientation of the surface *S* with respect to the recoils. The surface was rotated about a vertical axis through 45° with respect to its position in Fig. 1. This caused about a 30 percent decrease in the intensity of the recoil momentum spectrum, but practically no change in its shape. This means that the recoil spectrum is substantially independent of the orientation of the direction of the recoils with respect to the normal to the surface over a range of about $\pm 45°$. It also means that as a recoil makes a larger and larger angle with the normal, its probability of escaping, at least in a charged state, decreases. However, this decrease in escape probability seems to be about the same for all recoil momenta. This strengthens the arguments presented above that the surface does not selectively neutralize the recoil ions, thus distorting their momentum spectra.

Scattering of the electrons is a possible source of error. The backing on the source *S* has a thickness of 1 to 2 mg/cm², and this can cause the low energy electrons below about $1000H\rho$ to be strongly absorbed and scattered. However, the 15 mg/cm² mica windows that the electrons must penetrate to be detected cut out all electrons below $1{,}200H\rho$, and strongly absorb them up to still higher values of $H\rho$. To check the order of magnitude of the effect of *S* upon the electrons, a source of 1.4 mg/cm² thickness is mounted in its standard 0.009-cm diameter copper wire cradle a distance of about 6 cm from the Geiger counter. The active surface was

alternately faced toward, and away from the Geiger counter, with a total absorber of 15 mg/cm² in front of the Geiger counter. A total of about 2 percent difference in counting rate was observed. About half of this was accounted for by the shielding resulting from the wire cradle. Thus, at most, only a few percent of the electrons are affected by the backing material of the source.

The reproducibility of the data was rather good. Out of about 35 surfaces, 15 gave no usable data. Either no recoils escaped at all, or there were too few to get any data. This was probably due to some contaminating material covering up the radioactive surface. For five or six surfaces, instead of the typical 180° recoil spectra in Fig. 4, an excessively large number of low momentum recoil ions were observed. It is inferred that these surfaces were thicker than a monolayer. As a "good" surface slowly becomes contaminated in the vacuum, the number of low momentum recoils increases so that the spectrum is very similar to a "thick" layer spectrum. Also, the intensity of recoils diminishes as the originally good surface becomes contaminated. Four surfaces, including the three shown in Fig. 4, had fairly good statistics for all four angles, and agree fairly well with each other regarding the shape and relative amplitudes of the various curves in the high momentum region. In addition, 10 surfaces with poorer statistics agree with the data of Fig. 4.

A particularly important point is the reproducibility of the 180° curve. When cases having deviations from the typical runs were observed, they invariably had fewer high momentum recoil ions, and more low momentum recoil ions. This fact, coupled with the known purity of the original radioactive material, supports the assumption that the reproducible cases are due to true monolayers, or less, of P^{32}.

VII. COMPARISON OF RESULTS WITH NEUTRINO THEORY

Figure 5 shows the theoretical recoil momentum spectra for P^{32} calculated with the following assumptions:

(a) A neutrino, whose rest mass is small compared to the rest mass of the electron, is assumed to leave the nucleus in the beta-decay process. (b) The neutrino and the electron share the available energy of 1.72 Mev. The energy carried away by the nucleus is negligible. (c) Four different assumptions are made about the neutrino-electron angular correlation function:

1. The random neutrino. It is assumed that the probability of the neutrino entering the element of solid angle $d\Omega$ is $1/4\pi d\Omega$. In this case all elements of solid angle are equally probable, independent of the direction of the electron. If θ is the direction between the neutrino and the electron, and the solid angle element is $2\pi \sin\theta d\theta$, then the above expression becomes $(\frac{1}{2})\sin\theta d\theta$. This is the probability that the neutrino makes an angle θ with the electron, and enters an angle element, $d\theta$. Thus for the random neutrino the most probable direction is 90° with respect to the direction of the electron. This function is similar to those predicted by the tensor and axial vector forms of beta-interaction for an allowed transition in the Fermi theory.[7]

2. The probability that the neutrino makes an angle θ with respect to the electron and enters a solid angle element $d\Omega$ is $(1/4\pi)(1-\beta\cos\theta)d\Omega$. β is the ratio of the velocity of the electron to the velocity of light.

This function is predicted by both the scalar and pseudoscalar forms of interaction in the Fermi theory for an allowed transition.[7]

The most probable angle between the electron and the neutrino is about 120°.

3. The probability that the neutrino makes an angle θ with respect to the electron and enters a solid angle element $d\Omega$ is

$$\frac{1}{4\pi(p/2q+q/2p-1/3)}(1-\beta\cos\theta)(p/2q+q/2p+\cos\theta)d\Omega.$$

Here p and q are the magnitude of the electron and neutrino momenta, respectively.

This function is predicted for the first forbidden transition when the allowed transition has the correlation function of $(1-\beta\cos\theta)$.[7]

The most probable neutrino-electron angle for this function is 90° for those electrons near the middle of the spectrum. For electrons near either end of the electron spectrum, the most probable angle is near 120°.

4. With no theoretical suggestion, the following neutrino-electron angular correlation function was also used as a basis for calculation:

$$\frac{3}{16\pi}(1-\beta\cos\theta)^2 d\Omega.$$

For this function the most probable angle between the neutrino and the electron is 135°.

No plot is made on Fig. 5 of the correlation function predicted by the polar vector form of the Fermi theory,

$$\frac{1}{4\pi}(1+\beta\cos\theta)d\Omega.$$

Here the most probable angle between neutrino and electron is about 60°. This function gives a peak on the 180°

curve of Fig. 5 which is twice as high as is the peak for the random neutrino.

(d) There is no scattering of either the electrons or recoil ions. (e) The electron momentum spectrum is that measured by Lawson,[11] corrected for the absorption in the mica windows which are 15 mg/cm² in thickness. This spectrum is plotted in Fig. 6. (f) One hundred percent efficiency is assumed for the Geiger counter for electrons, and in the electron multiplier for recoil ions of 3000-volts energy.

The calculations plotted in Fig. 5 were done by a geometrical method, using numerical integration.

The disappearance at a definite point of the high momentum recoils for the 135°, 90°, and 45° theoretical spectra in Fig. 5 is characteristic of any neutrino hypothesis applied to the given geometry. This effect can be called the "geometrical cut-off," since the cut-off point varies systematically with the geometry of the detectors and is independent of the neutrino-electron angular correlation function.

The similarity between the experimental curves in Fig. 4 and the theoretical curves in Fig. 5 can be seen in Fig. 6. The average of four different experimental curves and the neutrino theory curves for the $(1-\beta\cos\theta)$ case are plotted in Fig. 6. Here the theoretical curves of Fig. 5 have all been divided by 18.5. This normalizes the peak of the 180° curve to the experimental 180° curve. Although there is fair agreement in the high momentum recoil region, it is apparent that the experimental curves show several times too many recoils in the low momentum region.

Several conclusions can be based on the high momentum regions of the recoil spectra, above 4000-$H\rho$ or 25-ev energy. It is in this region that the data are most reproducible, and where there is least evidence of surface effects.

The "no neutrino" curve drawn in Fig. 6 is identical in form to the electron-momentum spectrum, since in this case the recoil and the electron always have equal and opposite momenta. The great difference between this curve and the experimental curve makes it fairly certain that momentum is not conserved between the electron and the recoil nucleus. The reproducibility of this 180° curve under a variety of conditions is taken as one of the principle supports for this conclusion.

The fact that the experimental curves at 135°, 90°, and 45° show any recoils at all, and that these recoil spectra have about the same upper limit of momentum as that predicted by the neutrino hypothesis, is rather good evidence supporting this hypothesis. That the presence of these recoils and the high momentum "cut-off" effect can be due to the scattering of the recoils at the surface is, of course, a possibility. This would require, however, some very arbitrary assumptions about the dependence of scattering on recoil energy and direction in order to predict the observed facts in a quantitative manner.

The 180° experimental curve clearly favors the $(1-\beta\cos\theta)$ neutrino correlation function. If the large numbers of high momentum recoils predicted by the random neutrino, the $(1-\beta\cos\theta)$ first forbidden, or the $(1+\beta\cos\theta)$ theories were present, they would be very easily observed. For over 20 different surfaces from which recoils were observed, there was never any evidence of such large numbers of high momentum recoils. The failure to observe them may be due to energy losses at the surface causing a broadening of this sharp peak. It is hard to imagine how this broadening of the 180° peak could occur without also producing some scattering of the recoils. That high momentum recoils in the 6400–7200$H\rho$ region are not scattered through angles of even 45° is seen by the disappearance of these recoils in the 135° experimental curve.

It is concluded that the data definitely favor the $(1-\beta\cos\theta)$ neutrino-electron correlation function. This conclusion is only tentative, however, since the discrepancies with this theoretical assumption below 25 ev are very marked, and since the 135° curve does not fit the theory in the 4000- to 5500-$H\rho$ region. In some respects the $(1-\beta\cos\theta)^2$ function agrees as well with experiment as does the $(1-\beta\cos\theta)$ function.

More experiments are needed to positively rule out any of the neutrino-electron angular correlation functions mentioned above, with the exception of the $(1+\beta\cos\theta)$ function. It is difficult to see how the experimental data can be reconciled to this last function.

The region of recoil momentum below 4000$H\rho$ or 25 ev will now be considered.

[11] J. L. Lawson, Phys. Rev. **56**, 131 (1939).

First of all, it is not too surprising that peculiar effects occur in this region since the recoil energies begin to approach the chemical binding energies of the surface. In general, the agreement between theory and experiment gets progressively worse toward lower energies, and is worst of all in the 5 to 10 ev region.

An effort was made to see what particular region, if any, of the electron spectrum was causing the low momentum recoil peaks at 90° and 45°. It was observed for several different radioactive surfaces that these peaks were either completely removed, or greatly attenuated if aluminum filters were placed in front of the Geiger counter. For the 90° case, a filter of 136 mg/cm² was added to the 15 mg/cm² already present. This completely removed the peak. A filter of 68 mg/cm² merely removed the high momentum part of the peak. For the 45° case, 68 mg/cm² was adequate to greatly attenuate the peak. This shows that the peaks are due principally to the electrons between $1200H\rho$ (the electron cut-off for 15 mg/cm²) and three or four thousand $H\rho$. This behavior is predicted by any neutrino hypothesis.

Definite conclusions regarding the apparently anomalous intensity of the recoils below 25-ev energy can be reached only with the aid of further experiments.

It is interesting that ions with an ionization potential of 10.3 volts can escape charged from surfaces of SiO_2, LiF, and NaF. It may be possible to use this technique to investigate the binding energy for electrons on the surfaces of insulators. The use of different beta-active species would widen the range of investigation.

Since the recoil ions are extremely sensitive to any contaminating deposits from the vacuum, this technique may be useful in studying the manner in which freshly prepared surfaces reach equilibrium with low pressure gases.

VIII. CONCLUSIONS

1. There is good evidence that momentum is not conserved between the electron and the recoil nucleus in the beta-decay of P^{32}. This evidence is mainly the shape of the 180° recoil momentum spectrum, the presence of recoils at other angles, and the "geometrical cut-off" of high momentum recoils at other angles.

2. The $(1+\beta\cos\theta)$ function (polar vector interaction) is so strongly in disagreement with the experimental data that it is very probably not a possible neutrino-electron correlation function. It is safe to include in this category any function such as that predicted by the tensor interaction in which the neutrino and the electron most probably go into the same hemisphere.

3. In the region of recoil spectra above about 25 ev, the agreement is fair between the observed spectra and the spectra predicted by a neutrino whose angular correlation with the electron is given by $(1-\beta\cos\theta)$. This function is predicted by both the scalar and pseudoscalar forms of the Fermi theory for allowed spectra. This implies that P^{32} an allowed transition; however, the first forbidden transition can not positively be ruled out. Also, a function which predicts an even more strongly opposite neutrino, such as the $(1-\beta\cos\theta)^2$ function, can not be ruled out.

4. The random neutrino is less probable than those mentioned under 3 above, but it will probably be necessary for more experiments to fix the limits of error before even this case can be definitely discarded.

5. The unexplained difference between theory and experiment below recoil energies of 25 ev is the principle reason for limiting the above conclusions.

IX. ACKNOWLEDGMENTS

The author wishes to thank Dr. Paul Aebersold of the United States Atomic Energy Commission, and Mr. J. A. Cox of the Clinton Laboratories for their cooperation in obtaining the radioactive materials.

The author also extends his appreciation to Professor R. B. Duffield who performed chemical separation of the phosphorus, and to Mr. Oscar Sala for many stimulating discussions of the problem.

Second Sound and the Heat Conductivity in Helium II

WILLIAM BAND AND LOTHAR MEYER
Institute for the Study of Metals, University of Chicago, Chicago, Illinois
(Received October 15, 1947)

By introducing a time of relaxation in a wave equation for second sound (1) relations between the dispersion of second sound and ordinary sound are derived; (2) the high heat conductivity of He II is related to second sound in the same way as the normal heat conductivity is related to ordinary sound on Debye's theory; (3) values for the time of relaxation and the velocity of of the heat flow are computed which are practically the same as for the flow of liquid He II through narrow slits above the critical velocity, indicating that in both cases the restriction of the flow is due to the same mechanism.

1. INTRODUCTION

L. TISZA[1,2] and L. Landau[3,4] independently derived a wave propagation in helium II generally called "second sound," by considering helium II as a mixture of two sorts of particles with different energy contents. These waves consist of fluctuations of the relative density of the two sorts of particles, the total density remaining constant in first approximation. In their derivation of the wave equation both authors use separate and independent continuity equations for the motions of the different sorts of particles. This procedure implies that no interchanges take place between the two sorts of particles during the time of vibration.

A similar condition has been investigated for the transmission of ordinary sound in a dissociating gas by A. Einstein.[5] Here also two different sorts of particles with different energy contents take part in the vibrations. Usually the time of a cycle in ordinary sound is so long that the two sorts of particles can interact with each other sufficiently to maintain the state of equilibrium during all phases of the vibration. But if the frequency is increased sufficiently the time necessary to establish equilibrium (generally called the time of relaxation) becomes larger than the time of one cycle. Einstein showed that this causes a change in the velocity of sound, with a region of dispersion and absorption in the range of frequencies where the time of relaxation is comparable with the time of one cycle.

[1] L. Tisza, C. R. Acad. Sc. **207**, 1035, 1186 (1938).
[2] L. Tisza, J. de phys. et rad. **VIII**, 1, 350 (1940).
[3] L. D. Landau, J. Phys. U.S.S.R. **5**, 71 (1941).
[4] L. D. Landau, J. Phys. U.S.S.R. **11**, 91 (1947).
[5] A. Einstein, Sitzungsberichte Berl. Akad. **1920**, 380.

2. THE DISPERSION OF SECOND SOUND AND OF ORDINARY SOUND

It is the aim of this paper to show that by introducing the same conception of a time of relaxation in the equations for second sound, relations between the dispersion of second sound and of normal sound can be obtained, and furthermore the extremely high heat conductivity of helium II can be associated with second sound in practically the same way as the normal heat conductivity accompanies ordinary sound on Debye's theory,[6] yielding simultaneously very reasonable values for the time of relaxation.

In order to simplify the discussion we assume, like Tisza and Landau, that the energy content of the particles in the lower state of helium II is negligible compared with that of the others,[7] so that the density of these latter so-called "excited" particles alone determines the thermodynamic properties in first approximation. We therefore write the wave equation for fluctuations of the concentration of the excited particles ρ_e, including a relaxation term:

$$\nabla\cdot\nabla\rho_e=\frac{1}{v^2}\left[(\partial^2\rho_e/\partial t^2)+\frac{1}{\tau}\dot{\rho}_e\right] \qquad (1)$$

v being the velocity of second sound, and τ the time of relaxation. Physically this relation implies that as long as τ is great compared with the period of fluctuations of ρ_e, such a fluctuation

[6] P. Debye, *Vortraege ueber die kinetische Theorie der Materie* (Leipzig, 1914) p. 43.
[7] This assumption does not mean that we assume a Bose-Einstein condensation. It would hold equally well also for a hydrodynamical model of the Landau type, or even for an order-disorder model of the type suggested by H. Frohlich (Physica 's Gravenhage **4**, 6391 (1937)) and H. Jones (Proc. Camb. Phil. Soc. **34**, 253 (1938)).

can be propagated as a wave, but when τ is small compared with this period, a local change of ρ_ϵ is completely dissipated by a diffusion process and any "second sound" wave would suffer immediate damping.

Because ρ_ϵ is temperature dependent, fluctuations of ρ_ϵ will occur also in ordinary sound waves, in complete analogy to the fluctuations in concentration in a dissociating gas considered by Einstein. The time of relaxation introduced into (1) is then essentially the mean time between exchanges of excitation energy, just as in Einstein's theory (see, e.g., Rutgers[7]). This leads to the expectation that ordinary sound should show dispersion and absorption in the same frequency range as second sound.** The main difference between the two sets of phenomena would be that while ordinary sound should only change its velocity when passing through the critical frequency, showing an absorption maximum there, second sound can exist only at higher frequencies, and will be entirely damped out at all frequencies lower than the critical value.

3. THERMAL RESISTANCE

Second sound waves imply a transport of heat,*** just as ordinary sound waves do in Debye's theory;[6] the damping of the waves limits the conductivity to finite values. The following discussion of thermal resistance in terms of second sound relaxation therefore represents a complete analogy to Debye's theory in terms of ordinary sound. Its validity depends on the assumption that the resistance accompanying ordinary sound is very large compared with that accompanying second sound; the two resistances being effectively in parallel, so that only the latter is important.

To obtain the thermal resistance we transform the fluctuations of concentration (1) into fluctuations of temperature. Under completely relaxed conditions ρ_ϵ is a function of the equilibrium temperature T of the system:

$$\rho_\epsilon = \rho_\epsilon(T). \tag{2}$$

When the system is not completely relaxed we may still use this equation to define a temperature T_ϵ of the excited particles:

$$\rho_\epsilon = \rho_\epsilon(T_\epsilon) \tag{2'}$$

where in general T_ϵ will differ from a possibly measured temperature T by a certain quantity which depends on frequency. Putting (2') into (1) we obtain a temperature wave:

$$\nabla\cdot\nabla T_\epsilon = \frac{1}{v^2}\left[(\partial^2 T_\epsilon/\partial t^2) + \frac{1}{\tau}\dot{T}_\epsilon\right]. \tag{3}$$

It must be emphasized that T_ϵ in this wave equation is not the measurable thermodynamic-equilibrium temperature, but the temperature of the excited particles as defined by (2').† To obtain now†† the relation between the relaxation damping according to (3) and the heat resistance, we use the equation for the conservation of heat under completely relaxed conditions which apply to actual measurements of heat conductivity:

$$\nabla\cdot h = -\rho C_p \dot{T} \tag{4}$$

where C_p is the true heat capacity, and T the true equilibrium temperature, h the heat flow. Under general conditions we must write T_ϵ in place of T, and by using instead of C_p a different, suitably defined frequency-dependent value

[7] A. J. Rutgers, Ann. d. Physik **16**, 350 (1933).

** A difference in the two regions of dispersion could mean only that the damping of second sound is due also to other influences not present in ordinary sound, e.g., a mechanical viscosity between the two sorts of particles when vibrating in opposite directions. In helium II the exchanges of momentum and of excitation energy have usually been considered as the same process, but the experimental determination of the dispersion has to decide whether this assumption is true.

*** This is also consistent with Tisza's model, which leads to a simple classical picture of the nature of second sound: Helium II consists of two parts which may each transmit sound waves, (a) which are in phase with each other—ordinary sound, (b) in opposite phase to each other—second sound. Only so long as there is no appreciable relaxation between the two components can the second mode of vibration persist.

† The lack of temperature equilibrium between the two sorts of particles in second sound necessary to ensure propagation and not dissipation of a local fluctuation is overlooked in some derivations by introducing calorically measured thermodynamic quantities such as entropy, etc., which by definition are only valid for the state of equilibrium. (See, e.g., L. Landau,[3] page 85 and D. V. Gogate and P. D. Pathak, Proc. Phys. Soc. London **59**, 457 (1947).)

The use of separate and independent continuity equations for the relative motion of the two sorts of particles is inconsistent with the introduction of statically measured quantities as entropy and temperature which are only valid for the completely relaxed system.

†† This argument is similar to that of H. Jones (Proc. Camb. Phil. Soc. **34**, 253 (1938)) in terms of the flow of disorder.

C_p^*,††† we may retain (4) in the form:

$$\nabla \cdot h = -\rho C_p^* \dot{T}_e. \tag{4'}$$

As relaxation increases C_p^* approaches C_p, and $T_e \rightarrow T$. We may neglect the second derivative on the right side of (3) under partially relaxed conditions if the rate of change of T is small enough:

$$\nabla \cdot \nabla T_e = \dot{T}_e / \tau v^2. \tag{5}$$

Comparing this with (4') we obtain

$$h = -\rho C_p^* \tau v^2 \nabla T_e \tag{6}$$

which becomes, for complete relaxation as present in the irreversible heat flow experiment:

$$h = -\rho C_p \tau v^2 \nabla T. \tag{7}$$

The wave of concentration (1) together with partial relaxation implies a motion of excited particles. We may therefore regard the heat flow as a transport of excitation energy by excited particles diffusing with an average velocity u:

$$h = (\epsilon/\rho)\rho_e u \tag{8}$$

where ϵ/ρ means the excitation energy per unit mass associated with the excited particles. Under the simplifying assumptions made at the beginning, the energy content of the excited particles represents practically the total heat content ρQ_T of helium II, so we may write

$$(\epsilon/\rho)\rho_e = \rho Q_T = \rho \int_0^T C_v dT \tag{9}$$

since ρ is practically independent of T. Therefore (8) becomes

$$h = \rho Q_T u. \tag{10}$$††††

Using the measured values of Q_T and h,[8,9,10] we can compute from (10) the velocity u as a function of T. Table I contains these values for a temperature gradient of 0.001°K per cm. This table also shows the values of τ calculated from (7) and the same experimental data on h and the observed values of second sound velocity.[11]

From the experimental fact that $h \propto (\nabla T)^{\frac{1}{3}}$ it follows that $\tau \propto 1/h^2$. (See Eq. (7).‡) Taking into account that the energy supplied to the system in second sound measurements is at least ten times smaller than for the heat conduction experiments used in Table I (1/25 watt over a cross section of several cm² in the sound tube compared with between 1 and 3 watts per cm² in the heat conductivity measurements), it must be expected that the time of relaxation is in this case at least a hundred times greater than the values given in Table I. Dispersion and absorption ought therefore to appear in both kinds of sound (at such an energy input) at around 1 to 10 cycles per second. This is not in conflict with Peshkov's[12] results, in which no dispersion was

††† Under the simplifying conditions mentioned above $C_p = \partial(\rho_e \epsilon)/\partial T$ where ϵ is the "excitation" energy per particle at the temperature T. For the completely unrelaxed system $\tau \rightarrow \infty$, $C_p^* = \epsilon \partial \rho / \partial T$ as without interaction, the excitation energy carried by the particles cannot adjust itself to the temperature.

†††† Equations (7), (8), (10) have been derived by us earlier (Phys. Rev. 71, 828 (1947)) on the assumption that in the absence of a constriction the internal forces responsible for the fountain effect are still present, but produce an internal momentum density M according to the second law of motion:

$$\nabla p = \mu \nabla T = -dM/dt \tag{11}$$

where T is the temperature, p the fountain effect pressure difference and μ the fountain effect coefficient. L. Tisza (Phys. Rev. 72, 353 (1947)) criticized this equation, stating that we had omitted a factor ρ_2/ρ_e where ρ_2 is the density of the particles in the lower state. This is due to a misunderstanding: The above Eq. (11) was written simply as a definition of the momentum in terms of the fountain effect, but is not the momentum appearing in Tisza's model. Incidentally the momentum cancels from the equations leading to (7), so that Tisza's factor makes no difference to our evaluation of τ and u from the observed values of h, C_p and v.

The equivalence of both derivations can be shown as follows: Comparing (8) with (6) yields:

$$-(\rho/\epsilon)\rho C_p^* v^2 \nabla T_e = \rho_e u/\tau \tag{12}$$

where $\rho_e u$ represents a momentum density. Equation (12) has the form of the second law of motion under conditions of considerable relaxation:

$$-\nabla p = \dot{M} + M/\tau \doteq M/\tau. \tag{13}$$

Comparing (12) with (13) gives:

$$\nabla p = (\rho/\epsilon)\rho C_p^* v^2 \nabla T_e \tag{14}$$

which represents a fountain pressure relation:

$$\nabla p = \mu \nabla T_e. \tag{14'}$$

[8] W. H. Keesom, B. F. Saris, L. Meyer, Physica 's Gravenhage 7, 870 (1940).

[9] L. Meyer and J. H. Mellink, Physica 's Gravenhage 13, 197 (1947).

[10] W. H. Keesom, *Helium* (Elzevier, Amsterdam-New York, 1942).

[11] C. T. Lane, H. A. Fairbank, W. M. Fairbank, Phys. Rev. 71, 600 (1947).

‡ The derivation of Eq. (7) is, at least for one-dimensional flow as discussed here, practically unaffected by the fact that τ is a function of ∇T: Introducing into (5) instead of a constant τ, the expression

$$\tau = \gamma(\nabla T)^{-\frac{1}{3}}$$

leads to

$$h = 3\rho C_p v^2 \gamma (\nabla T)^{\frac{1}{3}} = 3\rho C_p v^2 \tau \nabla T.$$

[12] V. P. Peshkov, Vestnik Akademii Nauk 4, 117 (1945); Nature 157, 200 (1946); J. Phys. U.S.S.R. 10, 389 (1946).

found in the frequency range from 100 to 10,000 cycles per second.

The fact that the compressibility of helium II derived from measurements by Burton,[13] and by Findlay, Pitt, Grayson-Smith and Wilhelm,[14] on ordinary sound in helium II differs from the statically measured values at Leiden[10] by about 15 percent, may be due to the dispersion effect; the frequencies used (e.g., 1338 kc by Burton) were certainly higher than the critical value to be expected by our estimates of the relaxation time.

The sudden change in velocity of ordinary sound at the lambda temperature may also at least partly be due to this same dispersion. Above the transition, the time of relaxation has vanished, whereas below, it has already become long compared with the period of the waves.

The velocities u calculated from (10) are of the same order of magnitude as the critical velocities u_c for the frictionless flow through narrow slits[9] given in column 3.‡‡ It is very interesting that in the supercritical region—i.e., above the critical velocity—the velocity of flow through narrow slits is approximately proportional to $(\nabla T)^{\frac{1}{3}}$,‡‡‡ just as (10) demands for u. This leads to the conclusion that the restriction of the flow of particles in the heat current is the same as in the supercritical flow through slits, both being controlled by the time of relaxation.‡‡‡‡

TABLE I. Values of u and of τ.

T °K	u cm/sec.	u_c cm/sec.	τ sec.
1.2	19	25	$9.\ 10^{-4}$
1.5	15	20	$7.\ 10^{-4}$
1.8	11	13	$6.\ 10^{-4}$
2.0	5	8	$5.\ 10^{-4}$
2.1	2	3	$4.\ 10^{-4}$

We want to thank Professors J. E. Mayer, E. A. Long, A. W. Lawson and J. W. Stout for valuable discussions.

[13] E. F. Burton, Nature **141**, 970 (1938).

[14] J. C. Findlay, A. Pitt, H. Grayson-Smith and J. O. Wilhelm, Phys. Rev. **54**, 506 (1938); Phys. Rev. **56**, 122 (1939).

‡‡ The values of u_c contain with regard to their absolute magnitude an uncertainty up to about 25 percent due to the difficulties in measuring the exact width of the slit.

‡‡‡ Reevaluation of the Leyden Measurements by L. Meyer and J. H. Mellink[9].

‡‡‡‡ Experimental evidence (see reference 9) already lead to the conclusion that the friction in the supercritical flow is not produced in the slit itself but at its ends where the jet of "film" leaves or enters the bulk of the liquid.

Angular Distribution of the (d,p) Reactions Making Two Low States of O^{17}

N. P. HEYDENBURG
Department of Terrestrial Magnetism of The Carnegie Institution of Washington, Washington, D. C.

AND

D. R. INGLIS
Department of Physics, The Johns Hopkins University, Baltimore, Maryland

(Received October 27, 1947)

Angular distributions of the protons from deuteron bombardment of fairly thin oxide targets have been observed both for the long-range protons leading to the ground state of the residual nucleus O^{17}, and for the short-range protons leading to the first excited state. The deuteron energies ranged from 0.65 to 3.05 Mev, and the beam, obtained at each energy from one of two statitrons, was practically monoenergetic. The protons were observed by an ionization chamber, linear amplifier, and pulse height discriminator, while the monitoring was done by integrating target current. The yield of the short-range protons is about ten times that of the long-range protons at low bombarding energies, and the two yields become nearly equal at higher energies. Very pronounced variation of proton intensity with angle was observed for both ranges at almost all bombarding energies, the shape of the curves varying markedly with energy. At low bombarding energies the long-range protons are predominantly forward, the short-range predominantly backward. In the neighborhood of a peak in the excitation curves at about 1.8 Mev, the angular distributions become roughly symmetric about 90° for both ranges, and even almost isotropic for the long-range protons. It happens that the high energy side of this peak coincides rather closely with the threshold of the competing (d,n) reaction. This peak appears for both ranges in the excitation curves for the total yield, integrated over all angles, but not in the conventional 90° excitation curves. Two further peaks appear at higher energies. It is hoped that relationships between the angular momentum properties of the two low states of the final nucleus may be deduced from detailed angular information of the sort here presented.

KNOWLEDGE of the low states of the simpler light nuclei gives particular promise of being helpful in leading to an understanding of nuclear structure. Acquaintance with the properties of more than one state in a single nucleus might be expected to contribute to the problem in a manner somewhat analogous to that in which spectroscopic information on many levels of simpler atoms helped unravel the problem of atomic structure. The O^{17} nucleus is probably an unusually simple one when not too highly excited because the stability of the O^{16} nucleus and its "completed-shell" nature in either the central or the alpha model makes it likely that the low states of O^{17} may be better approximated by a single-particle model than may those of most nuclei. The experimental investigation here reported was motivated by the hope that it might make possible a comparison of the angular properties of the two low states of O^{17}. (The present state of the analysis is not such that this hope is realized.)

The two ranges of the protons from the $O^{16}(d,p)O^{17}$ reaction have been observed by Cockroft and Lewis[1] at right angles to their incident deuteron beam, which had an energy of 575 kev. The two ranges were resolved as rather sharp peaks, at about 4-cm and 8-cm air equivalent. The short-range peak was about $2\frac{1}{2}$ times as high as the long-range peak.

In the first phase of the present experiments, deuteron energies were used up to 1150 kev, this being the highest energy available from the small statitron at D.T.M. This atmospheric-pressure machine was selected as the one which could be put into operation most quickly after the recent prolonged hiatus in research activities. During the course of the investigation, the voltage control of this statitron has been improved by installation of equipment which utilizes the "voltmeter current," taken from the high voltage head through a 10^{10}-ohm resistor stack,[2] to control the corona current[3] allowed to leak from a corona arm back to the head. The behavior of the resistor stack was improved by installing more closely spaced shielding rings and corona points outside the textolite casing. The voltage regulation achieved is better than one-half percent although the calibration may

[1] J. D. Cockroft and W. B. Lewis, Proc. Roy. Soc. 154, 250 (1936).

[2] M. A. Tuve, Sci. Month. 47, 4, p. 8 (1938).

[3] A. O. Hanson, Rev. Sci. Inst. 15, 60 (1944).

gradually drift more than this because of temperature changes.

Toward the end of the first phase of the work, trouble developed in the ion source power supply of the small statitron which made necessary the start of some rebuilding at the completion of this phase. At about this time the large statitron[4] was brought into operating condition, and the second phase of the work consisted of carrying the measurements up to bombarding energies of 3 Mev with this machine. Modifications and improvements in this statitron which helped bring it into operating condition included the building of a new electrostatic voltmeter, the installation of a new set of fixed corona points and shunting sphere gaps, the installation of a system of variable corona gaps between the platforms at four-foot intervals up the supporting column, and the use of a rather soft mixture of "W" wax and "J" oil on the joints in the accelerating tube, where cracks had been developing in ordinary "W" wax during the cold weather of the winter. Lacking a voltmeter stack or electrostatic deflector, the voltage regulation is carried out on the large statitron by manual adjustment of the charging current, according to indications of the oscilloscope trace obtained from the generating voltmeter. The regulation of bombarding voltage was always good to about 1 percent, and under the most favorable conditions to better than $\frac{1}{4}$ percent.

EXPERIMENTAL ARRANGEMENT

Target Chamber

The target chamber found most satisfactory for measuring the angular distribution of the protons produced by the $O^{16}(d,p)O^{17}$ reaction is shown in Fig. 1. The chamber itself is the same one that was used earlier[5] at the Johns Hopkins Physics Department for the observation of alphas resulting from the proton bombardments, but the method of observing the product particles is quite different in the present work. The chamber had windows allowing observation at five angles, and more were added toward the end of this work. An ionization chamber and prepreamplifier are mounted on a screw-adjusted, radially traveling carriage which in turn is mounted on a swivel arm screwed to one face of the chamber, the pivot bolt being at the center of the face. A graduated circle is mounted around the edge of this face, so that the angular position of the swivel arm may be read. With the angular position adjusted to suit one of the windows, the distribution of the protons in

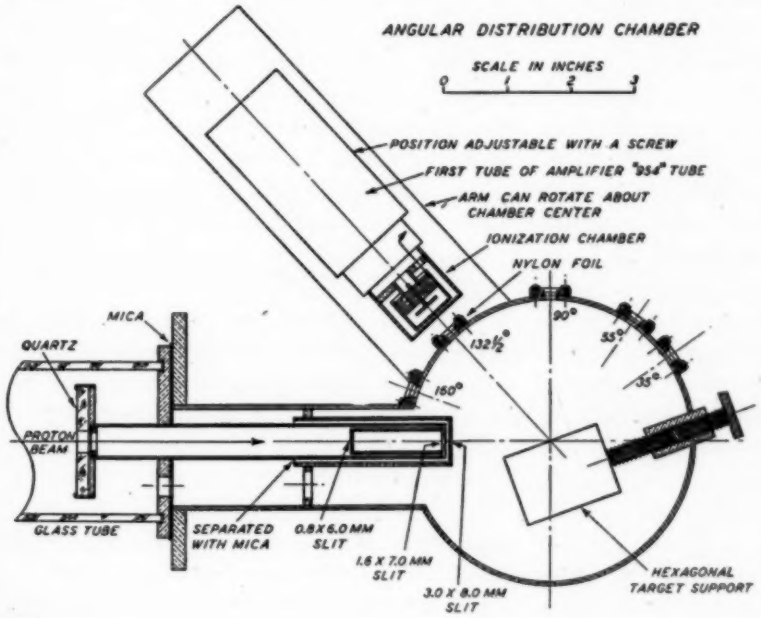

FIG. 1. Target chamber.

[4] Reference 2, p. 19.
[5] Swartz, Rossi, Jennings, and Inglis, Phys. Rev. 65, 80 (1944).

range is investigated by measuring the frequency of proton counts as dependent on the radial position of the carriage. Thus air at atmospheric pressure is used as the variable absorber. The discriminator bias is set at such a value that only those particles having the ends of their ranges near the back of the ionization chamber are counted.

The first of these experiments with this chamber were carried out with 0.0005-inch aluminum windows, but difficulties were experienced especially in variation of the shape of the peaks from one window to another. (The short-range peak was so close to the window that no adequate check could be obtained between the two peaks to make sure that the effect was attributable to the windows.) Some windows gave the appearance of a plateau on the short-range side of the long-range peak, as though perhaps one-third of the area of the window were about twice as thick as the rest. (The nominal thickness of the Al windows was 2-cm air equivalent, and the plateau was displaced about 1 or 1½ cm from the peak). Whatever the origin of these troubles, they vanished with the use of Nylon windows and the improvement of the electronic technique.

The great advantage of Nylon windows is that they are so thin as to make one confident that variations in their thickness cannot lead to appreciable uncertainties in the ranges of the particles. Their nominal thickness is 0.0005 in., which means an air equivalent of about 2 mm. The disadvantage is that they do not last long under particle bombardment. With primary currents of the order of a few tenths of a microampere getting through the slit system to the target, the life of the windows is only three or four hours. The secondary particles being counted amount to only a few dozen per square millimeter per second, but shorter-ranged primary particles scattered from the target are probably responsible for the short window life. It is convenient that the windows give warning by leaking slowly for some time before actually bursting, so that vacuum calamities may usually be avoided.

In the final arrangement used at the lower bombarding energies, each of the five Nylon windows is mounted in a window frame in such a way that its inner side is pressed around the edges against a $\frac{1}{16}$-in.$\times\frac{1}{16}$-in. Neoprene gasket which is sunk in a groove 3/64-in. deep. The lower plate of the window frame is shaped to fit the cylindrical surface of the target chamber, and is pressed against it with a flat ungrooved rubber gasket. The window itself measures 5 mm$\times$9 mm, being rounded toward the ends, and the direction of greatest strength in the Nylon is placed the short way across the window. Windows a couple of millimeters wider did not last as long as an hour.

At the higher bombarding energies the range of the short-range protons was sufficient that duraluminum windows of 6-cm air equivalent could be used and these were nicely homogeneous. Extra stopping foils of the same material were used to shorten the distance from target to counter and increase the counting rate.

The target chamber arrangement first used in this investigation appeared more elegant, but was not very successful because the connection between the collecting electrode and the first grid was so long that the pulses were only slightly higher than the noise level. This chamber had a swivel arm inside the vacuum, pivoting on a conical ground joint (as used formerly at D.T.M. for proton-proton and proton-helium scattering measurements[6]), and carrying a double chamber with two pressure tubes and a high voltage lead in addition to the pulse connection (which came out of the opposite face of the target chamber to the external pre-preamplifier). The first compartment of this double chamber was a variable-pressure absorption cell with an aluminum window at each end, and the second part was the usual ionization chamber.

Electronic Equipment

The pre-preamplifier which travels on the ionization chamber carriage is a 954 Acorn tube, which has been found consistently superior to other tubes tried for this purpose, now just as several years ago. It is connected by a short flexible connector to a 3-stage preamplifier consisting of three 6AK5 tubes in a negative-feedback loop. This in turn is connected by a longer lead to a rather new linear amplifier ("Model 100" as designed by W. A. Higinbotham for

[6] N. P. Heydenburg, L. R. Hafstad, and M. A. Tuve, Phys. Rev. 56, 1078 (1939).

faster counting than encountered here, with the input slowed down for total ion collection, to eliminate high-frequency noise) and this feeds the pulses into a discriminator and scale-of-eight recorder which has been in use in this laboratory for some time. During the second phase of the work, a discriminator and scale-of-64 of Higinbotham's design replaced the old scale-of-8 and seemed to discriminate just as dependably until the humidity of the summer was accompanied by trouble which was eliminated by a return to the old scalar.

The preliminary observations were made by integrating current over time visually, taking runs for a given time, because current integrators had not been found very accurate in earlier work in this laboratory. During the course of the investigation, two current integrators were built and tried. The first depended on the firing of a thyrotron and did not achieve a reliably functioning condition. The second is a more complicated circuit designed by M. Sands. It has been very satisfactory and has greatly facilitated the final measurements.

PROCEDURE

The target used for most of the measurements is in effect a fairly thin target of ordinary oxygen, but is actually an oxide layer on a tungsten surface. The tungsten surface was polished with emery cloth and then heated to a dull red glow. During the heating the spreading of successive layers of oxide across the surface could be seen in reflected light, and the target was considered completed when three or four such layers had appeared. The plate was then mounted on a hexagonal copper-block target mounting capable of being rotated from outside the target chamber through a screw which also allows advancement to a fresh target position after a target spot has become contaminated with superposed carbon deposited by the beam.

Alignment to place the target spot at the center of the chamber is aided by the possibility of turning a quartz target in place to make the spot easily visible, but a slight glow can also be seen on the oxide target itself for purposes of more accurate alignment. The possibility of sighting visually through the Nylon windows is also helpful. The most important requirement is that the edges of the windows should not partially eclipse the lines between the edges of the target spot and the edges of the ionization chamber aperture, and this is assured by picking the angle setting suited to each window by means of trial runs with given range settings and varying angle settings.

Some preliminary runs at fixed angle covered a domain of range wide enough to include both the 4-cm and the 8-cm peak and the region between them to verify the observation of Cockroft and Lewis that there are only two peaks in this domain. Subsequently attention was focused only on the peaks themselves. A typical curve showing the appearance of the peaks is shown in Fig. 2. It was taken toward the end of the work with the thin target on steel,

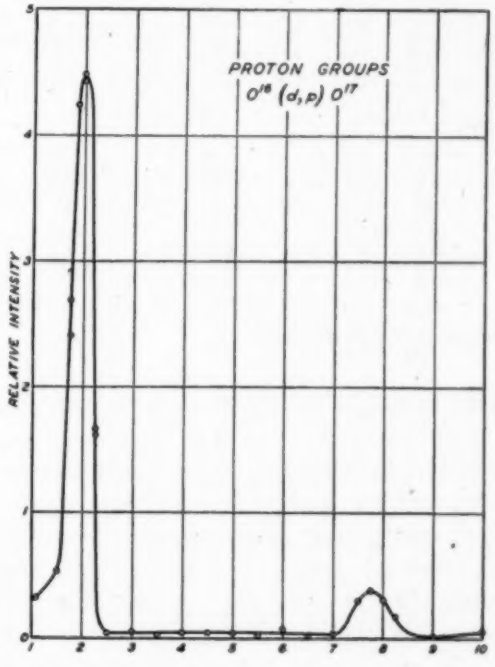

FIG. 2. A typical yield curve as a function of range, showing the appearance of the two groups of protons. This was observed at a bombarding energy of 1.15 Mev and $\theta = 90°$. Only the inverse-square correction has been made. To the observed range as plotted should be added the window thickness (5.2-cm air equivalent) and approximately the thickness of the ionization chamber (3 mm). The long-range peak is then at 13.2 and the short-range peak at 7.5 cm. According to Livingston and Bethe's range-energy curve, these correspond to 2.89 and 2.07 Mev. From these data we find the energy evolutions $Q_{l.r.} = 2.05 \pm 0.2$ Mev and $Q_{s.r.} = 1.18 \pm 0.2$ Mev, and the energy of the excited state of O^{17}, $Q_{l.r.} - Q_{s.r.} = 0.87 \pm 0.03$ Mev, which while consistently larger, are not in disagreement with the earlier values. From this $Q_{l.r.}$ we obtain $M(O^{17}) = 17.00908 \pm 0.0002$.

TABLE I. Intensities in the center-of-mass system at various angles and bombarding energies. The tabulated numbers are the numbers of protons recorded per current-integrator count (0.41μ coulomb) in a solid angle which would be subtended by the ion chamber aperture (area 0.13 cm²) at 10^{1} cm from the target. The angles listed are laboratory angles; for center-of-mass angles see Table II. The energies are laboratory bombarding energies. The target is slightly thick oxide on tungsten except where otherwise noted.

E/Mev	35°	55°	72.5°	90°	110°	132.5°	160°
Short range							
0.650	0.30	0.22		0.68		1.57	1.68
0.750	0.73	0.77		2.51		3.86	3.72
0.930*	2.74	4.03		11.56		13.64	13.54
0.933	1.97	2.89		9.76		10.94	11.02
1.070	5.94	7.17		15.4		17.6	15.72
1.150	7.23	8.19		17.8		19.5	17.49
1.52	9.58	14.5		33.7		33.1	22.0
1.71*	8.76	18.24	26.80	29.3	26.0	15.6	10.1
1.785	16.65	30.9		41.9		22.0	4.95
1.935	25.6	24.4		27.4		23.2	14.3
2.045	40.5	19.35		39.2		46.3	33.5
2.34	24.7	17.85		53.2		34.4	20.5
2.60	7.43	40.5		39.0		15.5	15.8
3.05	16.7	33.6		40.2		18.25	9.9
0.80**	0.66	0.51		2.08		2.94	2.93
0.93**	1.13	1.67		4.55		4.46	3.91
1.15**	0.57	1.30		3.34		2.43	1.40
1.62**	2.32	3.85	7.15	8.74	7.54	3.86	2.98
1.71**	3.70	5.50	7.11	7.40	5.82	2.90	2.33
1.825**	7.16	4.87	5.84	4.27	4.00	3.04	2.29
1.945**	9.60	3.24	5.26	8.16	6.94	7.10	5.98
2.045**	9.19	2.90	7.11	10.95	11.96	11.57	8.85
Long range							
0.933	2.64	3.63		2.40		1.26	0.914
1.070	3.99	4.96		2.93		1.68	1.36
1.525	9.9	15.4		12.5		10.84	10.25
1.71*	57.6	90.8	89.9	88.2	100.5	132.1	156.4
1.785	9.9	10.44		10.8		16.6	18.8
2.045	10.1	14.85		8.88		10.73	14.9
2.34	13.85	29.7		15.7		18.65	29.3
2.60	16.6	16.8		15.3		28.5	30.9
3.05	32.0	45.2		32.05		25.1	29.3

* Slightly thick oxide on steel.
** Thin oxide on steel.

at 1.15 Mev and 90° (with a bias of 80 volts on the "old" discriminator). The position of course varies with bombarding voltage and with angle in a way which can be calculated from conservation of energy and momentum in the collision. The observed range on the carriage vernier depends further on the amount the Nylon window is bowed in, and this varies from window to window and from run to run just sufficiently that it is considered necessary to take about three readings very close to the expected position of a peak in order to be sure to obtain the height of the peak. This procedure is followed in obtaining curves for the variation of the height of a peak with angle at a given bombarding voltage.

Because of gradual drift in the effectiveness of the discriminator bias and in the resistance of the voltmeter resistor or in the comparison potential governing the bombarding voltage, it is desirable to group consecutively measurements of which the comparison is most significant. We are primarily interested in angular dependence of the peak height, and secondarily interested in the variation of this property with bombarding voltage. Most runs were therefore made consecutively over different angles, observing either the short-range or the long-range peak at a given bombarding voltage. During such consecutive runs, observations at different bombarding voltages were made at single angles in order to make possible intercomparison with sets of data obtained on different days and under varying conditions. Finally a 90° excitation curve was made to extend this intercomparison over a broad range of energies.

The discriminator bias is kept at a constant value during all these runs. The value was picked in the first place, as a result of experience with preliminary measurements, in such a way as to give as frequent counts as possible without broadening the lines unduly beyond their inevitable width arising from straggling in range. It is to be noted that the cut-off for settings on the long-range side of the peak arises from most of

TABLE II. Center-of-mass angles.

E/Mev	35°	55°	72½°	90°	110°	132½°	160°
Short range							
0.65	36°40′	57°23′		92°54′		134°38′	161°
1.0	36°53′	57°41′		93°17′		134°55′	161°7′
1.5	37°5′	57°58′	75°57′	93°37′	113°24′	135°10′	161°14′
2.0	37°12′	58°9′	76°10′	93°51′	113°37′	135°20′	161°19′
3.0	37°22′	58°23′		94°8′		135°33′	161°25′
Long range							
1.0	36°35′	57°16′		92°56′		134°32′	160°57′
1.5	36°48′	57°34′	75°30′	93°8′	112°57′	134°49′	161°4′
2.0	36°56′	57°46′	75°44′	93°21′	113°11′	135°	161°9′
3.0	37°9′	58°4′		93°44′		135°15′	161°17′

TABLE III. Correction factor g = (center of mass intensity)/(lab. intensity).

E/Mev	35°	55°	90°	132½°	160°
Short range					
0.65	0.923	0.945	1.001	1.072	1.094
1.0	0.913	0.939	1.001	1.082	1.104
1.5	0.906	0.933	1.001	1.091	1.130
2.0	0.901	0.929	1.001	1.097	1.138
3.0	0.893	0.923	1.002	1.106	1.152
Long range					
1.0	0.926	0.948	1.001	1.071	1.089
1.5	0.918	0.941	1.000	1.068	1.110
2.0	0.912	0.936	1.000	1.081	1.119
3.0	0.902	0.930	1.001	1.094	1.137

the particles ending their paths after passing only part way across the chamber, whereas the cut-off on the short-range side arises from most of the particles spending the last and most highly ionizing part of their paths beyond the chamber. If there were no straggling and the bias were set to accept pulses considerably below the maximum, one could obtain a quite unsymmetrical peak from the difference in these two mechanisms of cut-off. The lack of marked asymmetry may be considered some evidence for the reasonableness of the bias setting.

The results as observed in the laboratory coordinate system are transformed to the center-of-mass coordinate system by use of the relation

$$\sin(\theta_r-\theta)=(V/v_r)\sin\theta, \qquad (1)$$

and by multiplying the observed relative intensities by the factor which relates the solid angle defined by the ionization chamber aperture in the two systems[7] (see Table III):

$$g(\theta)=\sin\theta d\theta/\sin\theta_r d\theta_r$$
$$=(\sin^2\theta/\sin^2\theta_r)\cos(\theta_r-\theta). \qquad (2)$$

The last substitution arises from differentiating (1) with respect to θ_r and solving for $d\theta/d\theta_r$. In order to find θ_r, the deflection angle in the c.m. system, from (1), the factor V/v_r is computed from the relation

$$(V/v_r)^2=(m_1m_2/m_0m_3)/(1+MQ/m_0E_1) \qquad (3)$$

which is obtained from the kinetic energy of the center-of-mass motion,

$$E_{\text{c.m.}}=(1/2)MV^2=(m_1/M)E_1$$

where M is the total mass and V the speed of the center of mass, and from the expression for the kinetic energy after the reaction, relative to the center of mass:

$$E_{\text{rel.}}=(1/2)m_2^2v_r^2(1/m_2+1/m_3)$$
$$=E_1+Q-E_{\text{c.m.}}=(m_0/M)E_1+Q.$$

Here the subscripts 0, 1, 2, and 3 refer to the target nucleus (O^{16}), the incident particle (deuteron), the product particle (proton), and the residual nucleus (O^{17}), respectively. The variation of θ_r and g with θ and E are shown in Table II, in a form convenient for interpolation.

[7] Haxby, Allen, and Williams, Phys. Rev. **55**, 142 (1939).

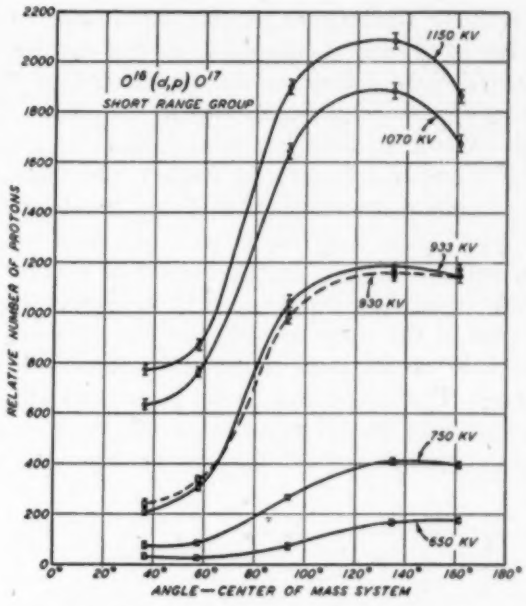

FIG. 3. Angular distributions at low bombarding energies. The solid curves were observed with the small statitron and a slightly thick oxide target on tungsten. The dotted curve was observed later with the large statitron and a slightly thick oxide target on steel.

The expansions in terms of the small quantity V/v_r,

$$\theta_r=\theta+(V/v_r)\sin\theta+(1/6)(V/v_r)^3\sin^3\theta+\cdots,$$

$$g(E,\theta)=1-2(V/v_r)\cot\theta$$
$$+(V/v_r)^2(3\cot^2\theta+\tfrac{1}{2})+\cdots,$$

are also sometimes useful. The last term given may usually be neglected.

RESULTS AND DISCUSSION OF TARGET THICKNESS

In making numerous observations like these it is desirable to strike a compromise between ideal thinness of a target and the demands of intensity. When the original target used in most of the observations was made by oxidizing tungsten to a thickness of about two wavelengths of yellow light, it was not realized that it was anything but ideally thin and no attempt was then made to seek a more appropriate metal. The only criterion used was that the lines seemed to have a width of the order of magnitude of that expected from straggling, and a satisfactory intensity. It turns out that this target is a little thicker than ideal, but the results obtained with it serve to give a good general

view of the variation of angular distribution with energy and are trustworthy except for some slight details. These results transferred to the center-of-mass coordinate system are shown in Figs. 3 and 4. They are also tabulated, along with more recent results, in Table I. The angular distributions shown in Fig. 3, for bombarding energies below 1.15 Mev, were obtained with the small statitron. In this region of energy it seems from these results that there is very little change in the shape of the curves with energy, but only an increase of over-all intensity with energy. The long-range group is predominantly forward and the much more intense short-range group predominantly backward. The results shown in Fig. 4 cover a larger range of bombarding energies and show that the appearance of the angular distributions undergoes wild fluctuations as the energy increases, while the over-all intensity of the long-range group becomes more nearly equal to that of the short-range group. There is a slight semblance of waves of intensity starting at the backward angles and moving forward as the energy is increased.

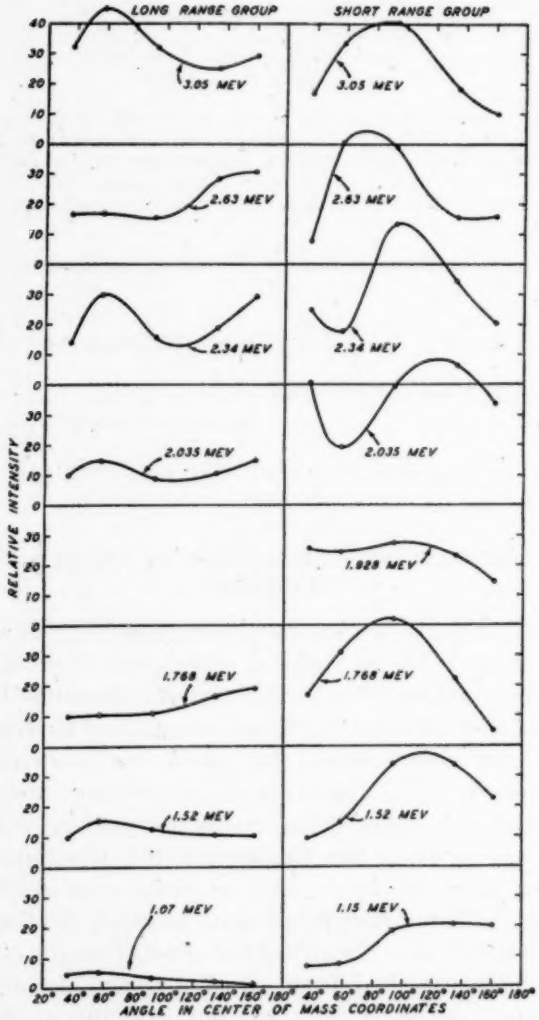

FIG. 4. General trends of the angular distributions over a wide range of energy. Slightly thick oxide targets were used.

The angle of incidence on the target is 22½°, and the most nearly forward angle at which observations were made is 35°, at which position the angle of emergence is as little as 12½°, nearly enough grazing that an appreciable part of the bombarded target area might be eclipsed if the target were microscopically uneven. Such an effect would falsify the angular distribution. To investigate this point, a polished mirror-like steel surface was prepared and oxidized to a dull blue by heating, with the intention to compare results from this with those obtained with the tungsten oxide surface on which most of the observations were made. It was found that this was not really a thin target: the peak width at the 35° position was about twice that at 90°, which latter was about the same as with the tungsten oxide target. (At 1.71 Mev, the short-range peak had a width at half-maximum of 1.2 cm at 90°, 2.4 cm at 35°.) In a repetition of this control experiment, the polished steel was oxidized more lightly, to a very faint bluish tinge, and this oxide layer gave evidence of being thin. The yield with the thin target on steel was about one-fourth that on the slightly too thick layer on steel, and the latter was about the same as that on tungsten in this respect. Observations made with this target are shown in Fig. 5, and also in Table I. These are considered more reliable than the other angular distributions.

ANALYSIS OF THE RESULTS IN ANGLE FUNCTIONS

The theory of the phenomenon here observed is beyond the scope of this paper. We confine ourselves to a few remarks about the formal analysis of the angular distributions in terms of angle functions, for the sake of preliminary orientation toward the theoretical problem. One of the most striking features of the results is the fact that, over a range of low bombarding

energies, the long-range group is preponderantly backward (with a considerable similarity between the one curve and the mirror image of the other). This is probably to be interpreted as arising from constructive and destructive interference of outgoing s and p waves, the phase relation between the s and p waves being different in the short-range and long-range transition.

Unless there be some unexpected selection rule (such as the failure of spin and orbital angular momenta to be mixed in the reaction), one would expect the observed intensity to be the superposition of several intensities each expressible as the square of a wave function corresponding to one arrangement of spin orientations. The rather nearly complete cancellation, at low bombarding energies, of s and p waves to give a markedly reduced intensity at some angle seems to indicate that the intensity arises preponderantly as the square of one wave function, or as the superposition of the squares of several wave functions but with similar angular properties. At some higher bombarding energies no low dip in the intensity appears at any angle, and there is thus no evidence that one wave function or type of wave function predominates. Whether there be one or several components of the intensity distribution, it would be expected that it could be expressed as a sum of terms of the form

$$\sin^m\theta_r \cos^n\theta_r,$$

with the exponents m and n going to values not more than twice the highest orbital angular momentum quantum number involved in the outgoing waves. With five observed values of the intensity, corresponding to the five angles of observation, one has only five values of a continuously varying function with which to determine the arbitrary parameters in terms of which it may be expressed. It would be hoped that there would be fewer than five terms of the above-mentioned form so as to allow some verification of the parameter determination. This does not seem to be the case, so the best one can do is to try to fit the five data with five parameters. This process ordinarily involves the use of fifth-order determinants and correspondingly lengthy computation. The computations are simpler if one limits m to zero and analyzes the intensity in powers of $x=\cos\theta_r$ from the zero power to the fourth power, inclusive. This is done

TABLE IV. Coefficients in some of the expansions in angle functions.

E/Mev Short range	A_0 (α_0)	A_1 (α_1)	A_2 (α_2)	A_3 (α_3)	A_4 (α_4)
0.65	0.61	−1.11	0.74	0.68	−0.29
	(0.28)	(−0.71)	(0.33)	(0.27)	(−0.07)
1.07	14.7	−13.1	−8.6	9.1	5.6
1.07	(12.9)	(−7.6)	(−2.5)	(3.6)	(1.3)
1.785	46.9	5.4	−59.7	−23.7	38.1
3.05	49.7	14.7	−52.0	−21.4	5.7
Long range					
1.07	3.1	4.1	1.7	−4.0	−3.1
	(3.1)	(1.7)	(−0.6)	(−1.6)	(−0.7)
1.785	10.6	−3.3	8.6	−2.3	5.7
3.05	41.0	40.2	10.8	−56.4	−31.7

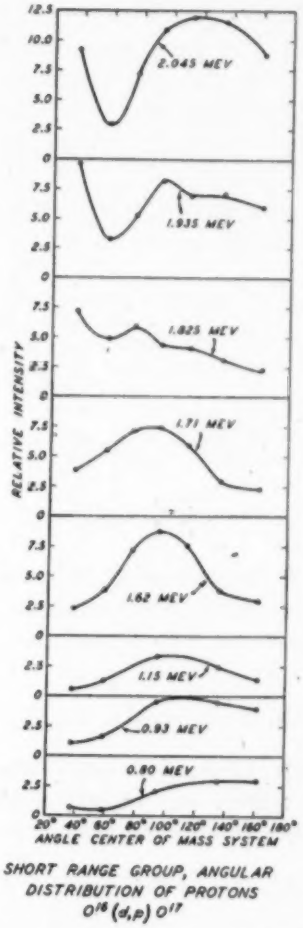

FIG. 5. Angular distributions of the short-range protons observed with a thin oxide target on steel.

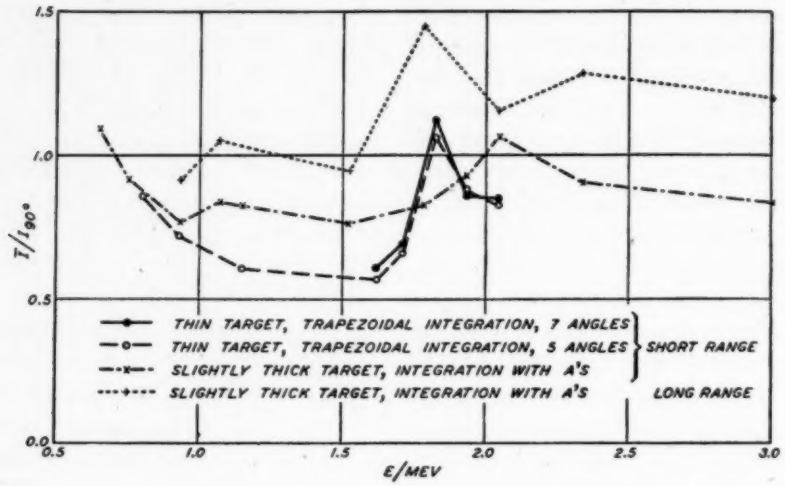

FIG. 6. Average intensity over the entire sphere, relative to the intensity at 90°.

by means of an expansion by products:[8] the five angles at which observations are made are numbered from $n=0$ to 4, and the intensity is written

$$I(x)=a_0+a_1(x-x_1)+a_2(x-x_1)(x-x_2)+\cdots$$

to five terms. Then the a_n are determined by putting $a_0=I(x_1)$, $a_1=(I(x_2)-I(x_1))/(x_2-x_1)$, etc. The terms so obtained are combined to give an expansion in powers of x, and this has in some cases been rearranged to give coefficients of the normalized Legendre functions:

$$I(x)=\sum_{k=0}^{4}A_k x^k=\sum_{l=0}^{4}\alpha_l P_l^0(x),$$

with the P_l^0's of course equal to $2^{-\frac{1}{2}}$, $(3/2)^{\frac{1}{2}}x$, $(5/2)^{\frac{1}{2}}(3x^2-1)/2$, $(7/2)^{\frac{1}{2}}(5x^3-3x)/2$, and $(9/2)^{\frac{1}{2}}\times(35x^4-30x^2+3)/8$, respectively. Some typical samples of the results of this analysis are given in Table IV.

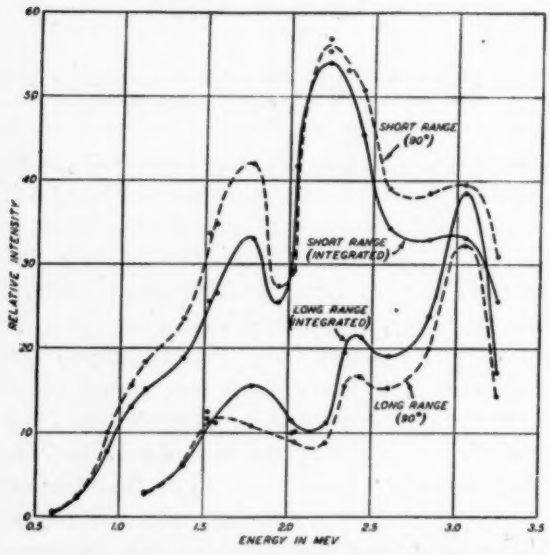

FIG. 7. Excitation curves for the short-range and long-range protons, obtained with slightly thick oxide targets. Both the 90° intensity and the average intensity are shown as functions of bombarding energy.

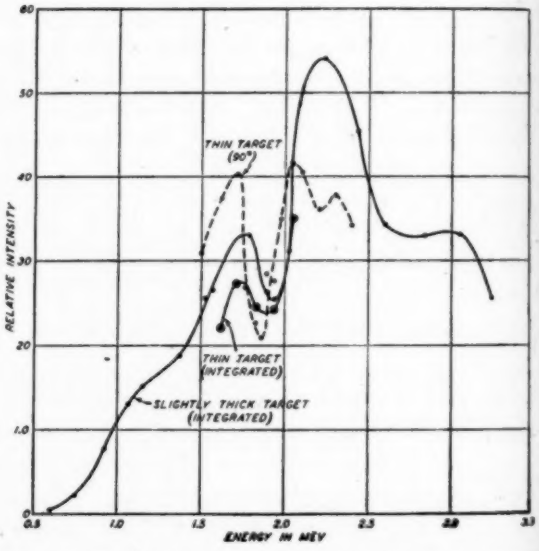

FIG. 8. Excitation curve for the short-range protons, obtained with a thin oxide target on steel. The average intensity curve for the short-range protons from Fig. 7 is repeated here for comparison.

[8] Runge and König, *Numerisches Rechnung* (Julius Springer Verlag, Berlin, 1924), p. 97.

If there were no transitions between incoming deuteron and outgoing proton in which spin and orbital angular momenta were interchanged, then the outgoing waves would have in common with the incoming waves the property of having no component of orbital angular momentum parallel to the axis of incidence, and this is the situation to which our trial analysis in powers of the cosine, or in the P_l^0's, corresponds. One would expect the terms with higher values of l to have extremely small coefficients because of the necessity of penetrating the "centrifugal barrier" (if the process does indeed involve a compound nucleus). That the higher a's and α's do not vanish probably indicates that the analysis should be carried out with a more general expression for the distribution function, including sine terms. This over-simplified analysis on the theoretically untenable hypothesis of very small spin-orbit interaction was tried merely as a preliminary exploration for an unexpected simplicity, so its failure to display convergence is not to be considered in any way disturbing.

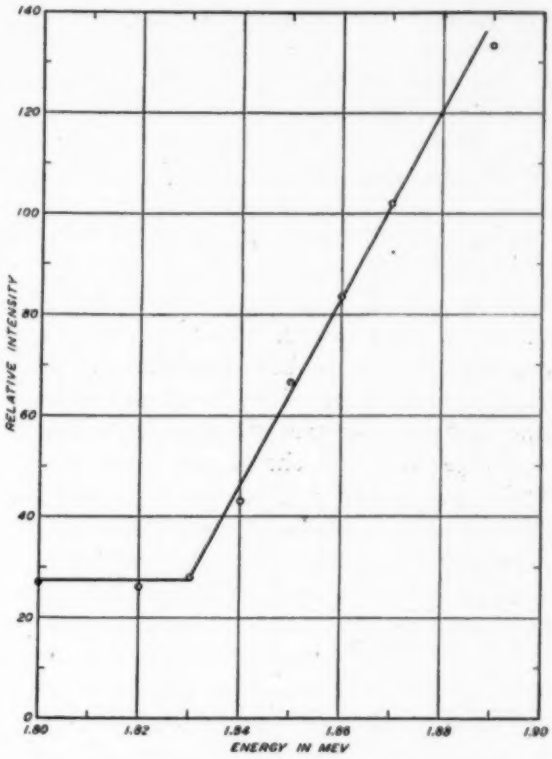

FIG. 9. 90° excitation curve of the competing reaction $O^{16}(d,n)F^{17}$ near its threshold.

INTEGRATED EXCITATION CURVES

The total yield $Y(E)$ of the reaction at a given energy, integrated over all directions of the product particle, may be obtained fairly reliably by interpolation between the five angles at which observations were made (and even more reliably in the cases where seven observations were made). The extrapolation to 0° and to 180° introduces little uncertainty because very little solid angle is involved near the poles. Several methods are available for carrying out the integration. In the cases where the spherical harmonic analysis was carried out, the most reliable integration is considered to be that over the smooth curve through the observed points provided by this analysis:

$$Y(E)=4\pi\bar{I}=2\pi\int_{-1}^{1}I(x)dx=2\pi\sum_{l=0}^{4}\alpha_l^2$$

$$=4\pi(A_0+A_2/3+A_4/5).$$

The demands on accuracy are not so great but that a simple trapezoidal integration may be considered about as satisfactory, and this has been used in cases where the spherical harmonic analysis was not carried out. In the formula used,

$$4\bar{I}=(y_1-y_2)(1-x_1)^2/(x_1-x_2)+y_1(2-x_1-x_2)$$
$$+y_2(x_1-x_3)+\cdots+y_5(x_4+x_4+2)$$
$$+(y_5-y_4)(x_5+1)^2/(x_4-x_5),$$

the first and last terms represent the difference between a linear and a leveled-off extrapolation to the poles and are practically negligible. The results of these calculations of total yield by integration of the intensity over the angles are shown in Fig. 6. The quantity plotted is the average intensity, $\bar{I}$, divided by the intensity at 90°. It is seen that the average intensity is at some energies greater than the intensity at 90°, and at some energies less. The ratio is a convenient quantity because it is a correction factor converting a ninety-degree excitation curve into an integrated excitation curve. At a few energies, observations were interpolated at two additional angles (Table II), and one sees in Fig. 6 that the average intensity obtained by use of all seven angles differs very little from that computed ignoring the extra angles, a fact which gives

confidence in the results obtained from observations at only five angles. One also notes that the peak in the ratio for the short-range curve with a thin target is sharper and lies at about 200-kev lower bombarding energy than the corresponding peak obtained with a thicker target.

As mentioned above, an excitation curve is most reliable if readings are taken consecutively at one angle and a succession of energies. For this reason ninety-degree excitation curves have been observed, as has been customary in investigations not concerned with angular distributions. The ninety-degree excitation curve for the long-range and the short range protons are shown with dotted lines in Fig. 7. Quite interesting structure appears, especially the peak in the short-range curve in the neighborhood of 1.8 Mev. Observations were made with the thin target at more closely-spaced energies near this peak, and in Fig. 8 a separate excitation curve is shown for these. In Figs. 7 and 8 are also shown, in solid lines, the more significant curves representing the average intensity or integrated excitation curve, obtained from the ninety-degree results and from the ratios plotted (with somewhat dubious interpolation at the higher energies) in Fig. 6. It is gratifying to note that the presumably more significant integrated excitation curves display a similarity between the resonances in the short-range and long-range results that was not apparent in the ninety-degree curves.

THE COMPETING REACTION $O^{16}(d,n)F^{17}$

The dip in the excitation curve beyond the peak at about 1.8 Mev comes near the threshold of the competing (d,n) reaction. This reaction was first observed, through the resulting positron activity, by Newson,[9] who found the threshold at about 2 Mev (perhaps 100 kev lower according to newer range-energy information). In order to establish this threshold on the same energy scale used for the (d,p) reaction and thus have a direct comparison with the position of the dip in the excitation curve observations have been made on the neutrons emitted at about 90° to the deuteron beam, from a slightly thick target on steel. A boron-lined ionization chamber was used, surrounded by about 5 cm of paraffin. The neutron intensity thus detected, as a function of bombarding energy, is shown in Fig. 9. The threshold thus determined lies at 1.83 Mev, which is indeed very close to the position of the dip in the short-range excitation curve. Incidentally, this gives

$$Q=-1.615\pm0.01 \text{ Mev}$$

and the mass of F^{17} as 17.007518 ± 0.000015 if we consider our absolute voltage scale[10] to be uncertain by ½ percent. (Here we have taken the deuteron and neutron masses 2.014721 ± 0.000006 and 1.008937 ± 0.000008).

One is tempted to attribute the peak near 1.7 Mev to the cutting of a cravass in an ascending slope by the competing reaction. However, the nature of the angular distributions seems to be compatible with the assumption that the peak is a resonance. If the resonance levels of the compound nucleus are at all separated, one expects from the dispersion formula that one resonance will have a dominant influence on the angular distribution at energies in the immediate neighborhood of that resonance. Since asymmetry about 90° arises from the interference of the outgoing waves from different compound states, one expects approximate symmetry about 90° when one state is dominant. The curves of Figs. 3 and 4 show a tendency to become more nearly symmetrical about 90° as the energy approaches from below the energy of the peak in the excitation curve, which leads one to believe that this peak is due to a resonance, not simply to (d,n) competition.

The one of us from a neighboring institution wishes to thank Dr. J. A. Flemming and Dr. M. A. Tuve, successive directors, for permitting and encouraging his use of the long-productive experimental facilities of the D.T.M. We express our gratitude also to W. D. Whitehead, Jr., for help in making the observations during the last phase of the work, to Mrs. D. R. Inglis for carrying out most of the computations, and to W. A. Higinbotham of the Federation of American Scientists for consultation concerning a circuit.

[9] H. W. Newson, Phys. Rev. **48**, 790 (1935).

[10] O. A. Hanson and D. L. Benedict, Phys. Rev. **65**, 33 (1944).

Angular Distribution from $Li^7(p,\alpha)\alpha$

N. P. HEYDENBURG, C. M. HUDSON,* D. R. INGLIS,** AND W. D. WHITEHEAD, JR.
Carnegie Institution of Washington, Department of Terrestrial Magnetism, Washington, D. C.
(Received October 27, 1947)

The angular distribution of alpha-particles from proton bombardment of lithium has been measured with an ionization chamber and linear amplifier at proton energies of 1.0 to 3.0 Mev. The yield as a function of angle in the center-of-mass system follows the form $Y(\theta)=Y(90°)\times(1+A\cos^2\theta+B\cos^4\theta)$, where the term in $\cos^4\theta$ is clearly present. The value of A shows a resonance peak at about 1 Mev and declines to a low value at 3 Mev. Values of B calculated from the data range from -0.1 to -1.2 but are not sufficiently well resolved to determine their dependence upon bombarding energy.

1. INTRODUCTION

THE angular distribution of charged particles emerging from reactions of light nuclei has been a useful means for distinguishing between various possible nuclear models, and in the case of alphas from the disintegration of Li^7 by protons has been studied by Young, Ellett, and Plain[1] who showed the departure from spherical symmetry in the form $Y(\theta)=Y(90°)(1+A\cos^2\theta)$, with A increasing rapidly from near zero at 0.1 Mev up to their peak bombarding energy of 0.4 Mev. Swartz, Rossi, Jennings, and Inglis[2] found evidence for a resonance near their peak bombarding energy of 0.9 Mev and Rubin, Fowler, and Lauritsen[3] extended the data to 1.38-Mev bombarding energy, locating the maximum value of A at about 1.0 Mev. Both of the latter measurements utilized photographic emulsions to detect the emergent alpha-particles, and were limited to angles in which $\cos^2\theta\lesssim 0.77$.

2. APPARATUS

The present observations were made on the large statitron at the Department of Terrestrial Magnetism with a target chamber having several thin foil windows permitting particles of sufficient energy to escape and be counted by an ionization chamber adjustable in angle with respect to the beam and in air range of the particles being observed. Details of the geometry and of the circuit arrangement are described in a separate paper on $O^{16}(d,p)O^{17}$ since the chamber was first used for work on this reaction. Near the end of the present work four portholes were added, making nine in all, so that the forward angles of large $\cos^2\theta$ could be observed together with additional intermediate angles.

Thin films of lithium were evaporated onto the tungsten plate and used for several runs each. It was intended to measure film thickness by observing the gamma-ray resonance at 440 kev, but obtaining an adequate beam at such low energy proved difficult. From previous measurements on films of comparable length of time for evaporation and yield under bombardment, it is estimated that films were not over 100 kev in effective thickness.

With increasing energy scattered protons from the incident beam began to enter the chamber at backward angles ($\theta=160°$ particularly) in sufficient numbers to jam it for any useful counting, and the thick tungsten target backing could no longer be used. The use of a thick beryllium backing was found to be an adequate precaution for energies close to 2 Mev, but at higher energies too many protons scattered from it, and thin foils first of Al and finally of Be were installed. The latter in particular have proved satisfactory, and in the later runs a thin Li film deposited on thin Be foil was used in a fixed position for particles emitted either forward through the foil or backward.

3. RESULTS

The data as shown in Fig. 1 are based upon approximately 3000 counts per point shown, and

* Office of the Chief of Ordnance, War Department, Washington, D. C.
** Johns Hopkins University, Baltimore, Maryland.
[1] V. S. Young, A. Ellett, and G. J. Plain, Phys. Rev. **58**, 498 (1940).
[2] C. D. Swartz, H. H. Rossi, B. Jennings, and D. R. Inglis, Phys. Rev. **65**, 80 (1944).
[3] S. Rubin, W. A. Fowler, and C. C. Lauritsen, Phys. Rev. **71**, 212 (1947).

often several times that number. Reductions included the inverse-square corrections for adjustments in the range to the ionization chamber, and transformation of the intensities and angles to the center-of-mass coordinate system. The transformed intensities are plotted against $\cos^2\theta$ in this system. In general, as a preliminary to each observation, the ionization chamber was moved through several adjacent ranges and left at the range where the α-particle ionization was at a maximum. In some cases, however, where there was a reliable "plateau" because no disturbing protons or α-particles of different range could enter, the chamber was set closer to the target and thereby data were obtained more rapidly. The input grid bias to the scaling circuit was frequently checked to insure that noise or unwanted particles did not count, and that a margin of sensitivity remained below the normal counts.

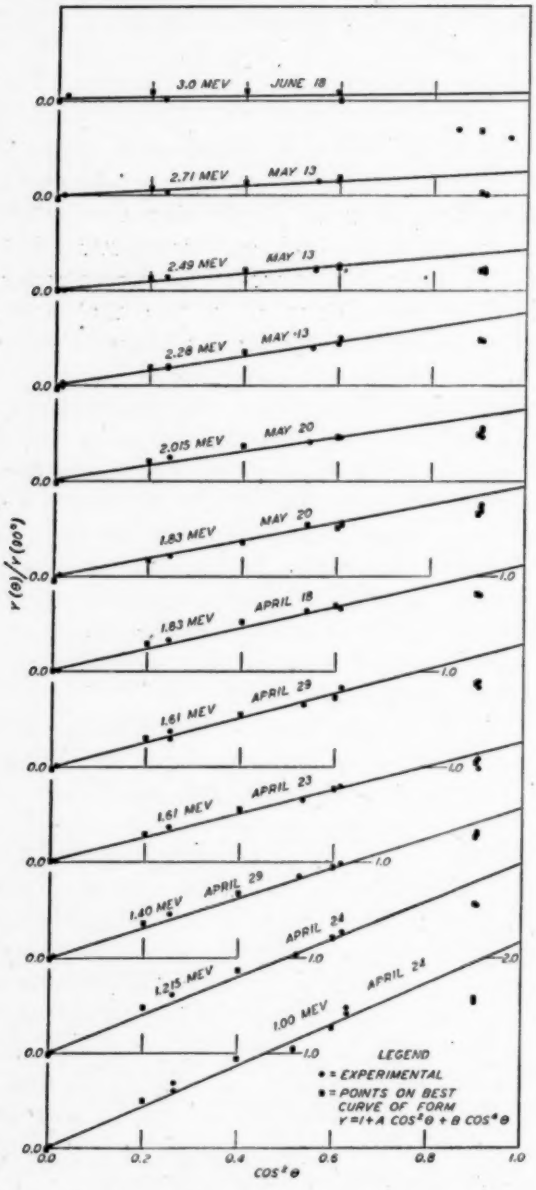

FIG. 1. Relative yields as functions of $\cos^2\theta$ for various proton energies. The angle θ is the deviation from the proton beam in the center-of-mass system. Points marked by a square box are calculated from least-squares fits to the form $Y=1+A\cos^2\theta+B\cos^4\theta$.

In conformity with prior papers, yields are shown, normalized to unity at $\cos^2\theta=0$, as a function of $\cos^2\theta$. The straight lines as shown in Fig. 1 are least-squares or best visual fits neglecting points of $\cos^2\theta>0.7$, to obtain values of A comparable to those found by previous investigators and to show up clearly the consistent departure from linear dependence on $\cos^2\theta$, which may be accounted for by a term in $\cos^4\theta$. Also in Fig. 1 a least-squares fit to the form $Y=1+A\cos^2\theta+B\cos^4\theta$ has been made for each energy and the value of the resulting function plotted at $\cos^2\theta=0$, 0.2, 0.4, 0.6, and 0.9. Values of A and B derived from this are given in Table I.

Figure 2 contains later data, obtained after the additional windows had been added.

In Fig. 3 the values of A are shown as a function of energy from 0 to 3 Mev, with results from previous investigators indicated for comparison. The new values of A here shown are obtained by considering only the values of $\cos^2\theta$ less than 0.7 so as to correspond more nearly to the prior observations. It will be noted that A, as obtained to fit $Y=1+A\cos^2\theta$, neglecting the strongly backward and forward angles, is considerably smaller than the A obtained by fitting the entire run to the parabolic curve $Y=1+A\cos^2\theta+B\cos^4\theta$. This is of course reasonable since the use of a negative B in fitting the points accounts for a considerable change in initial slope.

The dotted line in Fig. 4 shows the intensity at 90° as a function of bombarding energy, with the earlier data[4] matched to the present measurements near 1.0 Mev. The change in slope is

[4] L. R. Rumbaugh, R. B. Roberts, and L. R. Hafstad, Phys. Rev 54, 657 (1938).

TABLE I. Values of A and B to give best fit to form $Y=1+A\cos^2\theta+B\cos^4\theta$ for each run.

Energy in Mev	Date	A	B
1.0	Apr. 24	2.96	−1.27
1.0	July 29	2.02	−0.10
1.0	Oct. 10	1.99	−0.09
1.215	Apr. 24	2.59	−0.92
1.40	Apr. 29	1.94	−0.57
1.40	Oct. 10	2.13	−0.54
1.61	Apr. 23	1.47	−0.38
1.61	Apr. 29	1.80	−0.88
1.61	June 12	1.69	−0.40
1.83	May 20	1.23	−0.44
1.83	Apr. 18	1.58	−0.76
1.83	July 21	1.55	−0.60
2.015	May 20	1.25	−0.75
2.015	June 13	1.36	−0.53
2.28	May 13	1.33	−0.83
2.49	June 19	0.58	−0.35
2.49	May 13	0.82	−0.64
2.71	May 13	0.70	−0.70
3.0	June 18	0.73	−1.20

quite noticeable above 1 Mev, and is, of course, closely related to the changes in A, as shown in Fig. 3. The total yield, integrated over all angles, or the average intensity which is the same within a factor 4π, is a more significant quantity, as was pointed out in the preceding paper, and in this particularly simple reaction it is obtained very easily from the parameters describing the angular distribution by multiplying the ninety-degree intensity by a factor $(1+A/3+B/5)$. The average intensity so obtained is given by the solid curve in Fig. 4.

The Oct. 10 runs at 1.0 and 1.4 Mev were taken with especial care (up to 10,000 counts per point) to check the existence of a B term at low energy, and they were given double weight in averaging results for plotting. The data at 1.215 Mev were much less extensive and were given less weight in the drawing of Fig. 3.

The determination of B is even more sensitive than is the determination of A to small uncertainties in the measured intensities at specific angles, since B is directly related to the curvature of the plot against $\cos^2\theta$, whereas A is directly related to the slope. A conclusive determination of the coefficient B as a function of the energy would require somewhat more exact observation of the angular distributions than we have achieved with our present methods of monitoring and voltage control. This is apparent from the rather broad scatter displayed by the values of B from Table I when they are plotted against

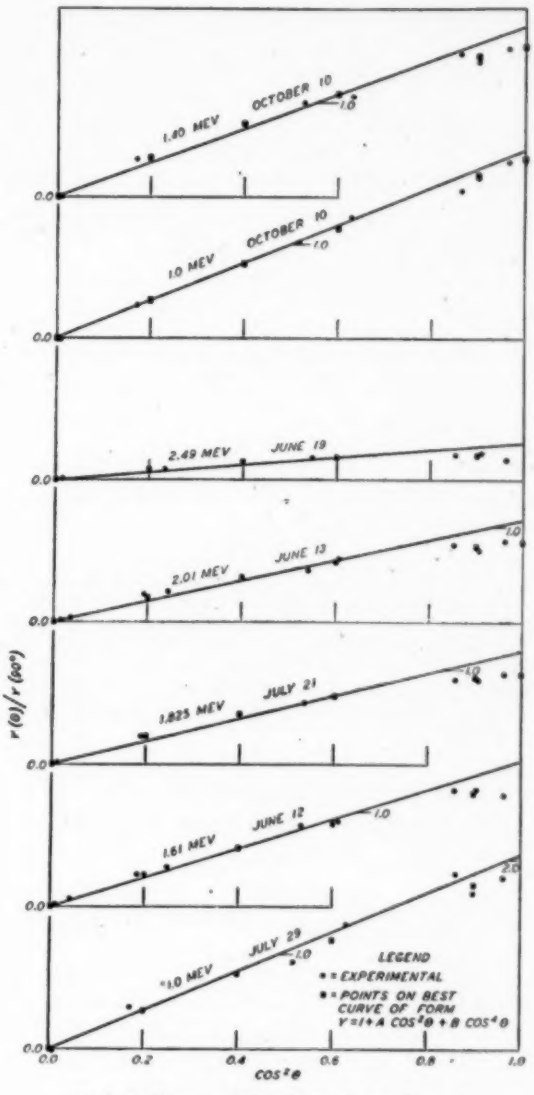

FIG. 2. Same as Fig. 1, for later data.

energy, as in Fig. 5. The most flagrant discrepancy from any possible regularity arises from the large negative value observed at 1 Mev on April 24. Two later measurements at the same voltage, one of them made much more carefully, agree closely on a much smaller negative value of B. It may be noted that the other badly errant point, at 1.215 Mev, was also taken on April 24. We have been unable to find any *a priori* reason to question these two data, and would not feel justified in ignoring them because of their rather wide divergence from the trend of the other data. It is, of course, not impossible that some undiscovered source of systematic

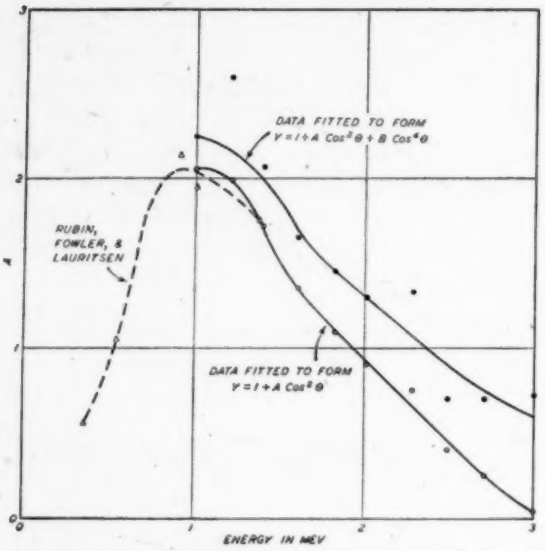

FIG. 3. Values of A as a function of bombarding energy. Data from Rubin, Fowler, and Lauritsen are shown for comparison. The lower curve extending from 1.0 to 3.0 Mev is obtained by best fit to the form $Y=1+A\cos^2\theta$, using only data for $\cos^2\theta$ less than 0.7. The upper curve is obtained by fitting all data for each run to the form $Y=1+A\cos^2\theta+B\cos^4\theta$ and averaging values of A for all runs at a given energy.

error may have been present that day. In view of the theoretical expectation that the $\cos^4\theta$ term, arising from an incoming f wave, should become unimportant at low bombarding energies, it seems appropriate to remark that all data except those taken on April 24 are not inconsistent with a negative value of B which grows from zero just below 1 Mev, and either continues to grow gradually throughout the region up to 3 Mev or levels off in that region. The levelling off is possible because the large negative value of B at 3 Mev is less reliable than the others, having been observed against an especially strong background of scattered protons.

The weighted mean value of B for 1 Mev corresponding to the weighted mean value of A, appearing in Fig. 3, would fall in Fig. 5 at $B=-0.4$, and this would not allow any curve representing B to show a tendency to drop toward zero near 1 Mev. If one were to accept a value of B as small in magnitude as -0.1, he should plot the 1-Mev point in Fig. 3 at $A=2.0$, and this would shift the maximum value of A to a somewhat higher energy.

Observations at the forward angles (from windows at 10°, 20°, 35°, and 75° to the beam) tend to fall in line consistently with those at backward angles, 112.5°, 132.5°, and 160° meas-

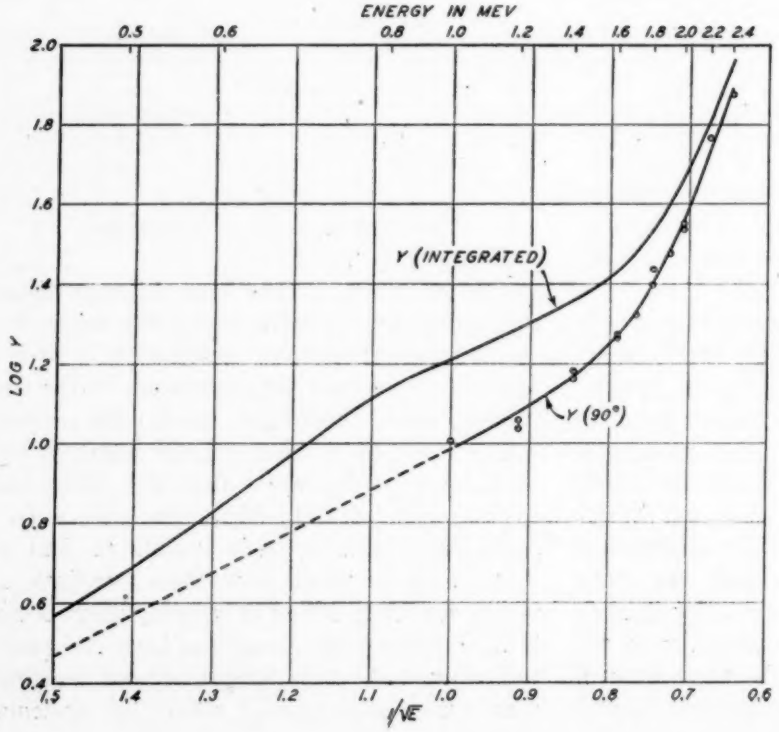

FIG. 4. Yield at 90° as a function of proton energy.

ured on the apparatus. This indicates that no odd powers of $\cos\theta$ appear in the distribution, as demanded by the Bose statistics of the product alphas. A theoretical discussion of the reaction is given by Critchfield and Teller,[5] who also questioned whether further experiment might not show up terms of higher power than $\cos^2\theta$.

Data were not discarded without experimental basis except for one erratic run at 1.4 Mev which could have been due to error in some one point. A run including all nine values of $\cos^2\theta$ at 1.0 Mev placed all nine points consistently but is not presented in Fig. 2 because it was later discovered that the lithium had been evaporating from the aluminum target backing during bombardment. The change, which was indicated to exceed 10 percent during the run, would give a misleading appearance to the data, in particular to the curvature.

The above data suffice to show unmistakably the presence of an even-powered term higher than $\cos^2\theta$ and give its sign and approximate magnitude, but do not resolve the energy dependence if any of that term. The $\cos^2\theta$ term is shown to exhibit a resonance at 1.0 Mev and to drop to a small value at 3.0 Mev.

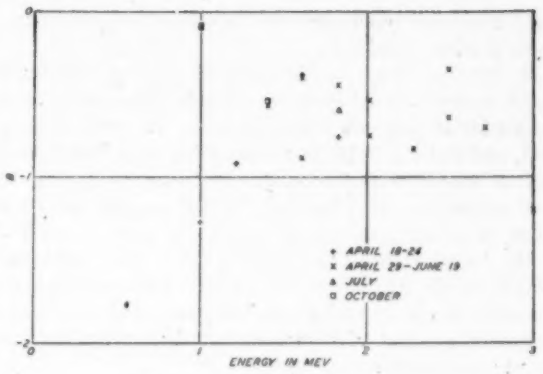

FIG. 5. Observed values of B.

We are grateful to Dr. Hugh Bradner, of the Radiation Laboratory of the University of California at Berkeley, for generously supplying thin Be foils of a type developed for the linear accelerator there.

[5] C. L. Critchfield and E. Teller, Phys. Rev. 65, 10 (1941).

PHYSICAL REVIEW VOLUME 73, NUMBER 3 FEBRUARY 1, 1948

The Cosmic-Ray Counting Rate of a Single Geiger Counter from Ground Level to 161 Kilometers Altitude

J. A. VAN ALLEN AND H. E. TATEL*
Applied Physics Laboratory, Johns Hopkins University, Silver Spring, Maryland
(Received October 16, 1947)

The cosmic-ray counting rate of a single Geiger counter has been measured from ground level to an altitude of 161 kilometers. The equipment was carried in a V-2 rocket at geomagnetic latitude $\lambda = 41°$N. Especial care was taken to avoid multiplicative effects from surrounding material. A value of the charged primary cosmic-ray flux of $j = 0.12$/sec./cm²/steradian, averaged over the upper hemisphere, is implied by the data above 55 km. This interpretation of the counting rate must be qualified by the as yet unknown contribution from secondaries which emerge from the atmosphere and execute orbits in the earth's magnetic field.

1. INTRODUCTION

THIS is one of a series of reports on cosmic ray experiments conducted by this laboratory in flights of V-2 rockets during the past year and a half. The data presented herein were obtained during the flight of July 29, 1947. They are believed to be reliable but are provisional in the sense that they have been obtained in only one flight. A description of this work is thought to be worthwhile at this time for several reasons:

(a) No previous comparable data are known to us.
(b) The technique of using high altitude rockets as vehicles for scientific measurements is not as yet very generally known.

* Now at Department of Terrestrial Magnetism, Carnegie Institution of Washington, Washington, D. C.

(c) The next opportunity for repeating these measurements is some time away.

(d) Previous data on the counting rates of single and double counters *vs.* altitude have been obtained by us in V-2 flights on July 30, 1946, December 17, 1946, April 1, 1947, and April 8, 1947. The counters in these flights were parts of another experiment, which will be reported in the near future. In these previous flights no such care was taken to separate the counter from the mass of material in the rocket itself. The counting rates were, therefore, influenced to an important extent by multiplicative processes in the immediate environment. The results are in general support of those reported herein but are not strictly comparable.

The specific objective of this experiment was to learn the counting rate of a single Geiger counter as a function of altitude and especially at altitudes sufficiently great to be considered "above the atmosphere." Particular care was taken to approach the ideal of an unshielded counter, isolated from all other material. Implications as to the absolute flux of charged cosmic ray primaries are discussed. A tentative flux figure is given on the basis of this discussion.

2. APPARATUS

The arrangement of apparatus is shown in Fig. 1. The Geiger counter P and the bundle of three Geiger counters Q, with a minimum of electronic and other associated equipment, were located in a long cylindrical cloth-filled bakelite tube affixed to the forward end of the missile by dural fittings. The cylinder was surmounted by a wooded cone, and was sealed airtight. The materials used were of minimum thickness, density, and atomic number, consistent with the physical strength required to resist the estimated aerodynamic forces during passage through the atmosphere. The counters P and Q were rigidly supported by a light fiber framework and were packed in glass wool. The 0.4 mm copper lining of the bakelite cylinder was introduced as an r.f. shield against pulses from the various ground and missile-borne radar equipments involved in tracking the missile.

The Geiger counter P was the heart of the apparatus. Its counting pulses were applied to two independent scale-of-eight circuits, whose output pulses were broadened and shaped for characteristic appearance, then applied to the radio telemetering set provided by the Naval Research Laboratory.[1] Pulses were recorded by ground stations during the flight on photographic film moving at the rate of three inches per second and were subsequently analyzed by visual count of the film.

Although it was believed that counter P was already well isolated from the rocket by geometrical considerations, the further bundle of three counters Q was, at the suggestion of Professor Schein, located so as to intercept all except a small fraction of charged particles coming from the warhead and rocket proper. Double coincidences PQ were likewise telemetered.

Significant electronic characteristics of the circuits used are as follows:

(a) By means of an "addition of (radium) sources" test, it was shown that the loss of counts of the over-all system due to resolving time of the scale-of-eight circuit and pulse forming circuit, and the reading of telemetering film was less than 1 percent at a rate of 100 counts/second. This rate was much higher than the highest observed in flight. The measured counter dead time was 400 microseconds.

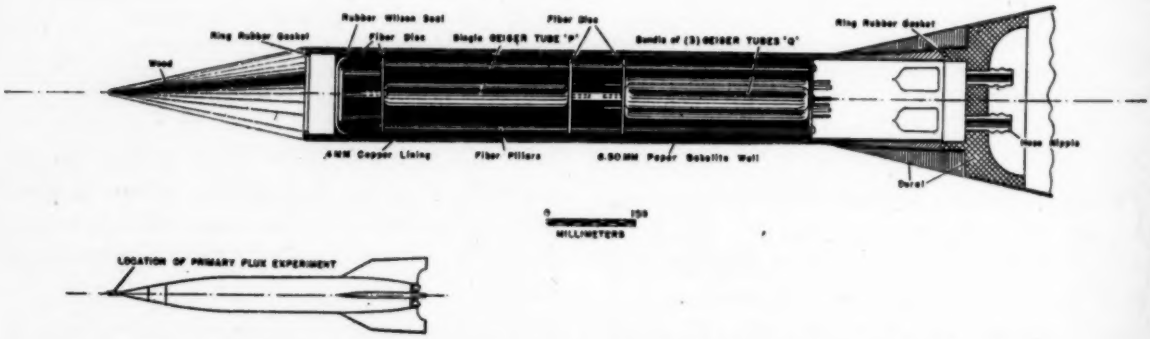

FIG. 1. Diagram of equipment, drawn to scale and showing location in V-2 rocket.

[1] V. L. Heeren, C. H. Hoeppner, J. R. Kauke, S. W. Lichtman, and P. R. Shiffleit, Electronics (March and April, 1947).

(b) The resolving time of the PQ circuit was measured as 5 microseconds by means of a "double pulser" giving two simulated Geiger pulses separated by an adjustable time interval. The resolving time was further checked by determining the increase in counting rate of the over-all coincidence system when the individual rates of P and Q were increased to 40 counts/second and 120 counts/second, respectively, by a suitably located 20 microgram radium source. A figure of 7 microseconds was obtained. During this latter measurement all equipment was operating on internal power with all voltages in final adjustment.

(c) Particular care was taken in assuring the constancy of all measured rates under a considerably wider variation of supply voltages than could reasonably be expected in flight. The Geiger voltage was supplied by a wax-potted stack of Minimax dry batteries. All circuit power was obtained from non-spillable Willard storage batteries and from dynamotors driven from them. The internal power supply operated all equipment satisfactorily for up to a half hour in laboratory tests. In final use it was run for five minutes on the launching platform immediately before take-off and for six minutes of flight.

(d) No amplitude-accuracy requirements were made on the telemetering system nor on any other part of the circuit. The characteristically shaped telemetered pulses were easily recognized in the presence of radio interference. In this flight, however, an exceptional clean telemetering record was obtained during all portions of the flight for which data are reported and the genuineness of all pulses is believed beyond question.

(e) The rate of P was obtained through two independent scaling circuits, pulse forming circuits, and telemetering channels. These rates were in complete agreement for all portions of the flight reported.

(f) The four Geiger counters were selected from a batch prepared to our specifications by the Geophysical Instrument Company of Arlington, Virginia. They were of "all metal" type with 0.8 mm thick copper walls, 0.10 mm tungsten wires, filled with a mixture of 10 cm argon and 1 cm absolute ethyl alcohol. The active volume of the counters was taken from geometrical construction as a cylinder 15.0 cm long and 2.38 cm in diameter. The counting rate due to a radium source *versus* voltage for the P tube is shown in Fig. 2. It will be noted that there was a slope of 3 percent per 100 volts in the operating region. As used, 15 volt pulses were obtained on the grid of the first tube. In auxiliary experiments the efficiency of these tubes for cosmic-ray particles was tested in coincidence telescopes and found to be greater than 99.3 percent. No appreciable effect on the counting rate of temperatures between 10°–100°C has been found.

3. FLIGHT OF THE MISSILE

The rocket[2] left the White Sands Proving Ground launching platform at 5:55 A.M. on July 29, 1947. (Geomagnetic Latitude 41°N.)[3] The propulsive period terminated at 63 seconds time of flight, altitude 37.5 km., velocity 1510 meters/second. During this period, except for a brief stabilizing period during the first five seconds, the axis of the missile did not deviate from the vertical by more than 6°.

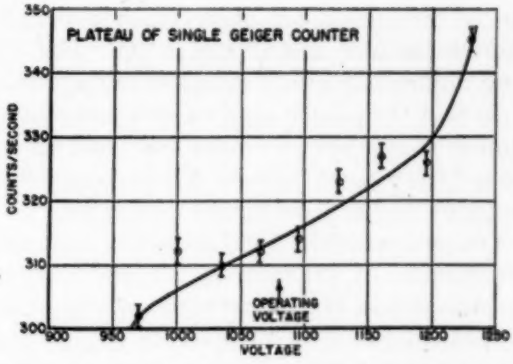

FIG. 2. Plateau of Geiger counter P, shown on enlarged vertical scale. The operating voltage in flight was 1080 volts.

Arrays of high power photo-theodolites and radar sets of the U. S. Signal Corps and the Ballistic Research Laboratories of the Aberdeen Proving Ground provided tracking data on the missile throughout flight.[4] This particular missile flew in a near vertical trajectory. A composite replot of the altitude-time data, kindly provided us by the B.R.L., is shown in Fig. 3. The accuracy of these data considerably surpasses the needs of this experiment. Note that the launching platform is at altitude 1.22 km. Time signals of the B.R.L. master oscillator were transmitted to all tracking stations and to the telemetering stations. It was thus possible to assign accurate altitude values to any time interval on the telemetering record.

At fuel burn-out the aerodynamic trim tabs were thrown "hard over" in order to augment the rate of roll of the missile expected from the slight measured fin asymmetry and to thus provide a measure of stabilization during the vacuum flight. By means of a photoelectric cell system, a roll period of six seconds was observed to have been produced. The zenith angle of the

[2] For description of the V-2, see H. S. Siefert, M. M. Mills, and M. Summerfield, Am. J. Phys. 15, 1, 121, 255 (1947) and J. M. J. Kooy and J. W. H. Uytenbogaart, *Ballistics of the Future* (Tech. Pub. Co. H. Stam, Haarlem, Holland, 1946).

[3] A. G. McNish, Terr. Mag. 41, 37 (1936); T. H. Johnson, Rev. Mod. Physics 10, 193 (1938).

[4] L. A. Delsasso, L. G. de Bey, and D. Reuyl, "Full-Scale Free-Flight Ballistic Measurements of Guided Missiles," Ballistic Research Laboratories, Aberdeen Proving Ground.

axis of the missile was observed by two B.R.L. photo-telescopes, a 4.5″ and a 10″. The data[5] were unfortunately not complete but sufficed to show that the missile began a slow end-over-end tumble soon after fuel burn out, had its nose toward the ground by about 110 seconds (94 km. altitude), and was continuing to tumble.

The peak altitude, 161 kilometers, occurred at 224 seconds. At 361 seconds, the forward part of the missile was severed from the after part by a distributed charge of two pounds of high explosive, detonated by radio command. This segregation of the missile was accomplished in order to improve the likelihood of recovering photographic film which was part of another experiment. No data were obtained beyond this time.

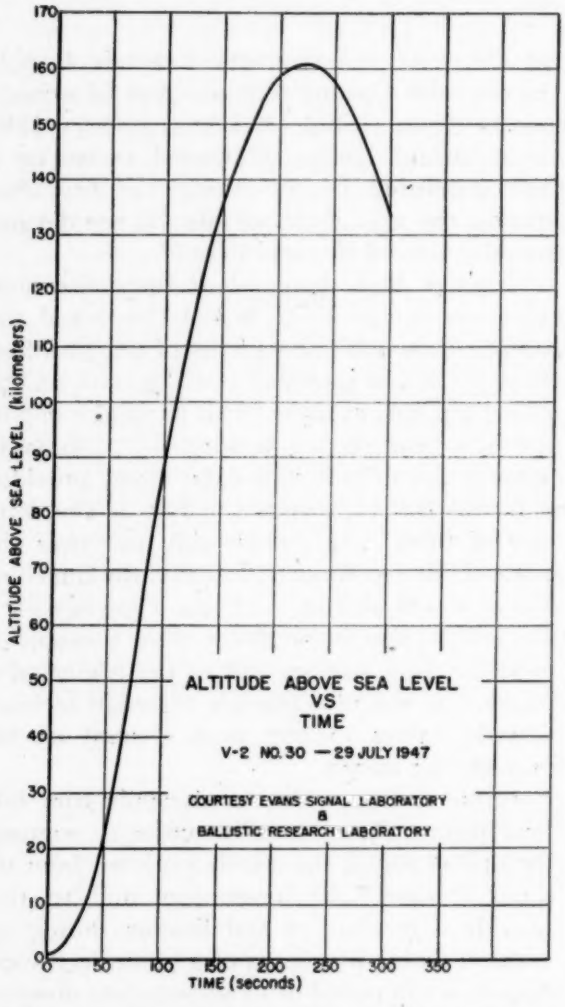

FIG. 3. Observed altitude above sea level *versus* time. Extrapolation of the curve to warhead blow-off (361 seconds) can be done with adequate accuracy by assuming free vacuum fall.

[5] Courtesy of Dr. D. Reuyl, Ballistic Research Laboratories, Aberdeen Proving Ground.

4. DATA

In Silver Spring, Maryland, altitude 0.12 km., with the apparatus vertical in a laboratory covered overhead by about 15 gm/cm² of concrete and wood, the rate of P was 1.39 ± 0.01/sec.; the rate of Q, 3.30 ± 0.05/sec.; and the rate of PQ, 0.0075 ± 0.0025/sec.

At White Sands Proving Ground, altitude 1.22 km., with all apparatus fully assembled onto the rocket nose in a thin roofed Quonset hut and in the open on the launching stand, the respective rates of P, Q, and PQ were 1.75 ± 0.01/sec., 3.49 ± 0.12/sec., and 0.010 ± 0.001/sec.

During 110 seconds of recorded data just before take-off the rate of P was checked at 1.75 ± 0.09/sec. Two PQ counts were obtained during this interval.

Data in flight from 0 to 360 seconds were obtained with the exception of a period between 15 and 28 seconds, portion of the period 143 to 214 seconds and portion of the period 320 to 360 seconds. In the earlier omitted period a large number of spurious counts was recorded by one scaling circuit, only a few by the other. It has been tentatively concluded that this was due to excessive vibration of the long cylinder during its passage through the trans-sonic aerodynamic region. Considerable noise on ionization chamber high gain amplifier channels was also noted in this well defined period. In the 143–214 second and the 320–360 second periods, the record was clearly readily in short sections totaling about one-half of the length of the periods.

Reading of the telemetered record is summarized as follows:

−110 to +15 seconds	Continuous
15 to 28 seconds	No data
28 to 143 seconds	Continuous
143 to 214 seconds	Partial
214 to 320 seconds	Continuous
320 to 360 seconds	Partial

In Fig. 4 are plotted the data on the counting rate of P versus altitude. The vertical bars indicate the statistical probable error of each point. A pressure scale in gm/cm² was derived

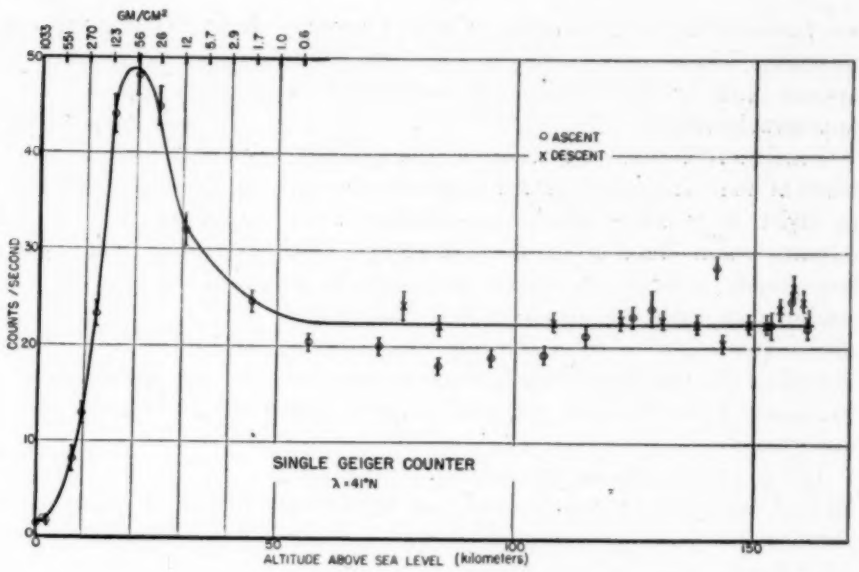

FIG. 4. Plot of the counting rate of Geiger counter P *versus* altitude above sea level. The curve has been drawn flat from 55 km to 161 km at the arithmetic mean counting rate above 55 km.

from standard tables[6] and is indicated at the top of the figure. Although the statistical accuracy of the various points is not sufficient to establish any fine features of this curve, the main features are unmistakable.[7]

A peak counting rate of about 49/second is reached at 19.8 km. (58 gm/cm²). The counting rate then falls off progressively. Between about 55 km. and the highest altitude reached, 161 km., there is a reasonably flat plateau. The average of all data in this range (5048 counts) is 22.4 ± 0.2 counts/second.

In Fig. 5, the smooth curve of Fig. 4 has been transformed to a pressure basis. Aside from the addition of the previously unknown point on the zero pressure axis, the curve resembles those of previous workers.[8] It may be noted that a single counter, being an omnidirectional detector, shares the physical characteristics of an ionization chamber more nearly than that of a counter telescope.[9]

The counting rates of the double coincidence set PQ are summarized in Table I. (A slight reduction of the observed counting rates for the two highest altitude points has been made for the finite resolving time of the coincidence set mentioned above.)

Thus, it is clear that the counting rate of the P tube is not appreciably influenced by stray effects from the rocket itself. The PQ rate is about 1 percent of the P rate in the "plateau" region.

Indeed, the rocket subtended a total solid angle of less than 1 percent of 4π at P.

With regard to vitiating effects of the immedi-

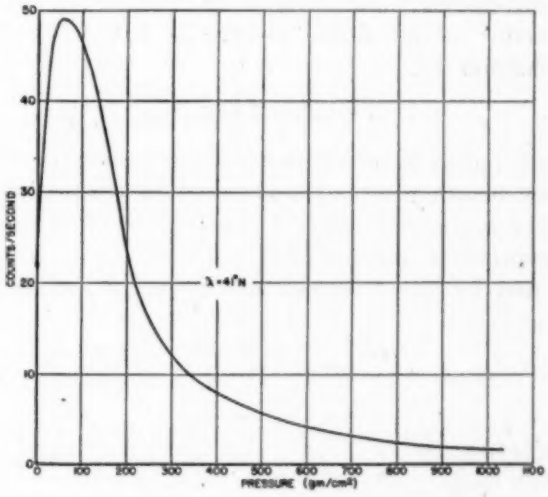

FIG. 5. Counting rate of Geiger counter P *versus* atmospheric pressure in units of gm/cm². This is a smoothed transformation from Fig. 4.

[6] Walter S. Diehl, "Standard Atmosphere—Tables and Data," N.A.C.A. Report No. 218; Calvin N. Warfield, "Tentative Tables for the Properties of the Upper Atmosphere," N.A.C.A. Technical Note No. 1200.

[7] This curve is in striking disagreement with the results of L. F. Curtiss, A. V. Astin, L. L. Stockman, B. W. Brown, and S. A. Korff, Phys. Rev. **53**, 23 (1938).

[8] I. S. Bowen, R. A. Millikan, H. V. Neher, Phys. Rev. **53**, 855 (1938).

[9] H. V. Neher and W. H. Pickering, Phys. Rev. **61**, 407 (1942).

ate surroundings of P, nothing is known experimentally. Yet an examination of Fig. 1 makes it appear unlikely that there could have been an appreciable effect.

Considerable care was taken in the arrangement of the counters to assure thermal isolation in flight. It is quite difficult to simulate aerodynamic skin heating in the laboratory. We have made a series of furnace tests which, in conjunction with the appearance of the equipment after recovery from the impact, has convinced us that no appreciable increase in spurious background should have occurred at any time in flight.

The apparent dip in the rate of P at about 80 km. during the ascent was not confirmed on the descent. It may be remarked that a somewhat similar dip has been suspected in the data of previous flights—flights in which the counters enjoyed much more complete thermal isolation.

From an over-all view, a slight reservation in judgment must be held on the subject of thermal effects. But it was especially clear from the furnace tests that no appreciable rise in temperature of the counters could have occurred as soon as 100 seconds. Therefore, a plateau rate of about 19/second is as low a value as would be admitted by present knowledge.

5. DISCUSSION OF DATA AND CONCLUSIONS

The counting rate of a single Geiger counter of unit efficiency for an ionizing ray crossing any portion of its active volume of length l and diameter a is

$$N=\tfrac{1}{2}\pi^2 alj(1+a/2l)$$

in a region in which the flux j is constant over one hemisphere and zero over the other hemisphere, a result which is independent of counter orientation (see Appendices I and II). As indicated by the foregoing discussion of the data from PQ, it seems safe to assume that this result is also independent of missile orientation in the plateau region.

If one neglects the counter's spurious background (which could scarcely exceed 0.5/sec.) and naively assumes that the observed plateau counting rate $N=22.4$/second arises from an isotropic charged primary flux over a hemisphere, then the result is

$$j=0.12/\text{sec.}/\text{cm}^2/\text{steradian}.$$

If the lower value of $N=19$/sec. (discussed above) be used, we find

$$j=0.095/\text{sec.}/\text{cm}^2/\text{steradian}.$$

Either of these values is more than twice the flux inferred from the measurements of Millikan and co-workers.[10]

A rough independent check on the operation of the P counter is provided as follows: Mr. J. F. Jenkins of this laboratory has measured with a counter telescope at the same geomagnetic latitude as White Sands the total flux at zenith angle zero from ground level to an altitude of 9.15 km.[11] Combining these flux figures, extrapolated, and Swann's zenith angle dependence of flux data,[12] we find that a P counting rate of 19/second should be expected at an altitude of about 11.3 km. This result is in satisfactory agreement with the results as shown in Fig. 4.

Measurements such as those reported herein should eventually yield an estimate of the loss of energy into secondary forms which are not revealed by ionization in the atmosphere and should provide direct information on the multiplication of the primary radiation. As yet it seems premature to attempt such interpretations until the contribution of re-entrant secondaries can be ascertained.[13]

TABLE I. Counting rate of PQ.

Place	Geomagnetic latitude	Altitude	Rate
Silver Spring, Md. (Ground level)	50°N	0.12 km	0.0075±0.0025/sec.
White Sands Proving Ground, New Mexico (Ground level)	41°N	1.22	0.010±0.001
In flight		1.2–13	0.025±0.017
		13–27	0.47±0.12
		27–161	0.17±0.02

6. ACKNOWLEDGMENTS

This work has been made possible by the support of the Navy Bureau of Ordnance under

[10] For example, T. H. Johnson, Phys. Rev. 53, 499 (1938); M. Schein and D. J. Montgomery, "Problems in Cosmic Ray Physics," 1946 Princeton Lectures.

[11] Equipment carried in a B-29 airplane (to be published).

[12] W. F. G. Swann, Rev. Mod. Phys. 11, 242 (1939).

[13] H. Kulenkampf, Naturwiss. 21, 25 (1933); T. H. Johnson, Phys. Rev. 56, 226 (1939); W. F. G. Swann, Rev. Mod. Physics 11, 242 (1939); G. J. Perlow and J. D. Shipman, Jr., Phys. Rev. 71, 325 (1947).

Contract NOrd 7386. The opportunity for conducting these experiments in the current series of V-2 firings is due to the Army Ordnance Department and to the White Sands Proving Ground. Time signals and missile tracking were provided by the Ballistic Research Laboratories of the Aberdeen Proving Ground and the Army Signal Corps. The cosmic-ray data were transmitted and received through the excellent telemetering equipment of the Naval Research Laboratory.

We are indebted to Professor M. Schein for several opportunities to discuss cosmic-ray problems during the past year.

Finally, the accomplishment of this experiment was in no small measure due to our associates of the Applied Physics Laboratory, in particular Messrs. L. W. Fraser and J. F. Jenkins.

APPENDIX I

Calculation of the counting rate N of an idealized Geiger counter of diameter a, length l, in a field of charged particles of flux j, isotropic over one hemisphere, zero over the other:

Case 1. *Axis of the tube parallel to the axis of the hemisphere.*

$$N=\int_{\text{Hemisphere}} j\cdot A\cdot d\Omega$$

with A being the projected area of the cylindrical counter on a plane perpendicular to the direction along which the elementary solid angle $d\Omega$ lies. If θ be the angle from the axis of the cylinder to this direction,

$$N=j\int_0^{\pi/2}(\pi a^2/4\cos\theta+al\sin\theta)2\pi\sin\theta d\theta,$$

$$N=\tfrac{1}{2}\pi^2 alj(1+a/2l). \tag{1}$$

Case 2. *Axis of the tube perpendicular to the axis of the hemisphere.*

Similarly to the above

$$N=j\int_0^{\pi/2}(\pi a^2/4\cos\theta+al\sin\theta)\pi\sin\theta d\theta$$

$$+j\int_{\pi/2}^{\pi}(-\pi a^2/4\cos\theta+al\sin\theta)\pi\sin\theta d\theta.$$

The result is identical to that of Case 1.

Case 3. *Axis of the tube at an arbitrary angle to the axis of the hemisphere.*

By simple geometric visualization, it is clear that this general case can be reduced to Case 1. Hence, we conclude that the counting rate of an idealized Geiger tube in a hemispherically isotropic field is independent of orientation and is given by Eq. (1).

APPENDIX II

The conclusions of Appendix I can also be reached by a general argument which applies equally well to a counter volume of any shape, provided the surface is everywhere convex outward. This treatment was suggested to us by Drs. H. E. Newell and N. M. Smith.

Thus the basic integral

$$\int_{\text{Sphere}} j\cdot A\cdot d\Omega$$

yields, in a *spherical* isotropic field,

$$N=\pi jS,$$

in which S is the total surface area of the counter volume.

Inasmuch as the integration involves equal contributions from diametrically opposite directions, the result for a hemisphere is

$$N=1/2\pi jS,$$

independent of orientation of the counter volume. In the case of a cylindrical counter Eq. (1) is obtained as by Appendix I.

Some Isotopes of Platinum and Gold

GEOFFREY WILKINSON
Department of Chemistry and Radiation Laboratory, University of California, Berkeley, California
(Received December 22, 1947)

A SURVEY of the lighter radioactive isotopes of platinum and gold has been made. Using the 60-inch Crocker Laboratory cyclotron, bombardments were made of iridium, with 38-Mev helium ions and 18-Mev deuterons, of platinum with 18-Mev deuterons, fast and thermal neutrons, and of gold with fast neutrons. After bombardments, the metal targets used were dissolved and radioactive isotopes separated by the usual carrier techniques. Iridium metal was dissolved by heating for a few hours at 300°C, with strong hydrochloric acid and sodium chlorate in a sealed tube.[1] Chemical separations of osmium, iridium, platinum, and gold were made using variations of the basic procedures: (*a*) distillation of osmium as tetroxide from nitric acid solution, (*b*) ethyl acetate extraction of gold in the oxidized state, with reduction to the metal by sulfur dioxide, (*c*) ethyl acetate extraction of platinum in the divalent state after reduction by stannous chloride,[2] (*d*) precipitation of iridium as potassium chloroiridate or as the dioxide.

Table I summarizes the properties of the longer lived gold and platinum isotopes of mass below 197, which have been here studied. The radiations are consistent with the assumption of decay by orbital electron capture, electrons arising from gamma-ray conversions in transitions from excited states of the product nuclei. Electron and soft electromagnetic radiations were resolved using the technique of differential absorption in the thin foils of aluminum and beryllium. Energies of radiations were obtained from absorption measurements.

In addition to the isotopes listed, the previously known[3] activities of Ir^{192} (70 days), Ir^{194} (19 hours), and Pt^{197} (18 hours), Pt^{199} (31 minutes) were obtained in good yields by d, p reactions on iridium and platinum. In addition, very low yields of Os^{191} (32 hours), Ir^{192}, and Ir^{194} were observed by the respective d, α reactions in iridium and platinum.

4.33-day platinum.—A platinum isotope with radiations similar to the one now observed has been reported previously[4] and allocated to Pt^{197}, but a half-life of about three days was given. In the present work the electrons and quantum radiation decay with the same half-life which has been measured through fourteen half-lives. The activity is attributed to Pt^{193} decaying by orbital electron capture for the following reasons. The isotope is formed in the deuteron, fast and thermal neutron bombardments of platinum, and also in the deuteron and α-particle bombardments of iridium in yields agreeing with allocation to mass 193. No iridium daughter activity of half-life greater than a few minutes has been found. There is no evidence for its formation in the decay of Ir^{194}. Separation of platinum from the gold fractions of both Pt+d and Ir+α bombardments show the growth of the 4.3-day activity from a parent of half-life 16±1 hours.

3.0-day platinum.—Previously unreported, this isotope which is distinguished from the 4.3-day isotope by its 0.5-Mev electron and strong 0.57-Mev γ-ray has been observed in low yield in Pt+d, Pt+fast neutron, and Ir+α bombardments, but in a yield comparable to that of the 4.3-day activity in the deuteron bombardment of iridium. No daughter activity has been observed. Growth of the 3.0-day activity from a parent of ~1-day half-life occurred in gold fractions from both Pt+d and Ir+α bombardments, together with the 4.3-day activity, but in a much lower yield. The electrons and electromagnetic radiation decay with the same half-life which has been followed through eight half-lives. The activity has been assigned provisionally to mass 191.

If the 3 and 4.3-day activities are correctly allocated to masses 191 and 193, respectively,

[1] E. Wichers, W. G. Schlect, and C. L. Gordon, Bur. Stand. J. Research **33**, 363 (1944).
[2] H. Wöbling, Ber. **67**, 773 (1934).
[3] G. T. Seaborg, Rev. Mod. Phys. **16**, 1 (1941).
[4] a. R. S. Krishnan and E. A. Nahum, Proc. Camb. Phil. Soc. **37**, 422 (1941); b. E. M. McMillan, M. Kamen, and S. Ruben, Phys. Rev. **52**, 375 (1937).

no activity of Pt^{190} formed by Ir d, $3n$ reaction has been observed, although this reaction would be expected to occur; the 10.7-day Ir^{190} isotope[5] which should be present in the iridium fraction if Pt^{190} had a short half-life was not found. Pt^{190} might be expected to have a long life and the results thus are not inconsistent with this consideration.

190-day gold.—A long-lived gold activity has been detected previously,[4a, 6] but has not been adequately characterized. This activity is produced in high yield in both Pt+d and Ir+α bombardments. The radiations and decay appear identical in both cases, but measurements have been made as yet only through just over one half-life. A sample of ~0.4-millicuries strength with high specific activity was prepared from a platinum target which had received 492 microamperes of deuterons over a period of three months, and had been decaying for four months. No evidence of any activities of half-lives between those of the 5.5-day and 190-day isotopes has been found, and the radiation characteristics of this sample are identical with the long-lived activity from the other bombardments. The sample has been studied on a "magnetic" counter. No positron emission, but only a single peak of conversion electrons has been observed. Chemical separation showed no evidence for any platinum daughter of half-life greater than about thirty seconds. Allocation to mass 195 is consistent with the yields and the half-life is consistent with expectations for a gold isotope of this mass number.

39.5-hour gold.—Previously unreported, this activity is formed in high yields in Pt+d and Ir+α bombardments. Chemical separations give no evidence of a platinum daughter activity of half-life greater than a few minutes.

15.8-hour gold.—Evidence for a gold isotope of half-life 16±1 hours, parent of the 4.3-day Pt^{193} was obtained in chemical separations from gold fractions of Pt+d and Ir+α bombardments and decay of the gold fraction in the latter showed an activity of 15.8-hours half-life. A half-life for Au^{193} longer than 16 hours and of the order of days might have been expected from considera-

TABLE I.

Element	Probable mass number	Half-Life	Energy of radiations (Mev) Particles	γ-Rays	Probable mode of formation
₇₈Pt	191	3.00±0.02 d	0.5	x-rays	Ir-d-2n
				0.57	Au (~1 day) decay
				1.8	Pt-n-2n
	193	4.33±0.03 d	0.10	x-rays	Ir-d-2n, Ir-α-p-2n
				1.7	Au (16 hour) decay
				~0.17	Pt-d-p
					Pt-n-γ, Pt-n-2n
₇₉Au	191	~1 d	?	?	Ir-α-4n
					Pt-d-3n
	192	4.7±0.1 h	~0.3	x-rays	Ir-α-3n
			>2	~3	Pt-d-2n
	193	15.8±0.3 h	<0.3	x-rays	Ir-α-2n, Ir-α-4n
					Pt-d-3n
	194	39.5±0.5 h	0.31	x-rays	Ir-α-3n
			~1.8	0.38	Pt-d-2n, Pt-d-3n
				1.9	
	195	195±5 d	0.08	x-rays	Ir-α-2n
				1.7	Pt-d-2n, Pt-d-3n
				0.17	Pt-d-n
	196	5.55±0.05 d	0.34	x-rays	Pt-d-2n, Pt-d-n
				0.41	Au-n-2n
				1.7	
	196	14±0.5 h	?	x-rays	Au-n-2n

tion of the stability of isotopes of elements of odd Z in this region, but since the allocation of Pt^{193} seems reliable, the gold parent has been allocated similarly. No activity which might be a longer lived isomer has been yet detected in the decay of the gold fractions from either Pt+d or Ir+α bombardments.

4.7-hour gold.—Previously unreported, this activity with a characteristic very hard gamma-ray has been observed in chemically separated gold fractions from both Ir+α and Pt+d reactions. Provisional assignment to mass 192 has been made on the basis of reaction yields, and absence of any daughter activity.

~1-day gold.—The 3.0-day platinum provisionally assigned to mass 191 grows in the chemically separated gold fraction from a parent of ~1-day half-life in both Ir+α and Pt+d bombardments. The yield is low in both cases, and the isotope has not been directly observed.

A search is being made for shorter lived activities, and a full report on isotopes of platinum and gold will be published subsequently.

I am much indebted to Dr. J. Hamilton, Mr. T. Putnam, Mr. B. Rossi, and the crew of the 60-inch cyclotron for their assistance in bombardments, to Professor Glenn T. Seaborg and Professor I. Perlman for their advice and encouragement, to Mr. K. Street and Mr. H. Hicks for assistance in part of the experimental work, and to the University of California for providing facilities.

[5] C. Goodman and M. L. Pool, Phys. Rev. 71, 288 (1947).
[6] a. J. M. Cork and O. Halpern, Phys. Rev. 58, 201A (1940); b. J. L. Lawson and J. M. Cork, Phys. Rev. 58, 580 (1940).

Letters to the Editor

PUBLICATION of brief reports of important discoveries in physics may be secured by addressing them to this department. The closing date for this department is five weeks prior to the date of issue. No proof will be sent to the authors. The Board of Editors does not hold itself responsible for the opinions expressed by the correspondents. Communications should not exceed 600 words in length.

On the Hamiltonian for a Particle in an Electromagnetic Field

PAUL I. RICHARDS**
Brookhaven National Laboratory, Upton, New York
December 19, 1947

IN connection with a study of the "infra-red catastrophe," it was found that a contact transformation may be used to eliminate certain low frequency divergences. The classical Lagrangian for a particle with charge e and mass m in a field specified by the potentials $\mathbf{A}$, ϕ is:

$$L_0=\frac{m}{2}|\dot{\mathbf{r}}|^2+\frac{e}{c}\mathbf{A}\cdot\dot{\mathbf{r}}-e\phi, \tag{1}$$

where dots indicate (total) differentiation with respect to time. This Lagrangian L_0 leads to the Hamiltonian usually given in the literature.

The equations of motion, however, are not changed when an arbitrary total time derivative is added to the Lagrangian. If we subtract $(d/dt)(\mathbf{A}\cdot\dot{\mathbf{r}})$ from (1), we obtain:

$$\begin{aligned}L&=\frac{m}{2}|\dot{\mathbf{r}}|^2-e\phi-\frac{e}{c}\mathbf{r}\cdot\frac{d\mathbf{A}}{dt}\\&=\frac{m}{2}|\dot{\mathbf{r}}|^2-e\phi-\frac{e}{c}\left(\frac{\partial\mathbf{A}}{\partial t}+\dot{\mathbf{r}}(\nabla\mathbf{A})\right)\cdot\mathbf{r},\end{aligned} \tag{2}$$

where $\nabla\mathbf{A}$ is the dyadic $\partial A_i/\partial x_j$. It may be directly verified that (2) gives the Lorentz force equations, though in highly disguised form.

The Hamiltonian derived from (2) is found to be:

$$H=\frac{1}{2m}|\mathbf{p}+\frac{e}{c}(\nabla\mathbf{A})\cdot\mathbf{r}|^2+\frac{e}{c}\mathbf{r}\cdot\frac{\partial\mathbf{A}}{\partial t}+e\phi. \tag{3}$$

It has been pointed out to the author* that (3) may also be obtained from the usual Hamiltonian by carrying out the quantum-mechanical contact transformation

$$\psi=\exp\left(\frac{e}{ic}\mathbf{A}\cdot\mathbf{r}\right)\psi'.$$

For a plane wave, those terms linear in $\mathbf{A}$ which arise from the first part of (3) are smaller than the second term by essentially the factor v/c. Thus it is legitimate to treat the perturbing energy as $-e\mathbf{r}\cdot\mathbf{E}$. This procedure eliminates those low frequency divergences which formerly arose upon taking matrix elements of

$$\frac{e}{c}\mathbf{A}\cdot\mathbf{p}_{ik}\approx(v_{ik}/v)(e\mathbf{r}_{ik}\cdot\mathbf{E}).$$

Since the two Hamiltonians involved are completely equivalent, the original divergence must have arisen from neglecting terms which were actually not small, though it is very difficult to see just where this is done in the usual treatment.

The form (3) is interesting in that it roughly splits the energy into elementary "moment" interactions. Thus, the second term is the electric dipole energy, while the linear parts of the first term are easily seen to contain the magnetic dipole and electric quadrupole interactions.

* Private discussion with H. S. Snyder.
** Research carried out at the Brookhaven National Laboratory under the auspices of the Atomic Energy Commission.

Nuclear Quadrupole Interaction in the ICl Rotational Spectrum*

RICHARD T. WEIDNER**
Sloane Physics Laboratory, Yale University, New Haven, Connecticut
December 22, 1947

RECENTLY reported[1] microwave absorption measurements with ICl vapor in the mm pressure range showed absorption peaks at 6980 and 6684 mc/sec. These were interpreted as arising from $J=0$ to $J=1$ rotational transitions in ICl^{35} and ICl^{37} and indicated rotational constants some 2 percent greater than the accepted values.[2] As a result of private communications with Dr. C. H. Townes this discrepancy has been removed and the observations reinterpreted. In the $J=3$ to $J=4$ spectrum of ICl Townes has found large nuclear quadrupole interactions, $eQ(\partial^2V/\partial Z^2)$, -2930 cm/sec. for the I nucleus and -82.5 cm/sec. for the Cl^{35} nucleus, and rotational constants in agreement with previous determinations.[1] Using these values, the $J=0$ to $J=1$ spectra have been recalculated assuming the Cl interaction as a perturbation of the I interaction. ICl^{35} and ICl^{37} each give three close-spaced triplets; the strongest of the ICl^{35} triplets and a weak ICl^{37} triplet fall near 6980 mc/sec., and a relatively strong ICl^{37} triplet is near 6684 mc/sec. The other three triplets predicted are outside of the frequency range of our measurements.

* Assisted by the Office of Naval Research under Contract N6ori-44, Task Order II.
** Now at Rutgers University, New Brunswick, New Jersey.
[1] R. T. Weidner, Phys. Rev. 72, 1268 (1947).
[2] W. E. Curtis and J. Patkowski, Phil. Trans. Roy. Soc. 232, 395 (1934).

Radioactive Carbon of High Specific Activity*

L. D. NORRIS AND ARTHUR H. SNELL
Clinton National Laboratories, Oak Ridge, Tennessee
December 22, 1947

AS we have described briefly elsewhere,[1] the first 225 millicuries of carbon 14 to be produced and distributed under the isotope program of the Atomic Energy Commission were made in an apparatus which circulated saturated ammonium nitrate solution through an irradiation tube in the Clinton nuclear reactor. The major portion of the carbon 14 was found to be converted to $C^{14}O_3$

which was carried out of the ammonium nitrate solution by the gases resulting from radioactive decomposition of the solution itself. The gas stream was passed through bubblers containing saturated barium hydroxide, and the $C^{14}O_2$ thereby precipitated as $BaC^{14}O_3$. However, at the time the apparatus was installed, it was also expected that some carbon 14 would be converted to $C^{14}O$, and that if this were the case, the isotopic enrichment might be considerable inasmuch as there would be little possibility of dilution by natural carbon from the air. Therefore, the exhaust gas from the first barium hydroxide bubblers was passed over an oxidizing agent (hot CuO), and then led through a second series of barium hydroxide bubblers.

After several long periods of operation, very little $BaC^{14}O_3$ precipitate seemed to be present in the second series of bubblers, and we, therefore, assumed that negligible evolution of $C^{14}O$ occurred. Recently we have cleaned these bubblers thoroughly, scraping off all the solid material clinging to the sides of the bubblers and to the walls of their stems. This solid material, when examined for activity, was found to be very rich in carbon 14. As a result, we now have two samples, each weighing approximately 250 mg, which have specific activities corresponding to an isotopic concentration of 27 percent in the one case, and 19 percent in the other, on the basis of $T_{\frac{1}{2}}=5100$ years. These samples, which are nominally $BaC^{14}O_3$, in all likelihood contain certain solid impurities (i.e., silica, barium hydroxide), and thus the isotopic concentrations may in fact be somewhat higher than indicated by specific activity measurements.

Since the ammonium nitrate solution factory has been out of operation for some months, no more of this material can be expected from that source. The samples at hand, however, are sufficient to permit work on the spin determination, the beta-spectrum, the (p, n) threshold, and other interesting problems.

* This document is based on work performed under Contract No. W-35-058-eng-71 for the Manhattan Project and the information covered therein will appear in Division IV of the MPTS, as part of the contribution of the Clinton Laboratories.

[1] L. D. Norris and Arthur H. Snell, Science **105**, 265 (March 7, 1947).

New Bands in the Second Negative or Ultraviolet Band System of O_2^+ Molecule ($^2\pi_g \rightarrow {}^2\pi_g$)

LALJI LAL
D. A. College, Kanpur, India
December 10, 1947

THE ultraviolet O_2^+ bands have been produced by high frequency (750–850 kc/sec.) discharge (output power less than 10 watts) in oxygen produced by heating $KMnO_4$ crystals. They were photographed on a small (baby) Hilger Prism Spectrograph.

During the course of the present investigation we have observed many new bands, which are marked with an asterisk in (v', v'') Table I. Here only as much part of the (v', v'') table is produced as is required to accommodate the new bands.

TABLE I. (νvac).

v' \ v''	0	1	2	3	4	5	6
0					(2, 5)	29393?	27710?
						207	538
1				33735*	32009	30303	28611
				—	31803	084	420
2		38196*	36365*	34572	32841	31131	—
		001*	182	380	628	30938	29254
3		38990*	37167	35409	33657	31940*	30259*
		784*	36954	197	463	747*	—
4		39768	37960	36182	34447	32750*	
		564	765	35998	239	550*	
5		40539	38732	36954			
		340	551	753			
6	43120	41279	39473	37682			
	42900	079	283	491			
7	43813	41986	40174	38412*			
	613	788	39982	196*			

We have proposed these quantum assignments† to our newly discovered bands after a serious consideration of the mean vibrational differences for the initial and final states and that of the (O−C) values of the band heads. The underlined bands, v_4, 38,196 and 36,182 have been assigned two vibrational quantum numbers from a consideration of the intensity distribution. The bands (0, 5)i and (0, 6)i are marked as doubtful with "?" because their observed values given in the (v', v'') Table I are a little too different from their extrapolated values.

Besides these bands, a good many other bands with a striking difference of nearly 200 cm^{-1} have also been observed. Some of these were observed by Johnson[1] also who attributed them to the O_2^+ molecule but they have found no place in the present-day accepted (v', v'') scheme of the second negative system. These bands, however, must fit in either this (v', v'') scheme or in some other (v', v'') scheme, involving as their v'' (i.e., the final) level, the $2\pi_g$ level. All such attempts with the known structure and the known levels of the O_2^+ molecule have failed. It is, however, possible to include these bands in the (v', v'') table of the second negative system if we are prepared to have a narrow intensity distribution curve instead of a broad one (accepted at present). This change affects the internuclear distance (r_e) of the O_2^+ molecule, the accepted value of which is well established and hence cannot be discarded easily.

Work on this point is in progress, and as soon as some definite conclusions are arrived at they will be published along with the details.

Our thanks are due Professor R. K. Asundi of the Hindu University, Benares, under whose guidance this work has been done.

† Expressed in the given (v', v'') table.
[1] Johnson, Proc. Roy. Soc. **105**, 683 (1924).

He^3 Separation by a Heat Flux in Liquid Helium II*

C. T. LANE AND HENRY A. FAIRBANK
Sloane Physics Laboratory, Yale University, New Haven, Connecticut
AND
L. T. ALDRICH AND ALFRED O. NIER
Department of Physics, University of Minnesota, Minneapolis, Minnesota
December 16, 1947

ACCORDING to current ideas, liquid helium in the temperature interval between absolute zero and 2.19°K (λ-point) can be envisioned as behaving like two interpenetrating fluids—a so-called "superfluid" phase and a "normal" phase. The density of superfluid states (ρ_s) and normal states (ρ_n) bear a temperature dependent relationship to each other such that all the atoms are in ρ_s states at absolute zero and all are in ρ_n states at, and above, the λ-point. The macroscopic current density (j) is given by

$$j=\rho_s v_s+\rho_n v_n,$$

where the v's refer to the respective velocities of flow. Thus it is possible to have countercurrent flow of the two phases in the liquid without giving rise to a macroscopic current. Such a case is believed to occur if a temperature gradient is maintained in liquid helium II. Here ρ_s atoms flow from the cold region to the hot, are there raised in energy to ρ_n levels, and a balancing flow of ρ_n atoms returns to the cold region, the process being such that $j=0$.

Just prior to the war, L. Onsager advanced the hypothesis that He^3 atoms might be expected to participate in the ρ_n flow but not in a ρ_s type flow because of the different kind of statistics obeyed by He^4 and He^3 atoms.[1] Recently, Daunt, Probst, Johnston, Aldrich, and Nier[2,3] have tested this hypothesis by allowing liquid helium II to flow through a superleak filter. The latter permits the flow of ρ_s atoms but not ρ_n atoms. The results showed that He^3 was at least partially filtered out by flow through the superleak but the effect was small, the concentration of He^3 being reduced by about a factor of 4 or 5.

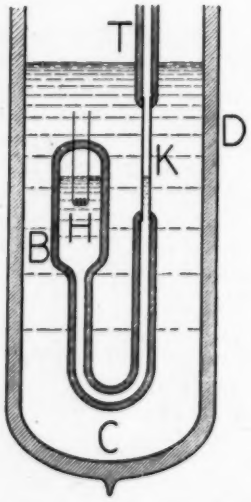

FIG. 1. Schematic drawing of the cryostat.

TABLE I. Summary of experimental data.

Sample	V_s Volume of gas used to produce liquid cm^3(STP)	He^3/He^4 in V_s $\times10^8$	Heat supplied watts	Time during which sample was held at temp. T min.	T °K	He^3/He^4 measured $\times10^8$
0	2040	1.3	—	—	300	1.3
1	2040	1.3	0	35	2.01	4.4
2	2032	1.29	0	—	2.01	10.4
3	2025	1.26	0.017	10.5	2.01	170
4	2016	0.63	0.017	—	2.01	52
5	2006	0.34	0	40	1.82	0.8
6	2000	0.34	0.017	15	1.82	<0.04
7	1963	0.34	0.023	14	1.82	<0.04
8	1932	0.34	0	2	1.82	<0.04

It occurred to us that perhaps a more clear-cut approach was to make use of the internal convection mentioned above due to a heat flux. Figure 1 is a schematic of our apparatus. A thick-walled glass bulb, B, contains an electrical heater, H. The bulb is connected *via* a 1½-mm glass capillary, C, a 1½-mm Kovar tube K, and thence *via* a 1½-mm capillary T to the outside of the cryostat. The whole was immersed in a bath of liquid helium contained in Dewar D and approximately 2.5 cm^3 of liquefied atmospheric helium condensed in the bulb, the level of the liquid being approximately as indicated. The temperature was now reduced below the λ-point to 2.01°K.

The procedure used in sampling and the results obtained are summarized in Table I. Sample 0 gives the amount of and He^3 concentration in the unrefrigerated gas. Sample 1 was evaporated from the liquid surface in the Kovar tube after the liquid had remained at 2.01°K for 35 minutes. The sampling time in this and subsequent samples was 1 minute. Sample 2 was taken immediately after sample 1. Sample 3 was taken after heat had been supplied to H for 10.5 minutes. Sample 4 was taken immediately after sample 3. The temperature was now reduced to 1.82°K and samples 5 through 8 taken under the conditions shown in the table. The last column in the table gives the value He^3/He^4 as measured for each sample by the mass spectrometer. Due correction has been made (columns 2 and 3) for depletion of He^3 resulting from sampling.

Samples 1 to 4 show conclusively that the He^3 isotope moves in the direction of the heat flow, and this supports the hypothesis that these atoms move only with the ρ_n flow, at least for these very dilute solutions. The lower concentration of sample 4 over sample 3 is to be expected inasmuch as 50 percent of the total He^3 was removed in sample 3. We note that both samples 1 and 2 show a considerably greater He^3 concentration than would be expected from our previous measurements either for the liquid or the vapor in equilibrium at this temperature.[4] We believe this is due to the small heat flux, in the same direction as that produced by the heater, produced by the evaporation in the Kovar tube during sampling.

It will be seen that the samples taken at 1.82°K all show very small He^3 concentration irrespective of the heat flux. We believe the explanation of this lies in our previous measurements on vapor-liquid equilibrium below the λ-

point.[4] In these measurements we showed that the concentration of He^3 in the vapor, while finite at 2.0°K, was immeasureably small at 1.82°K and quite possibly zero. The higher value for sample 5 is probably due to residual gas from sample 4 in the withdrawal line.

In view of an enrichment factor of 130 in sample 3, it appears that a very efficient He^3 separation apparatus could be designed using this heat flux method.

* The work at Yale University was assisted by the Office of Naval Research under Contract N6ori-44 and that at the University of Minnesota by grants from the Research Corporation and the Graduate School.

[1] See Pollard and Davidson, *Applied Nuclear Physics* (John Wiley and Sons, Inc., New York, 1942), p. 183. We understand from Professor Pollard that the idea was due to Onsager. See also J. Franck, Phys. Rev. 70, 561 (1946).

[2] J. G. Daunt, R. E. Probst, H. L. Johnson, L. T. Aldrich, and A. O. Nier, Phys. Rev. 72, 502 (1947).

[3] J. G. Daunt, R. E. Probst, and H. L. Johnson, J. Chem. Phys. 15, 759 (1947).

[4] H. A. Fairbank, C. T. Lane, L. T. Aldrich, and A. O. Nier, Phys. Rev. 73, 256 (1948).

Search for Gamma-Radiation in the 2.2-Microsecond Meson Decay Process

E. P. Hincks and B. Pontecorvo
National Research Council, Chalk River Laboratory, Chalk River, Ontario, Canada
December 9, 1947

THE meson decay process which is identified by a mean life of 2.2 microseconds[1] has been usually thought of as consisting of the emission of an electron and a single neutrino, as suggested by the well-known Yukawa explanation of the ordinary beta-process in nuclei. However, the Yukawa theory is at variance with the results of the experiment of Conversi, Pancini, and Piccioni,[2] and since there remains no strong justification for the electron-neutrino hypothesis,[3] a direct experiment to test an alternative hypothesis—*that the decay process consists of the emission of an electron and a photon, each of about 50 Mev*—has been performed.

The apparatus, illustrated in Fig. 1, consists of three rows of Geiger-Müller counters, A, B, and C, each having an effective area of approximately 38 cm×20 cm. Above A there are 15 cm of lead, and between A and B, 1.5 cm of lead. Mesons traversing A and B, and stopped in a graphite absorber 38 cm×19 cm×5 cm thick, produce decay electrons which may be detected in either B or C. Decay photons, if present, could also be detected in B or C, whose efficiency for gamma-radiation was increased by introducing 2.1 mm of lead between the graphite and both B and C. The twofold function of B—first, detection of the passage of a meson by a coincidence with A (event "(A, B)"), and second, detection of a decay electron (or photon) following "(A, B)"—is permitted by the circuit design. Although one of the eight counters of B (that through which the meson passed) is insensitive to the decay particle because of the long counter dead time, the use of B in this manner allows an advantageous geometry. The outputs of the three rows are mixed by circuits whose function is schematically shown in the diagram, and the following delayed events are finally recorded:

Table I. Delayed single and coincidence counting rates.

	$(B)_{del}$ (Counts/hr.)	$(C)_{del}$ (Counts/hr.)	$(B)_{del}+(C)_{del}$ (Counts/hr.)	$(B, C)_{del}$ (Counts/hr.)
With graphite plus lead—(104.2 hours of observation)	11.93±0.34	12.26±0.34	24.19±0.48	0.21±0.05
Without graphite plus lead—(77.2 hours of observation)	6.48±0.29	4.64±0.25	11.12±0.38	0.43±0.08
Net effect due to decay electrons from graphite plus lead	5.45±0.45	7.62±0.42	13.07±0.62	

1. "$(B)_{del}$;" discharges of B occurring between 0.6 and 5.3 microseconds after "(A, B),"
2. "$(C)_{del}$;" discharges of C occurring between 0.6 and 5.3 microseconds after "(A, B),"
3. "$(B, C)_{del}$;" coincidences of B and C occurring between 0.6 and 5.3 microseconds after "(A, B)."

Runs were made with and without the graphite plus lead between B and C, and the results are presented in Table I. Other runs with graphite only, with lead only, and with other thicknesses of graphite and lead, were performed and these will be reported in a more complete account of the experiment. Check runs with a 1.6- to 6.3-microsecond delay gave results consistent with a mean life of 2.2 microseconds.

The observed rate $(B, C)_{del}$ could be due to the following causes:

(i) genuine electron-photon coincidences from the meson decay,

(ii) single decay electrons which traverse both B and C,

(iii) casual events.

The casual rate (iii), which is due essentially to mesons traversing B and C between 0.6 and 5.3 microseconds after an event "(AB)," has been estimated from the measured double and triple coincidence rates and from the characteristics of the circuits to be 0.22±0.02 counts per hour. It is independent of the presence or absence of graphite plus lead. Effect (ii) should be detected only in absence of graphite plus lead, since otherwise the total thickness of material between B and C is of the order of the expected range of the electrons. We observe, in fact, that $(B, C)_{del}$ increases appreciably when the graphite plus lead is removed. The presence of this effect was verified by a sub-

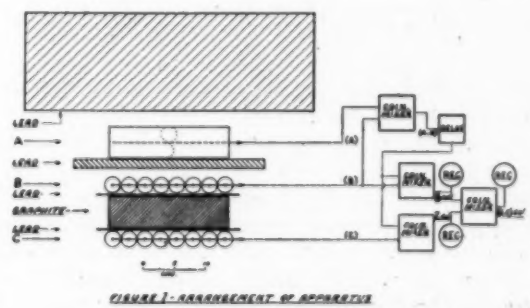

FIG. 1. Arrangement of apparatus.

sidiary experiment in which the number of decay electrons traversing both B and C was intentionally increased.

It is apparent, therefore, that the change in the contribution of effect (ii) to $(B, C)_{del}$ prevents an estimate of the contribution of effect (i)—electron-photon coincidences—being made by comparing the rates $(B, C)_{del}$ with and without graphite plus lead. However, we can compare $(B, C)_{del}$ with graphite plus lead with the estimated casual rate (iii) to conclude *that each decay electron is not accompanied by a photon of about 50 Mev.* The difference $(B, C)_{del}$ with graphite plus lead minus the casual rate is $0\begin{cases}+0.06\\-0\end{cases}$ counts per hour. We expect, on the other hand, that the contribution of effect (i), if present, to $(B, C)_{del}$ would be about one count per hour. This is a conservative estimate based on the number of single decay particles from graphite plus lead detected in B and C (13 per hour), assuming an average efficiency of 15 percent for detection of a 50-Mev gamma-ray in our system,* and taking into account losses of coincidences due to geometry.

Our negative result is consistent with the experiments on the genetic relationship[4] between the hard and soft components in the lower atmosphere. The mechanism of the 2.2-microsecond decay process remains, however, unknown. Should it consist of the emission of an electron and a neutral meson, as recent evidence[5,6] seems to indicate, the nuclear *capture* of a light negative meson may be accompanied by the emission of one neutrino, as previously suggested.[3]

* The absorption coefficient for a 50-Mev gamma-ray in lead was taken as 1 cm^{-1}. The secondary pair of electrons would be emitted in a strongly forward direction with an average range of about 10 g/cm^2.

[1] N. Nereson and B. Rossi, Phys. Rev. **64**, 199 (1943); M. Conversi and O. Piccioni, Phys. Rev. **70**, 859 (1946).

[2] M. Conversi, E. Pancini, and O. Piccioni, Phys. Rev. **71**, 209 (1947); for further discussions see E. Fermi, E. Teller, and V. Weisskopf, Phys. Rev. **71**, 314 (1947) and J. A. Wheeler, Phys. Rev. **71**, 320 (1947).

[3] B. Pontecorvo, Phys. Rev. **72**, 246 (1947).

[4] We are indebted to Professor G. Bernardini for drawing to our attention his discussion of this subject at the Nuclear Physics International Conference, Cambridge, England (1946) and a comprehensive article by G. Bernardini, B. N. Cacciapuoti, and B. Querzoli, Nuovo Cimento **3**, 349 (1946).

[5] C. D. Anderson, R. V. Adams, P. E. Lloyd, and R. R. Rau, Phys. Rev. **72**, 724 (1947).

[6] C. M. G. Lattes, G. P. S. Occhialini, and C. F. Powell, Nature **160**, 453, 486 (1947).

On the Phase Shift Approximation in the Theory of Pressure Broadening of Spectral Lines

ALEXANDER JABŁOŃSKI
Physics Department, Nicholas Copernicus University, Toruń, Poland
August 11, 1947

THE collision damping theory of broadening of spectral lines is still widely used in discussions of experimental results. Lately, some new contributions to this theory have been published.[1] Former attempts to give a quantum-mechanical foundation to the collision damping theory were discussed in a previous paper.[2] A new attempt in this line has been made recently by Foley.[3] According to Foley the wave mechanical theory proposed by the present writer[2] leads to the Lorentz line form for the conditions assumed in collision damping theories (phase shift approximation). Unfortunately, Foley's argument is liable to criticism. Foley adopts the distribution $e^{-T_i/T_0}/T_0$ in the parameter $T_i=R_0/v$, in which R_0 is the radius of the container, v the velocity of gas molecules, $T_0=R_0/\bar{v}$, and $\bar{v}$ their average velocity. This distribution does not result from Maxwell's distribution law[4] and thus does not correspond to the real distribution. This alone suffices to invalidate Dr. Foley's results.

But even if this incorrect distribution be adopted, further calculations, if carried out correctly, lead to results differing from those of Foley. Because of the dropping of a "numerical factor" (normalization factor, which, as inspection shows, depends on T_i!), the evaluation of "overlap" integral in phase shift approximation leads Foley to the expression

$$A(\omega_i)=\frac{\sin\omega_i T_i}{\omega_i}\,,^5$$

instead of

$$A(\omega_i)=\frac{\sin\omega_i T_i}{\omega_i T_i}\,.^6$$

If the corrected expression for $A(\omega_i)$ is used and another factor, the density of translational energy levels[7] (also omitted by Foley) taken into account, the integral

$$\int_0^\infty dT_i \frac{\sin^2\omega_i T_i}{\omega_i^2 T_i}\frac{e^{-T_i/T_0}}{T_0}=\frac{\log(1+4\omega_i^2T_0^2)}{8T_0\omega_i^2}\,,^8$$

is obtained instead of Foley's

$$\int_0^\infty dT_i \frac{\sin^2\omega_i T_i}{\omega_i^2}\frac{e^{-T_i/T_0}}{T_0}=\frac{T_0^2}{1+4\omega_i^2T_0^2}\,.$$

However, the "overlap" integral in Foley's approximation may be useful in the calculations of the intensity distribution in the core of the broadened line, if "collisions" with large collision parameters (small phase shifts) are also taken into consideration. Clearly, the last type of collisions must contribute considerably to the intensity in the core of the line.

Some further remarks should be added. According to Foley, "any line broadening theory which considers a single perturbing atom and then averages over-all transitions of this system will always yield a line form which diverges at the center." Actually, the asymptotic distribution (Kuhn's distribution) obtained in the above way in the previous paper[2] diverges at the line center. However, the discussion of applicability of this distribution[2] shows that it does so only owing to the approximations made by its derivation. The same discussion shows that its applicability is not restricted to high concentrations of perturbing atoms, as supposed by Foley. It can be used up to the lowest concentrations if other factors do not cause its failure.

On the whole the situation remains as it was before the publication of Foley's paper. One has either to demonstrate rigorously that the Lorentz formula can be obtained from the quantum-mechanical theory proposed by the writer or to modify (or to reject) one of these theories.

The subsequent note by Dr. Foley obviously contains not only modifications of some of the assumptions on which his original calculations were based ($T_i=R_i/v$ with R_i

variable and v = const., instead of $T_i = R_0/v$ with R_0 = const. and v variable, is introduced), but also a modification of the present writer's theory itself (in the original theory a container with a constant radius R_0 was considered). The writer sees no physical grounds for introduction of such assumptions, and, besides, is unable to see how Dr. Foley's new partition formula can be shown to be compatible with the conventional theory of fluctuations. As to the other points of disagreement the writer should like to refer to the original papers (cf., H. M. Foley, reference 3, p. 618 left column and page 627 left column).

[1] E.g., J. H. Van Vleck and V. F. Weisskopf, Rev. Mod. Phys. **17**, 227 (1945).
[2] A. Jabloński, Phys. Rev. **68**, 78 (1945).
[3] H. M. Foley, Phys. Rev. **69**, 616 (1946).
[4] Such a distribution derived from Maxwell's law would be $\frac{4T^3}{3!}e^{-T^2/T_0^2}$.
[5] See reference 3, Eq. (35).
[6] The last expression for $A(\omega_i)$ is, as it must be, dimensionless, the square of it denoting probability.
[7] $ds/dE = \mu^3 R_0/\pi\hbar(2E)^{\frac{1}{2}} = T_i/\pi\hbar$ (cf., A. Jabloński, reference 2).
[8] A T_i-independent factor is omitted in this expression.
[9] Cf., A. Jabloński, reference 2.

The Theory of the Pressure Broadening of Spectral Lines: A Reply

H. M. FOLEY
Columbia University, New York, New York
November 22, 1947

IN the preceding communication a section of a paper by the author[1] is criticized by Dr. Jabloński. The author regrets that the conciseness of his treatment, together with an error in notation, caused confusion.

In the classical treatment of collision broadening the distribution in the time intervals between collisions is of the exponential form $(e^{-T/T_0}/T_0)dT$. This distribution is not a consequence of the Maxwell-Boltzmann velocity distribution but results from the random spatial distribution of the perturbing atoms. In the simple derivations of the expression for the shape of a collision broadened line, the velocities are taken to be constant:[2] in any case the velocity distribution must be taken into account separately as was done by the author in another section of his paper.[1] In the wave mechanical treatment it is necessary to take into account this fluctuation in the density of perturbers by averaging over an ensemble of systems with varying radii and with a weight factor proportional to $(R_i/R_0)e^{-R_i/R_0}$ for each of the n colliding atoms. n is the number of perturbers in the container which have angular momenta small enough to effect a collision with the radiating atom, and is given by $n = 2\pi a^2 N R_0$ with N the density and πa^2 the cross section. In the case $n = 1$ the probability that the colliding atom be located at a distance R in an interval dR is $2\pi N a^2 dR = dR/R_0$, consequently the probability of finding a single such atom within a distance R is $(R/R_0)e^{-R/R_0}$. For $n > 1$ the intensity distribution must be averaged independently over the distributions in these radii according to the weight factors given above. In the author's paper these weight factors were expressed in the parameter T_i, and the calculation was carried out without further explanation. The definition of T_i should be R_i/V instead of R_0/V.

It is, of course, true that the squared amplitude for each perturber contains the normalization factor $1/T_i^2$ or $1/R_i^2$. Multiplication by the translational energy level density[3] introduces one factor R_i, and the averaging process over the density fluctuations brings in another factor proportional to R_i for each perturber. The radial dependence due to the normalization factor is thus eliminated, and the author's result (reference 1, Eq. 37) is clearly correct.

In his paper[1] the author pointed out that the condition for the validity of the Kuhn-Margenau distribution depends on the density and the velocity of the perturbing atoms.

[1] H. M. Foley, Phys. Rev. **69**, 616 (1946).
[2] V. Weisskopf, Physik. Zeits. **34**, 1 (1933).
[3] A. Jabloński, Phys. Rev. **68**, 78 (1945).

The Ratio of Positives to Negatives in Cu^{64}

L. CRANBERG AND J. HALPERN
University of Pennsylvania, Philadelphia, Pennsylvania
December 15, 1947

THE work of Backus[1] on Cu^{64}, which decays to Ni or Zn by β-emission, indicates positron-electron ratios in excess of values predicted by theory at energies below 50 kv. This has suggested a review of the earlier work by Tyler[2] and Townsend[3] for comparison of positron-electron ratio with theory. The results are shown in Fig. 1. The data of Tyler are those for his thinnest source (2.2 mg/cm² with paper backing of 1.8 mg/cm²). Backus' source thickness is not known; his support was a 0.03-μ collodion film. Townsend's source and support are unspecified.

The theoretical curves in the figure are one fitted by Backus and one fitted to Tyler's data using the relation given by the Fermi theory:

$$\ln\frac{N+}{N-} = 2\ln\frac{W_+ - W}{W_- - W} - \frac{2\pi\alpha ZW}{(W^2-1)^{\frac{1}{2}}} + k,$$

where the approximation $Z = Z_{Ni} = Z_{Zn}$ has been made.

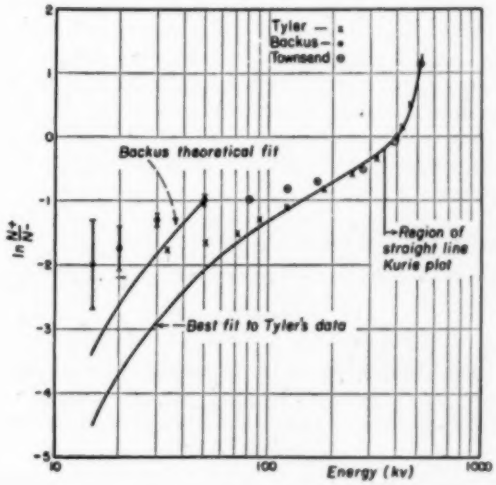

FIG. 1. Positron-electron ratios from Cu^{64} as a function of energy.

This approximation introduces negligible error above 5 kv. The end points W_+ and W_- are taken from Tyler's data to be 2.29 and 2.13 mc^2, respectively. The energy W is in relativistic units, $Z=29$, $\alpha=1/137$. The quantity k is the ln of the ratio of the square of the matrix elements between the initial and final states of the heavy particle, for transitions yielding a positron and an electron. The value for best fit with Tyler's data is 0.8. The corresponding value from Backus' fit is 1.9.

Tyler's curves show deviation from straight-line Kurie plots at 350 and 320 kv for positrons and electrons, respectively, while his ratios show close agreement with theory down to 100 kv. An excess of positrons at low energies is evident in all cases. Using the theoretical curve which fits Tyler's data so well from 100 kv up to the end point, one finds discrepancy between Backus' results and theory greater than was estimated by a factor of 2.9 in the ratio $N+/N-$.

The suggestion of Backus that scattering of positives and negatives in the source and support will distort the separate spectra in a manner that should cancel in the ratio helps explain the extension of the range of agreement with theory. This suggestion does not apply with equal strength at the lowest energies. In the case of inelastic scattering, cancellation of effects is contingent upon the similarity of the true spectra. According to the Fermi theory, however, in the region 0–50 kv the electrons comprise 14 percent, but the positrons only 1.2 percent of their respective totals. Thus, since more nearly equal numbers will be scattered into this region from higher energies, the effect of such scattering on the ratio is in the same direction as the experimental deviation from theory. The smallness of the ratio predicted by theory (1/90 at 15 kv from the theoretical fit to Tyler's data) suggests special care must be taken to minimize the number of spurious low energy positrons from this and other sources.

Referring to Backus' separate spectra for electrons and positrons, Lewis and Bohm[4] note that whereas the positron spectrum conforms to theory, the electron spectrum decreases with decreasing energy, the theory requiring approximate constancy at low energy. The possibility of scattering effects compensating in one case but not the other should be reckoned with, however. Until the effects of scattering on the individual spectral shapes are better understood, the ratios offer a better means of checking the theory at lower energies than the individual spectral shapes, since some cancellation of scattering effects is to be expected.

[1] John Backus, Phys. Rev. **68**, 59 (1945).
[2] A. W. Tyler, Phys. Rev. **56**, 125 (1939).
[3] A. A. Townsend, Proc. Roy. Soc. London **A177**, 357 (1941).
[4] Harold Lewis and David Bohm, Phys. Rev. **69**, 129 (1946).

Light Scattering in Supersonic Streams

J. H. McQueen, J. W. Beams, and L. B. Snoddy*
Department of Physics, University of Virginia, Charlottesville, Virginia
December 22, 1947

IN many types of experiments carried out in wind tunnels or free jets it is often important to know the amount of turbulence or density variations in the air stream. In subsonic air streams the turbulence has been successfully determined by measuring the heat transferred from a small wire placed in the air stream.[1] However, in supersonic air streams an object placed in the stream usually gives rise to a shock wave which complicates these measurements. Schlieren and shadow photographs taken with a short duration light source (10^{-7} sec. duration) reveal the density variations in supersonic air streams, but unless great care is taken it is very difficult to determine just where they occur in the stream. For example, in shadow photographs the density variations in the boundary layer often are difficult to differentiate from those near the axis of the stream.

For some time we have been determining the density variations in supersonic air streams by means of light scattering. An intense beam of parallel light is directed, say perpendicularly, through the air stream and the intensity of the scattered light measured at several different angles to the air stream and the light beam, respectively. From these data it is possible to estimate the average density variation at any point in the stream. With sunlight incident at 90° on a particle-and-droplet-free, one-inch supersonic free jet sufficient light is scattered for good photographs to be taken with an F 2 lens in about one-tenth of a second. The polarization of the scattered light is found to be in close agreement with light scattering theory so that further information on the density variations in the air stream can be obtained from measurements of the characteristics of the scattered light. Under certain conditions the shock waves can be observed directly.

* This work was carried out under Contract NOrd-7873 with the Bureau of Ordnance of the Navy.
[1] Dryden, *Aerodynamic Theory* (Durand, 1934), Vol. VI.

The Scattering of Protons by Deuterons

H. S. W. Massey and R. A. Buckingham
University College, London, England
December 22, 1947

IN a recent number of The Physical Review, Sherr, Blair, Kratz, Bailey, and Taschek[1] have reported measurements of the absolute intensity of scattering of protons by deuterons. We have recently extended the calculations which we have carried out of neutron-deuteron scattering[2] to cover proton-deuteron collisions. These calculations include the case of 1.85-Mev protons which may be compared with values interpolated from the results of Sherr and co-workers who cover the energy range from 1.51 to 3.49 Mev. The results of the comparison are given in Table I.

The agreement with the calculated results assuming exchange-type forces is remarkably good and clearly better than is obtained with ordinary forces.

Just as for the neutron-deuteron calculations the interaction between the nucleons was taken to be of the form

$$V(r)=A(mM+hH+bMH+\omega)e^{-2r/a},$$

where M is the Majorana operator interchanging position

TABLE I. Comparison of observed and theoretical values of the Ratio R of the scattered intensity to that given by the Rutherford formula.

Angle of scattering (C.M. system)	30°	45°	60°	90°	120°	150°
R observed (interpolated)		5.1	11.8	37	112	310
R calc. (exchange forces)	1.77	4.96	11.5	40.6	119	249
(ordinary forces)		8.10	17.3	43.2	176	503

but not spin coordinates, and H the Heisenberg operator interchanging all coordinates. The constants A and a were taken to be those derived by Present and Rarita[3] from the binding energies of the light nuclei. For ordinary forces $m=h=0$, $\omega=\frac{1}{2}(1+\kappa)$, $b=\frac{1}{2}(1-\kappa)$; and for the exchange forces $m=2b=\frac{1}{2}(1+3\kappa)$, $h=2\omega=\frac{1}{2}(1-3\kappa)$, κ being taken as 0.6 to give the observed energy of the ^1S state of the deuteron. The technique of the calculation was exactly as for the neutron-deuteron investigation.[3]

We are indebted to the Government Grant Committee of the Royal Society for a grant to enable us to employ the Scientific Computing Service to assist in the numerical solution of certain of the integro-differential equations which arose.

[1] R. Sherr, J. M. Blair, H. R. Kratz, C. L. Bailey, and R. F. Taschek, Phys. Rev. **72**, 662 (1947).
[2] R. A. Buckingham and H. S. W. Massey, Proc. Roy. Soc. **A179**, 123 (1941); Phys. Rev. **71**, 558 (1947).
[3] R. Present and W. Rarita, Phys. Rev. **51**, 788 (1937).

On the Penetrating Component of Air Showers

G. SALVINI AND G. TAGLIAFERRI
Institute of Physics, University of Milan, Milan, Italy
December 10, 1947

THE present note is a preliminary report of some measurements which have been taken at an altitude of 2100 m to gather further information as to (a) accompanying, (b) origin, and (c) frequency of penetrating particles (p.p.) in air showers.[1,2]

One of the arrangements used is represented in Fig. 1. To compare in the same measure the frequency under Fe and Pb, counters P_1, P_2, P_3 and F_1, F_2, F_3 were covered, respectively, with 30 cm of Pb and 10 cm of Pb+30 cm of Fe. The unshielded counters (or trays of counters in parallel) A_1, A_2, B, C, D, L, M, N were situated on the same horizontal level over the shielded counters. Recording took place with neon lamps, thus indicating which of the counters P_1, P_2, P_3, F_1, F_2, F_3, B, C, D, L, M, N were discharged simultaneously with the coincidences of the master counters A_1, A_2.

TABLE I. Experimental results—column 1: order of the coincidences; column 2: frequency (min.$^{-1}$) of the showers that have discharged at least the counters of col. 1; column 3: average density (m^{-2}) of the showers of col. 2; column 4: frequency (min.$^{-1}$) of the coincidences between any one of the shielded counters and the showers of col. 2; column 5: ratio [col. 2×col. 3] /col. 4.

1	2	3	4	5
$A_1+A_2+B+C+D+L+M+N$	$4.9\pm0.3\times10^{-3}$	119 ± 8	$2.2\pm0.11\times10^{-2}$	265 ± 47
$A_1+A_2+B+C+L+M+N$	$6.7\pm0.3\times10^{-3}$	100 ± 7	$2.4\pm0.11\times10^{-2}$	279 ± 45
$A_1+A_2+C+L+M+N$	$9.9\pm0.3\times10^{-3}$	63 ± 4	$2.8\pm0.12\times10^{-2}$	223 ± 31
$A_1+A_2+L+M+N$	$13.1\pm0.4\times10^{-3}$	51 ± 3	$3.0\pm0.13\times10^{-2}$	223 ± 30
$A_1+A_2+C+L+M$	$16.0\pm0.4\times10^{-3}$	48 ± 2	$3.5\pm0.14\times10^{-2}$	219 ± 23
A_1+A_2+L+M	$24.2\pm0.6\times10^{-3}$	41 ± 2	$4.2\pm0.15\times10^{-2}$	230 ± 26

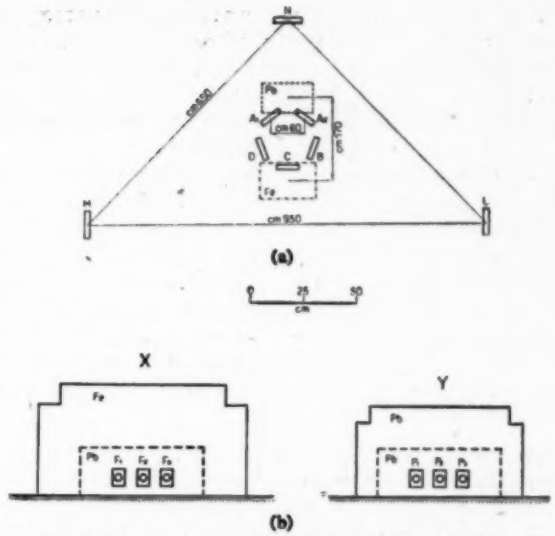

FIG. 1(a) Experimental arrangement. The dotted rectangles indicate the positions of the penetrating particles sets. Surfaces of the counters (or trays of counters in parallel) in cm²: $A_1=A_2=488$; $B=D=112$; $C=224$; $L=456$; $M=N=152$.
(b) Cross sections of the penetrating particles sets X and Y. Surface of each counter: 152 cm².

To clear up point (a) concerning the ratio between the frequency of the soft particles and that of the p.p. associated in showers, we have evaluated the ratio: (frequency of the showers×average density):(frequency of the p.p.) for various average densities Δ of the showers detected by the unshielded counters. As can be seen (Table I, column 5), this ratio is just about constant between $\Delta=119$ m^{-2}, and $\Delta=41$ m^{-2}. This seems to indicate that the p.p. are produced by the soft component, and perhaps not far from the apparatus; if another component generated the p.p., it should be present in the showers with a side distribution like that of the soft component.

(b) Recent works[2,3] suggest that the p.p. are produced in a good percentage in the absorbers. We have seen that the side distribution of the p.p. is not Poissonian, but presents particular associations. In fact, when several shielded counters in the two sets X and Y are discharged at the same time, events are more numerous in which two or three counters are discharged in the same set in comparison to those of two or more counters in different sets. Furthermore, in the same set the coincidences between counters near to each other (1+2, or 2+3) are more frequent than the coincidences 1+3. We think that this result indicates

TABLE II. Coincidences between the shielded counters and the showers having discharged counters A_1+A_2+ at least one of the counters B, C, D, L, M, N. Column 1: number of coincidences with one shielded counter (P_1, or P_2, or P_3; and corresponding F_1, or F_2, or F_3); column 2: the same with two adjacent shielded counters (P_1+P_2, or P_2+P_3; and corresponding); column 3: the same with two non-adjacent shielded counters (P_1+P_3; and corresponding); column 4: the same, with three shielded counters ($P_1+P_2+P_3$; and corresponding); column 5: total number of the events in each penetrating particles set.

	1	2	3	4	5	
Set X	593 ± 25	74 ± 9	15 ± 4	26 ± 6	708 ± 27	Time: minutes
Set Y	554 ± 24	77 ± 9	7 ± 3	33 ± 6	671 ± 26	20,690

that the p.p. are produced, partly at least, in the absorbers and in groups. In the alternative hypothesis that the p.p. are nearly all produced in the air, they should be associated in very narrow showers arising not far from our apparatus. In Table II the association between the events of the same set is given as an example.

(c) Within the limits of statistic fluctuations, we have observed the same frequency and distribution of penetrating events in the two sets X and Y (Table II). In agreement with several authors,[2-4] our measurements indicate that the p.p. are produced with a cross section proportional to Z^2, provided that production takes place in the absorbers by the soft component. It may be noted, however, that in the intermediate hypothesis of a production in the air, as well as in the absorbers, the exponent of Z might be less than two.

[1] G. Cocconi, A. Loverdo, and V. Tongiorgi, Phys. Rev. **70**, 852 (1946); A. Mura, G. Salvini, and G. Tagliaferri, Nature **159**, 367 (1947) and Nuovo Cimento **4**, 10 (1947); D. Broadbent and L. Jánossy, Proc. Roy. Soc. **A190**, 497 (1947).
[2] G. Cocconi and C. Festa, Nuovo Cimento **3**, 293 (1946).
[3] L. Jánossy, private communication. We thank Professor Jánossy for this communication.
[4] B. Ferretti, Nuovo Cimento **3**, 301 (1946).

Range of Nuclear Forces in the Neutron-Proton Triplet Interaction

C. G. SHULL, E. O. WOLLAN, G. A. MORTON,* AND W. L. DAVIDSON**
Clinton National Laboratory, Oak Ridge, Tennessee
December 12, 1947

MEASUREMENTS of the coherent scattering of neutrons by hydrogen[1] permit the evaluation of the scattering amplitudes characteristic of the two spin states of scattering, *viz.*, when the neutron and proton spins are parallel or antiparallel. Such evaluation also permits a determination of the range of nuclear forces present in the triplet interaction.

It can be shown that the coherent scattering amplitude for hydrogen in a crystal is given by

$$f_H = 2[\tfrac{3}{4}a_1 + \tfrac{1}{4}a_0], \quad (1)$$

where a_1 and a_0 are the triplet and singlet scattering amplitudes of a free proton when the spins of the proton and the incident neutron are, respectively, parallel and antiparallel. Also, the total scattering cross section of a free proton can be expressed as

$$\sigma_f = 4\pi[\tfrac{3}{4}a_1^2 + \tfrac{1}{4}a_0^2]. \quad (2)$$

Equations (1) and (2) permit evaluation of a_1 and a_0. From neutron diffraction experiments on hydrogen containing crystals, the coherent scattering amplitude has been determined to be

$$f_H = +0.472 \pm 0.040 \times 10^{-12} \text{ cm}.$$

Using this value of the coherent scattering amplitude and Hanstein's[2] value of 21×10^{-24} cm^2 for the total scattering cross section for a free proton, one obtains for the triplet scattering amplitude

$$a_1 = -0.498 \pm 0.025 \times 10^{-12} \text{ cm}.$$

The singlet scattering amplitude determined by this procedure is dependent almost completely upon the value of the free proton cross section and turns out to be $+2.44 \times 10^{-12}$ cm.

Hamermesh and Schwinger[3] have discussed the relationship between the scattering amplitudes and the range of nuclear forces, and when the above values are inserted into their calculations, the range of the neutron-proton triplet interaction becomes

$$r_0 = 1.2 \pm 0.4 \times 10^{-13} \text{ cm}.$$

This value is definitely smaller than the value 2.8×10^{-13} cm ascribed to the singlet proton-proton interaction and is slightly smaller than that found by Sutton, Hall, and others[4] from the scattering of neutrons by *ortho-* and *para-hydrogen*, namely 1.5×10^{-13} cm. This latter difference is, however, within the suggested error of the diffraction result.

Further details on the neutron diffraction experiments will be published in the near future.

* On leave (July 1946 to August 1947) from R.C.A. Laboratories, Princeton, New Jersey.
** On leave (July 1946 to August 1947) from B. F. Goodrich Company, Akron, Ohio.
[1] W. L. Davidson, G. A. Morton, C. G. Shull, and E. O. Wollan, Phys. Rev. **72**, 168 (1947).
[2] H. B. Hanstein, Phys. Rev. **59**, 489 (1941).
[3] M. Hamermesh and J. Schwinger, Phys. Rev. **71**, 678 (1947).
[4] R. B. Sutton, T. Hall, E. E. Anderson, H. S. Bridge, J. W. DeWire, L. S. Lavatelli, E. A. Long, T. Snyder, and R. W. Williams, Phys. Rev. **72**, 1147 (1947).

Cross Section for the Reaction $C^{12}(n, 2n)C^{11}$ at 90 Mev

EDWIN M. MCMILLAN AND HERBERT F. YORK
Radiation Laboratory, Department of Physics, University of California, Berkeley, California
December 18, 1947

THE formation of C^{11} by high energy particle impact on C^{12} has been studied extensively in this laboratory;[1-3] it has been found that the cross sections for its formation by deuterons, helium ions, and protons become constant above a certain bombarding energy, and this constant absolute cross section in the latter case has been found to be 0.073×10^{-24} cm^2. We have no information on the excitation curve in the case of neutron activation, but an extension of the theory would indicate that it should be flat above about 60 Mev as it is for protons. Whether or not there may be a peak between 20 and 60 Mev depends on the relative importance of "intermediate nucleus" processes compared to non-capture processes. However, such a peak of moderate size would not seriously affect the measurements reported here because of the small number of neutrons in this energy range. Theoretically, the yield on the flat part of the excitation curve should be less for neutrons than for protons if exchange collisions occur, because a (p, n) exchange can lead to C^{11} by evaporation of a proton, while an (n, p) exchange cannot lead to C^{11}.

The measurements reported here were made in a neutron beam produced by stripping deuterons[4,5] in a $\frac{1}{2}$ in. thick Be target in the 184-in. cyclotron, and collimated into a width of $2\frac{1}{2}$ in. by passing through an aperture in the

cyclotron shield. The mean neutron energy is 90 Mev, and the width of the distribution at half-maximum is about 27 Mev; these theoretical figures now have some experimental support. The neutron flux was measured by apparatus set up by one of us (H.F.Y.) for examining the angular distribution in neutron-proton scattering; since it will be described in full when that work is published, only an outline is given here. A thin scatterer of paraffin was put in the neutron beam at 52 feet from the source, and the recoil protons detected by a line of four proportional counters in coincidence. The solid angle for accepting protons was accurately defined by a hole in a copper plate, and an absorber between the counters limited the protons counted to those corresponding to neutron energies above 66 Mev. Protons coming from the carbon were eliminated by making another count with pure carbon in place of the paraffin. Then, knowing the counting rate at a given angle, the angular distribution of the protons (as found with this apparatus and in Dr. Wilson Powell's cloud chamber) and the total neutron-proton cross section,[6] the neutron flux can be computed. The neutrons whose energy lies below 66 Mev were not counted, and a 6 percent correction based on the fraction theoretically expected below this energy has been made. The neutron fluxes determined in the three runs made were 38, 8.5, and 8.8×10^{4} neutrons cm^{-2} $sec.^{-1}$. At full beam intensity the flux would have been about 10^{6} neutrons cm^{-2} $sec.^{-1}$ at 52 feet from the target, which from the known angular distribution would correspond to a total yield of 2×10^{11} neutrons per sec. for a deuteron current of the order of 1 microampere.

The rest of the measurement consisted of a determination of the C^{11} activity induced in the paraffin scattering blocks during the above experiments. The counting rate due to the paraffin was compared with that of a uranium standard, then in a separate experiment these blocks and a 5-mil polystyrene sheet were exposed simultaneously to a stronger beam, and the ratio of their counting rates was observed. Using the latter ratio, the activity that the polystyrene would have acquired in the weaker beam (which would have been too weak for accurate measurement) could be computed, and from this the disintegration rate free of self-absorption corrections. These disintegration rates per carbon atom in the polystyrene combined with the neutron fluxes lead to activation cross sections of 0.021, 0.024, and 0.022×10^{-24} cm^{2} in the three runs. The mean value, with an estimate of the over-all error, is $(0.022\pm0.004)\times10^{-24}$ cm^{2}.

Thus it is seen that the high energy cross section for the (p, pn) reaction is greater than that for the $(n, 2n)$ reaction in carbon as expected from the action of exchange collisions. The experimental ratio of these cross sections is 3.3. Another interesting comparison is with the total cross section of carbon for 90-Mev neutrons,[6] which is 0.55×10^{-24} cm^{2}. If the total proton cross section is assumed to be the same, and half of these cross sections is assumed to be due to diffraction, then activation to C^{11} is caused by 27 percent of the proton impacts and 8 percent of the neutron impacts. A theoretical basis for treating these reactions has been given by Serber,[7] and detailed computations leading to results in reasonable agreement with experiment have been made by Heckrotte and Wolff.[8]

Another experiment was made in an attempt to measure the ratio of the proton activation to the neutron activation directly. One carbon block was put in the neutron beam and another in a position to intercept protons from the same target; these were exposed simultaneously and the cross section ratio computed, assuming equal neutron and proton yields from the target and the theoretical angular and energy distributions for both particles. The ratios found were 2.5 using a $\frac{1}{2}$-in. Be target, 4.0 using a $\frac{1}{16}$-in. Cu target, and 2.9 using a 0.05-in. U target. Since this method is not very precise, the differences of these values from each other and from the value of 3.3 given above are probably not significant, but the rough check indicates that no gross error has been made in the various assumptions underlying this comparison.

The authors wish to express their appreciation to Warren W. Chupp, J. Hadley, and C. E. Leith for their help. This work was done under the auspices of the Atomic Energy Commission under Contract No. W-7405-eng-48.

[1] R. L. Thornton and R. W. Senseman, Phys. Rev. **72**, 872 (1947).
[2] W. W. Chupp and E. M. McMillan, Phys. Rev. **72**, 873 (1947).
[3] E. M. McMillan and R. D. Miller, Phys. Rev. **73**, 80 (1948).
[4] A. C. Holmholtz, E. M. McMillan, and D. C. Sewell, Phys. Rev. **72**, 1003 (1947).
[5] R. Serber, Phys. Rev. **72**, 1008 (1947).
[6] L. F. Cook, E. M. McMillan, J. M. Peterson, and D. C. Sewell, Phys. Rev. **72**, 1264 (1947).
[7] R. Serber, Phys. Rev. **72**, 1114 (1947).
[8] W. Heckrotte and P. Wolff, Phys. Rev. **73**, 265 (1948).

A Nuclear Evaporation Recorded in an Emulsion Near Sea Level

HERMAN YAGODA
National Institute of Health, Laboratory of Physical Biology, Bethesda, Maryland

December 15, 1947

DISINTEGRATIONS of component nuclei in thick layered emulsions by cosmic radiation have been recorded in plates exposed at high altitudes. At sea level the probability of this occurrence is very low and has been estimated at 10^{-9} event per ml per sec.[1] From available reports[2-4] only four evaporations have been observed in the microscopic survey of plates exposed near sea level. The event described in Fig. 1 and Table I was recently

TABLE I. Analysis of recorded track lengths.

Track	Length* microns	Direction	Number of grains**	Mean grain spacing	Particle	Probable energy (Mev)
A	39.1	air	72	0.55	alpha	(10)***
B	53.0	glass	36	1.52	proton	6.9
C	17.0	air	16	1.13	proton	5.4
D	56.5	glass	57	1.01	proton	5.0
E	24.1	glass	12	2.19	proton	8.9
F	42.3	glass	33	1.32	proton	6.2
G	2.0	emulsion		0	recoil(?)	

* Corrected for dip and gelatin contraction.
** Counted at 1250× under oil immersion and transmitted light.
*** Portion of track recorded corresponds to 7.2 Mev.

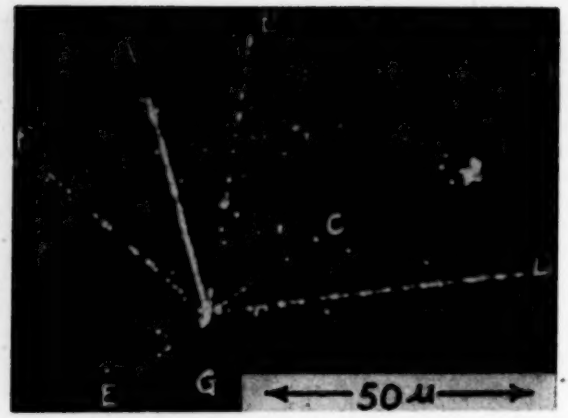

FIG. 1. Photomicrograph of the nuclear evaporation. ×44 dry objective with aperture reduced by dark field stop, 12.5× compensating eyepiece. The short recoil track, G, may not be visible in the reproduction.

observed in an Eastman NTA emulsion coated 30 microns thick, which resided in the laboratory at an elevation of 89 meters for 165 days prior to development.

On the basis of the mean grain spacing of the recorded track lengths, one trajectory can be attributed to an alpha-particle, and five to protons of varying energy. The short dense track *C* appears to terminate in the emulsion and may represent the recoil of the compound nucleus or the terminal track portion of the entrant particle. Its short length and unfavorable position near the center of the star does not permit evaluation of its grain density. If an equal number of neutrons accompanied the ejection of the protons, the event is consistent with the disintegration of an N^{14} atom in the gelatin layer. When observed under conditions of high resolving power the tracks are directed spatially in varied directions, two terminating in air and four entering the glass backing.

The energy of the protons was estimated from their grain counts with the aid of calibration data on grain density at the beginning of full length proton tracks recorded in an emulsion of identical stopping power. A study of the tracks of recoil protons produced in the emulsion by neutrons from a Be-Po source shows that the grain spacing near the track termination is essentially independent of proton energy, whereas at the beginning of the track it increases progressively with the total track length. This regularity permits an extrapolation of the proton energy, as the beginning of the tracks is sharply defined by the center of the star. Similar data is not available for high energy alpha-particles, but since the mean grain spacing of track *A* is only a trifle less than that observed in ThC′ alpha-tracks (0.56±0.02 microns) its total energy probably does not exceed 10 Mev.

The energy of the five protons totals 32 Mev and if an equal magnitude be assigned to the associated neutrons, then the disintegration is accompanied with the release of about 74-Mev energy. The breakdown of N^{14} into $He^4+5H^1+5n^1$ is endothermic and requires an additional energy expenditure of 76 Mev. The cosmic-ray particle causing the disintegration must therefore undergo a mass conversion equivalent to 150 Mev. The event is consistent with the entry and annihilation of a particle of about 300 electronic masses. The entrant particle might be a heavy meson, which according to Marshak and Bethe[5] has a mass of 250 electron masses.

[1] E. Gross, S. Kusaka, and G. Snow, Bull. Am. Phys. Soc. 22, 6 (1947).
[2] A. Zhadanov, Comptes Rendus U.R.S.S. 46, 359–61 (1945). Describes two events with 35- and 50-component tracks.
[3] G. R. Evans and T. C. Griffiths, Nature 159, 879 (1947). Observes star composed of eleven particles.
[4] R. R. Roy, Nature 160, 498 (1947). Describes nuclear burst with 22 tracks.
[5] R. E. Marshak and H. A. Bethe, Phys. Rev. 72, 506 (1947).

Excitation Function of the Reaction $C^{12}(p, pn)C^{11}$ at High Energies

W. HECKROTTE AND PETER WOLFF
Radiation Laboratory, Department of Physics, University of California, Berkeley, California
December 22, 1947

THE excitation curve for the reaction $C^{12}(p, pn)C^{11}$ at high energies has been measured recently by Chupp and McMillan.[1] Using the model of the nucleus described by Serber,[2] the excitation curve of the above reaction has been calculated for energies up to 100 Mev. The excitation of the nucleus is determined on the basis that the incident proton makes individual collisions with the nucleons, the transferred energy exciting the nucleus. The mean free path of a high energy nucleon in the C^{12} nucleus was taken to be $4.75\cdot10^{-13}$ cm at 100 Mev; and the radius of the C^{12} nucleus $3.7\cdot10^{-13}$ cm. These numbers are chosen to give a total cross section equal to the experimental value, $\sigma_t=0.55$ barn.[3] The distribution curve for the energy transferred to the nucleus in one or more collisions was calculated by Mr. Baumhoff of this laboratory. $n-p$ collisions are taken to be three times more probable than $n-n$ or $p-p$ collisions. The calculations were made for both a pure $n-p$ exchange force and a half-exchange, half ordinary force.

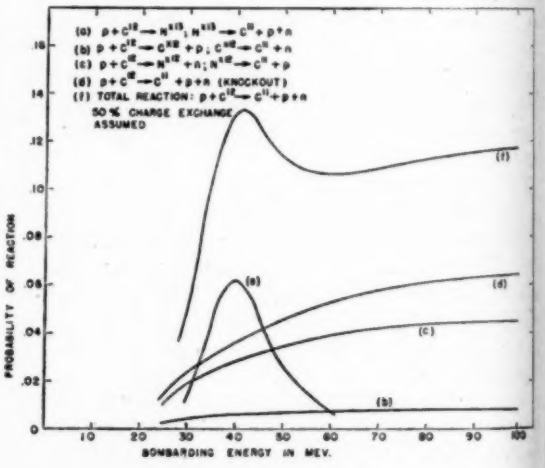

FIG. 1

The decay of the excited nucleus is treated by the usual evaporation model.

On the above basis, the reaction can go in four ways:

(a) $p+C^{12} \rightarrow N^{*13}$; $N^{*13} \rightarrow C^{11}+p+n$,
(b) $p+C^{12} \rightarrow C^{*12}+p$; $C^{*12} \rightarrow C^{11}+n$,
(c) $p+C^{12} \rightarrow N^{*13}+n$; $N^{*13} \rightarrow C^{11}+p$,
(d) $p+C^{12} \rightarrow C^{11}+p+n$ (knock out).

The part played by each of these separate reactions to give the total reaction is shown in Fig. 1 for 50 percent exchange. Reaction (a) contributes chiefly in the 40-Mev region. This is the result (1) of the high probability in this region of the incident particle giving up all of its energy in a few collisions and thus of being captured; and (2) of the energy dependence of the $N^{13} \rightarrow C^{11}+p+n$ reaction. Above the 40-Mev region there is an increased probability of boiling off three or more particles, and below the 40-Mev region, only one particle. Reaction (b) takes place when the incident proton passes through the nucleus and makes few collisions before emerging with most of its original energy. Because of the much greater probability of excited C^{12} breaking down into three α-particles, this reaction contributes very little to the total reaction. It does contribute somewhat more for 50 percent exchange since a one collision non-exchange process can then contribute. Reaction (c) is made possible by a net exchange taking place when the incident proton passes through the nucleus, so that it emerges as a neutron. Excited N^{12} is formed as the intermediate product. For small excitation energies (~10 Mev)N^{13} will definitely boil off one proton, but this probability rapidly drops off for higher excitation energies because of competing processes coming into play. As a result of this only a single $p-n$ exchange collision is effective in giving reaction (c), a two (or more) collision process leaving too much excitation energy. This results in making the reaction practically directly proportional to the amount of exchange, which, accordingly, exerts a direct influence on the yield of the total reaction at high energies. Reaction (d) is the knock-out reaction. It is assumed that a knock-out reaction can occur only if the nucleon struck by the incident particle travels from the point of collision to the outside of the nucleus without colliding with other nucleons. Otherwise the struck nucleon excites the nucleus by its collisions with the other nucleons and so stays in. The knock-out reaction (d) is probable only if the incident proton makes just the one collision near the edge of the nucleus.

The total reaction for both 50 percent and 100 percent exchange is plotted on a range scale in Fig. 2, assuming 140-Mev protons incident on a carbon block. The attenuation of the incident beam is taken into account. The experimental curve (1) for the reaction is given by the dotted line. The ordinate has been adjusted to bring it into approximate agreement with curve I.

The calculated cross section for the reaction at 62 Mev is: 0.046 barn for 50 percent exchange and 0.062 barn for 100 percent exchange. The experimental value[4] is 0.073 ±0.010 barn for 62-Mev incident protons.

The authors wish to express their great appreciation to Professor Robert Serber for his continued assistance throughout the course of these calculations.

This paper is based on work performed under Contract No. W-7405-eng-48 with the Atomic Energy Commission in connection with the Radiation Laboratory, University of California, Berkeley, California.

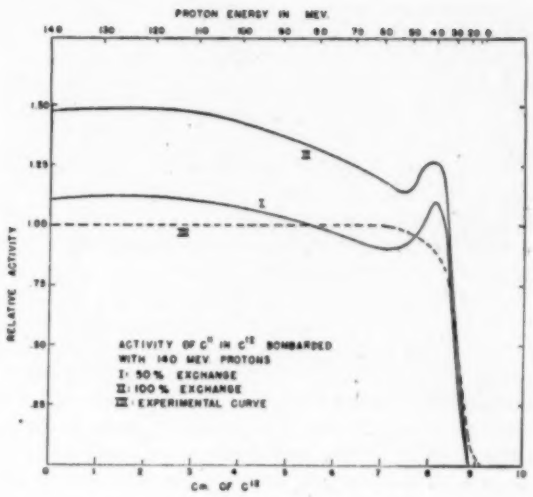
PROTON ENERGY IN MEV
RELATIVE ACTIVITY
ACTIVITY OF C11 IN C12 BOMBARDED WITH 140 MEV PROTONS
I: 50% EXCHANGE
II: 100% EXCHANGE
III: EXPERIMENTAL CURVE
CM OF C12

FIG. 2.

[1] W. W. Chupp and E. M. McMillan, Phys. Rev. **72**, 873 (1947).
[2] R. Serber, Phys. Rev. **72**, 1114 (1947).
[3] L. J. Cook, E. M. McMillan, J. M. Peterson, and D. C. Sewell, Phys. Rev. **72**, 1264 (1947).
[4] E. M. McMillan and R. D. Miller, Phys. Rev. **73**, 80 (1948).

Excitation Function of the Reaction $C^{12}(n, 2n)C^{11}$ at High Energies

W. HECKROTTE AND PETER WOLFF
Radiation Laboratory, Department of Physics, University of California, Berkeley, California
December 22, 1947

THE excitation curve for the reaction $C^{12}(n, 2n)C^{11}$ has been calculated for energies up to 100 Mev. The calculations were done as described in the preceding letter for the similar reaction of C^{12} under proton bombardment.

The reaction can go in three ways:

(a) $n+C^{12} \rightarrow C^{*12}$; $C^{*12} \rightarrow C^{11}+2n$,
(b) $n+C^{12} \rightarrow C^{*12}+n$; $C^{*12} \rightarrow C^{11}+n$,
(c) $n+C^{12} \rightarrow C^{11}+2n$ (knock out).

The results of the calculations for 50 percent exchange are shown in Fig. 1. The calculated cross section for the reaction at 90 Mev is: 0.010 barn for 100 percent exchange and 0.012 barn for 50 percent exchange. The experimental value is 0.022±0.004 barn.[1]

The ratio of the cross section of the reaction $C^{12}(p, pn)C^{11}$ to the cross section of the above reaction at 90 Mev is: 5.8 for 100 percent exchange and 3.8 for 50 percent exchange. The experimental ratio is 3.3 at 90 Mev.[1]

This difference in cross sections between the two reactions is established by two factors. First, there is the part played by exchange in the $C^{12}(p, pn)C^{11}$ reaction which

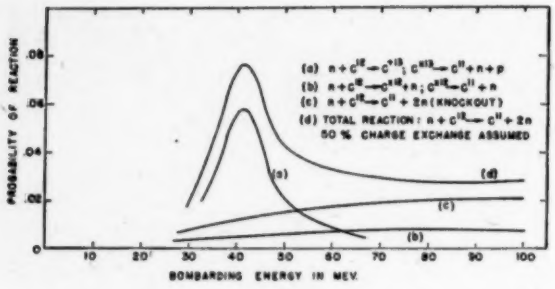

FIG. 1.

leads to excited N^{12} with the subsequent boiling off of a proton, while a similar exchange process cannot take place for the $C^{12}(n, 2n)C^{11}$ reaction. Secondly, there is the difference between the contributions of the knock-out process as a result of the difference in the $n-p$ and the $n-n$ cross sections, which favors the $p+C^{12}$ knock-out reaction. It will be noted that the parts of the reactions which go through excited C^{12}, while practically equal, are so small that they do not greatly affect either reaction.

Although the results of these calculations do not agree too closely with the experimental results, they are probably as good as are to be expected because of the crudity of the assumed model. The results do, however, seem to give a good qualitative picture of the contributing factors affecting the total reactions. Finally, it would seem that the assumption of 50 percent exchange gives better agreement.

The authors wish to express their great appreciation to Professor Robert Serber for his continued assistance throughout the course of these calculations.

This paper is based on work performed under Contract No. W-7405-eng-48 with the Atomic Energy Commission in connection with the Radiation Laboratory, University of California, Berkeley, California.

[1] E. M. McMillan and H. F. York, Phys. Rev. 73, 262 (1948).

Low Energy Pair Production

P. V. C. HOUGH
Laboratory of Nuclear Studies, Cornell University, Ithaca, New York
December 15, 1947

THE appreciable effort required to get numerical results from the exact Bethe-Heitler differential cross section for pair production[1] has suggested its imitation by a simpler expression. We first consider the well-known high energy limit,[2] without screening, of the exact formula.

Errors in the high energy formula are positive and <1.5 percent (differential cross section) or <1 percent (total cross section), for $k \geq 15$. (Energies throughout are in units of the electron rest energy.) If one fits the differential formula to exact values at the "midpoint," i.e., for equal electron and positron energies, these limits become +1 percent and +½ percent, respectively. Comparisons below, however, are to the unfitted formula. Errors for $k>20$ are roughly $(20/k)^2$ times the above limits, for either type of approximation.

The high energy integral formula usually quoted[2] is *not* as good as just stated; one lower power of k must be kept, making the total cross section

$$\Phi = (28/9)\ln 2k - (218/27) + (6.45/k). \quad (1)$$

Here, and throughout, cross sections are in units of $(Z^2/137)(e^2/mc^2)$.[2]

As a formula suitable for $2 \leq k \leq 15$ and having reasonable overlap with the high energy formula at the upper limit, we propose the following:

$$\phi_x = \phi_0 \varepsilon[1+0.135(\phi_0-0.52)\varepsilon(1-\varepsilon^2)]. \quad (2)$$

$x=(E_+-1)/(k-2)$ is the fraction of *kinetic* energy, $k-2$, given to the positron; $\varepsilon=2[x(1-x)]^{\frac{1}{2}}$; ϕ_x is the cross section per nucleus per unit x (cf. Heitler, p. 199); ϕ_0 is ϕ_x at $x=\frac{1}{2}$. *The second term in the square bracket is to be dropped when it becomes negative (below $k=4.2$).*

ϕ_0 appears in (2) because no simpler, good k-dependence has been found. At $x=\frac{1}{2}$ the exact formula simplifies appreciably (if not spectacularly), giving

$$\phi_0 = (1-\gamma)[\tfrac{1}{3}(4-\gamma^2)(L-1)-\gamma^2\alpha(\alpha-1)-\gamma^4\alpha(L-\alpha)], \quad (3)$$

with $\gamma=(2/k)$, $L=[2/(1-\gamma^2)]\ln(k/2)$, $\alpha=[1/(1-\gamma^2)^{\frac{1}{2}}] \times\ln[(k/2)+((k/2)^2-1)^{\frac{1}{2}}]$. Table I gives ϕ_0 for several values of k. (For comparison, several high energy values are also shown.)

Our formula (2) is, of course, exact at $x=\frac{1}{2}$; its performance at small x (and hence near $x=1$) is shown in Table II. We may suppose on this basis that for $2 \leq k \leq 15$ (2) deviates from the exact formula by <2 percent, that deviations of more than 0.2 percent occur only for $x<0.2$ or >0.8, and accordingly, that total cross sections from (2) are wrong by <½ percent (and <0.1 percent for $k \leq 10$).

We get from (2) for the total cross section

$$\begin{aligned} \Phi &= 0.776_0\phi_0 + 0.0180\phi_0^2 \quad (k>4.2) \\ &= 0.785_4\phi_0 \quad (k<4.2). \end{aligned} \quad (4)$$

Values calculated from (4) are presented in Table III,

TABLE I. Differential cross section at $x=\frac{1}{2}(\phi_0)$.

k		3	4	6	10	20	50
ϕ_0	exact	0.1116	0.4157	1.1419	2.3816	4.3163	6.953
	high energy				2.367	4.342	6.961

TABLE II. Exact, Eq. (2), and high energy differential cross sections compared.

		x = 0.2	0.1	0.05
$k=4$	exact		0.2492	
	Eq. (2)		0.2494	
$k=6$	exact	0.937		
	Eq. (2)	0.936		
$k=10$	exact	2.046	1.565	1.122
	Eq. (2)	2.043	1.567	1.130
	high energy	2.006	1.497	1.018
$k=20$	exact	3.968	3.194	2.324
	Eq. (2)	3.963	3.100	2.222
	high energy	4.009	3.238	2.343

TABLE III. Total cross section.

k	3	4	6	10	20
Eq. (4)	0.0876(0)	0.3265(±1)	0.9096(±8)	1.950(±2)	3.69(−2)
Heitler	0.085	0.32	0.89	1.94	3.75
Eq. (1)				1.89	3.73(+2)

where we have also reproduced results given by Heitler,[4] and at $k=10$, 20 numbers from the high energy formula (1). The figures in parentheses are expected errors in the last digit shown. One should note the considerable improvement in accuracy over Heitler's results, and the overlap of (4) and (1) at $k=20$. At $k=15$, the two are still closer.

The low energy form of (2), $\phi_s=\phi_0 s$, was found by expanding the exact formula in powers of the excess energy, $k-2$; the limiting k-dependence found for ϕ_0 is

$$\phi_0=(\tfrac{1}{3})(k-2)^3 \quad (k-2)\ll 1. \tag{5}$$

(5) is interesting in that the coefficients of three lower powers of $(k-2)$ vanish, so there results a higher order of contact of the total cross section curve at $k=2$ than might have been expected. The range of validity shown in (5) must be taken seriously: at $k=2.5$ (5) is already almost double the true value. As pointed out to me by Professor H. A. Bethe, multiplying (5) by $(2/k)^3$ gives the best possible power law approximation for large k; the improved formula is 12 percent low at $k=3$, 50 percent low at $k=6$, and gives a total cross section at high energies ~ 2 instead of actual limits (if screening is included) of ~ 12.

I wish to thank Professor Bethe for suggesting these calculations and for helpful discussions of many points while carrying them out.

[1] H. Bethe and W. Heitler, Proc. Roy. Soc. **146**, 90 (1934), Eq. (21); or W. Heitler, *Quantum Theory of Radiation* (Oxford University Press, 1936), p. 196, Eq. (8).
[2] W. Heitler, *Quantum Theory of Radiation* (Oxford University Press, 1936), p. 197, Eq. (9).
[3] See reference 2, p. 200, Eq. (15).
[4] See reference 2, p. 200, Table V.

On the Structure of Grain Boundaries in Metals

T'ING-SUI KÊ
Institute for the Study of Metals, The University of Chicago, Chicago, Illinois
December 15, 1947

THERE is no method known at present of determining the structure of grain boundaries in metals. Considerations based on the atomistic viewpoint suggest that the grain boundary is a transition region, where the atom positions represent a compromise between the crystalline arrangements in the two adjoining grains. Extensive experiments on internal friction and related effects have demonstrated that this transition region behaves in a viscous manner in the sense that it cannot sustain permanently a shear stress and it has a coefficient of viscosity decreasing with an increase of temperature.[1,2] This does not, however, tell us about the structure of this transition region, since any layer of disturbed crystallinity when considered as an entity may manifest a viscous behavior.

A study of the activation energy associated with the viscous slip along grain boundaries seems to contribute to our understanding of the structure of the grain boundary. It has been found that the activation energy associated with the grain boundary slip in alpha-brass is close to the value for the diffusion of zinc in alpha-brass of the same composition.[3] Recently, in the study of the anelastic effects in alpha-iron,[4] the value obtained for the activation energy of grain boundary slip agrees, within experimental error, with the value for the self-diffusion in alpha-iron reported by Birchenall and Mehl.[5] Such an agreement has also been found in the case of aluminum. The activation energies for volume diffusion and grain boundary slip of these metals are summarized in the second and third columns of Table I.

If such an agreement in activation energies were found to be a general phenomenon in all metals, this would indicate that the grain boundary slip involves the same mechanism as does volume diffusion. This would also indicate that, at least as far as the local order is concerned, the structure of the transition region at the grain boundary cannot be markedly different from that of the interior of the grains. The grain boundary slip can thus be considered as creep on a microscopic scale, and this creep occurs at a lower temperature than creep in single crystals because of the disturbed crystallinity at the grain boundary. This viewpoint is strengthened by the findings that the activation energies for the creep in these metals (shown in the fourth column of Table I) are comparable with that of grain boundary slip.

The upper limit of the width of grain boundary has been suggested to be five atomic diameters on the basis that the forces between atoms in solids are of short-range type extending with appreciable intensity only over a few atomic distances.[6] It seems that the boundary region within which creep may take place must have a width of at least a few atomic diameters. Actually the mere fact of short-ranged forces in solids does not necessarily imply that the transitional region can only be very thin. Reference can be made

TABLE I. Different types of activation energy of a few metals (in calories per mole).

Type of metal	Volume diffusion	Grain boundary slip	Creep
Alpha-brass	41,700[a,*]	41,000[b,*]	42,000[c,**]
Alpha-iron	78,000[d,***]	85,000[e,***]	90,000[f]
Aluminum	37,500[g]	34,500[b,†]	37,000[i,†]

* 29 percent Zn.
** 40 percent Zn.
*** Westinghouse Puron.
† 99.99 percent aluminum.
[a] A. E. Van Arkel, Metallwirtschaft **7**, 656 (1928); see also R. F. Mehl, Trans. A.I.M.E. **122**, 11 (1936).
[b] See reference 3.
[c] H. Tapsell, A. Johnson, and W. Clenshaw, Eng. Research Report No. 18, Dept. Sci. and Ind. Research, London (1932).
[d] See reference 5.
[e] See reference 4.
[f] J. J. Kanter, Trans. A.I.M.E. **131**, 385 (1938).
[g] Estimated on the basis of binding energy and of melting temperature according to an empirical rule for face-centered cubic metals observed by W. A. Johnson, Trans. A.I.M.E. **143**, 107 (1941); also private communication to the writer.
[h] See reference 1.
[i] S. Dushman, L. W. Dunbar, and H. Huthsteiner, J. App. Phys. **15**, 108 (1944); extrapolated to zero stress by C. Zener and J. H. Hollomon, J. App. Phys. **17**, 69 (1946).

to magnetic domain boundaries the width of which has been computed to have a value of between 30 to 100 atomic diameters.[7]

[1] T. S. Kê, Phys. Rev. **71**, 533 (1947).
[2] T. S. Kê, Phys. Rev. **72**, 41 (1947).
[3] T. S. Kê, J. App. Phys. (in the press).
[4] T. S. Kê, communicated to Trans. A.I.M.E.
[5] C. E. Birchenall and R. F. Mehl, Mining and Metallurgy (November 1947).
[6] F. Seitz and T. A. Read, J. App. Phys. **12**, 538 (1941).
[7] F. Bloch, Zeits. f. Physik **74**, 293 (1932); also R. Becker and W. Doring, *Ferromagnetismus* (Verlag Julius Springer, Berlin, 1939), p. 189.

Erratum: Interaction of Neutrons with Electrons

[Phys. Rev. **72**, 1254 (1947)]

J. M. JAUCH AND K. WATSON
Department of Physics, The State University of Iowa, Iowa City, Iowa

IN a recent letter to the editor[1] we erroneously estimated the expected scattering cross section of neutrons on electrons due to the polarization of the meson cloud in the field of an electron. While this effect no doubt exists theoretically it is much less important than the effect due to the spreading of the meson charge over a finite region in the nucleus as shown in the recent paper by Fermi and Marshall.[2] The conclusion at the end of the letter must therefore be withdrawn.

[1] J. M. Jauch and K. Watson, Phys. Rev. **72**, 1254 (1947).
[2] E. Fermi and L. Marshall, Phys. Rev. **72**, 1139 (1947).

Structure, Electrical, and Optical Properties of Barium Titanate*

B. MATTHIAS AND A. VON HIPPEL
Laboratory for Insulation Research, Massachusetts Institute o Technology, Cambridge, Massachusetts

December 10, 1947

SEVERAL letters to the editor have appeared recently in this journal[1,2] and in Nature[3,4] dealing with observations on $BaTiO_3$. Since some of the statements made are somewhat misleading, and others present results anticipated by publications from this Laboratory,[5] a short account concerning the properties of barium titanate as they appear today on the basis of our recent investigations may be in order.

N. J. Field, A. P. DeBretteville, and H. D. Williams reported[1] two kinds of barium titanate crystals with different infra-red absorption, distinguishable by their bluish and yellowish colors. This coloration is due to dissolved platinum, and we can add to the color scale crystals from light green to deep red by varying the method of growing the material in Pt crucibles. The pure crystals without oxygen defect are colorless and may, for instance, be grown with the proper precautions in carbon crucibles.

A microscopic investigation reveals that, regardless of color, the crystals are subdivided into ferroelectric domains. The faces of these domains parallel to the polar axis are, in general, covered with a system of stripes oriented at 45° to the cube edges and apparently represent slip bands. In the direction of the polar axis the crystals appear clear and sometimes intersected by stripes parallel to the cube edges. In polarized light the structure of the domains is enhanced by various stress colors, and black boundary lines mark the regions in which the opposing stresses of several domains balance.

By the application of an electric field, the domain boundaries may be seen to shift some domains growing at the expense of others, and, finally, the polar axes change orientation in sudden jumps by 90° or 180°. Increase of the temperature to the Curie point makes first the 45° stripes and then the domains themselves disappear; they reappear on cooling in various arrangements, depending on the thermal history. By cooling in an electric field from above the Curie point, the whole crystal may be forced more or less into a single domain, but such a state breaks down later into several domains forming arrangements of lower energy. The domain structure can also be influenced by pressure; in short, all the domain phenomena derived by indirect evidence in the case of ferromagnetics can be made visible in these ferroelectric crystals.

$BaTiO_3$ crystals are generally biaxial because of the stresses set up by their domains, but we have succeeded in producing single crystals of such large domain areas that they appear nearly tetragonal in polarized light. According to our present evidence, the c axis represents the polar axis, and can be turned in electric fields; x-ray back-reflection photographs of these large domains are being made to decide the question.

At low field strength, the dielectric constant parallel to the polar axis is relatively small ($\leqq$600 at 25°C) and, perpendicular to it, is high ($\leqq$2000 at 25°C); they are nearly alike in the two latter directions. The crystals are piezoelectric, and their resonance vibrations disappear as the dielectric constant begins to increase towards its maximum. The vibrations of titania ceramics, discovered by Roberts in this Laboratory, should, therefore, not be treated as an electrostrictive phenomenon as done by Mason,[3] because a normal electrostrictive effect increases with dielectric constant.[6] The mechanical deformation of $BaTiO_3$ single crystals appears as the superposition of a linear and a quadratic piezo effect.

In addition to the cubic modification of $BaTiO_3$, there exists, among others, an hexagonal form[7] which is not ferroelectric.

A more extensive paper on titania single crystals and their interaction in ceramics is in preparation. Photographs of the domain effects will be shown at the annual meeting of the American Physical Society in New York.

* This work was supported by ONR Contract N5ori-78, T.O. 1.
[1] N. J. Field, A. P. DeBretteville, Jr., and H. D. Williams, Phys. Rev. **72**, 1119 (1947).
[2] W. P. Mason, Phys. Rev. **72**, 869 (1947).
[3] H. F. Kay and R. G. Rhodes, Nature **160**, 126 (1947).
[4] J. K. Hulm, Nature **160**, 127 (1947).
[5] A. von Hippel, R. G. Breckenridge, F. G. Chesley, and L. Tisza, J. Ind. Eng. Chem. **38**, 1097 (1946); S. Roberts, Phys. Rev. **71**, 890 (1947); B. T. Matthias, R. G. Breckenridge, and D. W. Beaumont, Phys. Rev. **72**, 532 (1947).
[6] *Handbuch der Physik* XII, 493, 556.
[7] H. Blattner, B. Matthias, and W. Merz, Helv. Phys. Acta **20**, 225 (1947).

Saturation and Power Broadening of Microwave Resonance Lines*

PAUL I. RICHARDS AND HARTLAND S. SNYDER
Brookhaven National Laboratory, Upton, Long Island, New York
December 15, 1947

AN expression extending the results of Van Vleck and Weisskopf[1] for the power absorption by a gas in the neighborhood of a resonance line in the microwave region and which shows the effects of saturation and power broadening has been obtained. The quantum-mechanical result is

$$p=\frac{4\pi|\mu|^2h\nu_0\Delta NG}{3h^2c\tau[(\Delta\nu)^2+(1/2\pi\tau)^2+(8\pi|\mu|^2G/3h^2c)]},$$

in which p is the power absorbed per unit volume of gas, $|\mu|$ is the effective dipole moment of the gas molecule, ν_0 is the resonance frequency, ΔN is the difference in population of molecules in the two energy state per unit volume, G is the incident power per unit area, τ is mean collision time, and $\Delta\nu$ is the difference between the applied frequency and the resonance frequency. This equation checks qualitatively with the results obtained by Pond and Cannon.[2] A detailed paper on this calculation is being prepared.

* Research carried out at the Brookhaven National Laboratory under the auspices of the Atomic Energy Commission.
[1] J. H. Van Vleck and V. F. Weisskopf, Rev. Mod. Phys. **17**, 227 (1945).
[2] T. A. Pond and W. F. Cannon, Phys. Rev. **72**, 1121 (1947).